Localization and topology in surface states of disordered topological insulators

Mateo Moreno González

LOCALIZATION AND TOPOLOGY IN SURFACE STATES OF DISORDERED TOPOLOGICAL INSULATORS

Inaugural-Dissertation

zur

Erlangung des Doktorgrades

der Mathematisch-Naturwissenschaftlichen Fakultät

der Universität zu Köln

vorgelegt von

MATEO MORENO GONZALEZ

aus

San Rafael, Antioquia, Kolumbien

Köln 2024

Berichterstatter:	Prof. Dr. Alexander Altland
(Gutachter)	Prof. Dr. Achim Rosch

Vorsitzender der Prüfungskommission: Prof. Dr. Joachim Krug

Tag der mündlichen Prüfung: 19.11.2024

ABSTRACT

In condensed matter physics topology has fundamentally reshaped our understanding of phases of matter and the transitions between them. New phases, such as topological insulators, have introduced innovative perspectives on band theory, where for each band in the bulk of these systems topological invariants can be defined. One significant consequence of bulk topological invariants is the emergence of topologically protected gapless boundary states that are robust against symmetry-preserving perturbations.

However, all real systems exhibit some degree of impurities or disorder. Disorder breaks translation invariance, a critical feature for band theory, and can lead to the localization of states through Anderson localization. Anderson localization and topology act as opposing forces in electronic systems: while topology protects gapless states, Anderson localization tends to localize them. Consequently, Anderson localization can potentially drive a topological insulator through topological phase transitions.

This thesis investigates the impact of disorder on topological insulators in two and three dimensions. First, it presents a comprehensive study of the disordered Chern insulator, detailing its phase diagram and identifying the energy positions of delocalized states responsible for quantized Hall responses. Secondly, it explores disordered higher-order topological insulators, examining the preservation of boundary modes and topological invariants under disorder. Lastly, it addresses the surface states of three-dimensional chiral topological insulators, revealing their fragility and localization properties. These questions are addressed using analytical methods from topological quantum field theory and by deriving non-linear σ models from microscopic models. These findings allow us to comprehend the interplay between Anderson localization and topology in some topological insulators in two and three dimensions.

ZUSAMMENFASSUNG

In der Physik der kondensierten Materie hat Topologie unser Verständnis der Phasen der Materie und der Übergänge zwischen ihnen grundlegend verändert. Neue Phasen, wie z. B. topologische Isolatoren, haben innovative Perspektiven für die Bandentheorie eröffnet, in der für jedes Band des Systems topologische Invarianten definiert werden können. Eine wichtige Konsequenz der topologischen Invarianten ist das Auftreten von topologisch geschützten Randzuständen ohne Energielücke, die gegenüber symmetrieerhaltenden Störungen robust sind.

Alle realen Systeme weisen jedoch ein gewisses Maß an Verunreinigungen oder Unordnung auf. Unordnung bricht die Translationsinvarianz, eine entscheidende Voraussetzung für die Bandtheorie, und kann zur Lokalisierung von Zuständen durch Anderson-Lokalisierung führen. Anderson-Lokalisierung und Topologie wirken in elektronischen Systemen als gegensätzliche Kräfte: Während die Topologie Zustände ohne Energielücke schützt, neigt die Anderson-Lokalisierung dazu, sie zu lokalisieren. Folglich kann die Anderson-Lokalisierung einen topologischen Isolator potenziell durch topologische Phasenübergänge treiben.

In dieser Arbeit wird der Einfluss von Unordnung auf topologische Isolatoren in zwei und drei Dimensionen untersucht. Zunächst wird eine umfassende Studie über den ungeordneten Chern-Isolator vorgestellt, in der das Phasendiagramm detailliert beschrieben und die Energien der delokalisierten Zustände identifiziert werden, die für die quantisierten Hall-Antwort verantwortlich sind. Zweitens werden ungeordnete topologische Isolatoren höherer Ordnung erforscht, wobei die Erhaltung von Randmoden und topologischen Invarianten unter Unordnung untersucht wird. Schließlich werden die Oberflächenzustände dreidimensionaler chiraler topologischer Isolatoren behandelt, wobei deren Zerbrechlichkeit und Lokalisierungseigenschaften aufgezeigt wird. Diese Fragen werden mit analytischen Methoden aus der topologischen Quantenfeldtheorie und durch die Herleitung nichtlinearer σ-Modelle aus mikroskopischen Modellen behandelt. Diese Erkenntnisse ermöglichen es uns, das Zusammenspiel zwischen Anderson-Lokalisierung und Topologie in einigen zwei- und dreidimensionalen topologischen Isolatoren zu verstehen.

CONTENTS

1 Introduction 1
2 Localization and disorder 5
2.1 Effect of impurities on electronic systems 5
2.2 Scaling theory of localization 7
2.3 Field theory approach to the disordered electron gas 9
2.4 Quantum Hall effect 18
2.4.1 Field theory of the quantum Hall effect 24
2.5 Multifractality 26
2.6 Summary 28
3 Chern insulators and disorder 29
3.1 Berry phase 29
3.2 Chern Insulators 32
3.3 Disorder 36
3.3.1 Effective field theory of the disordered Chern insulator 37
3.3.2 Topological action 40
3.3.3 Gradient action 41
3.3.4 Beyond the weak disorder limit 42
3.4 Numerical multifractal analysis 44
3.5 Comparison between different approaches 45
3.6 Summary 47
4 Surface states of higher order topological insulators 49
4.1 The tenfold way 49
4.2 Higher order topological insulators 52
4.2.1 Mirror symmetric AIII HOTI 53
4.2.2 Inversion-symmetric insulator with chiral hinge modes 54
4.3 Conclusion 60
5 Fragility of spectral flow in class AIII topological insulators 63
5.1 Fragility of the spectral flow 64
5.1.1 Bulk 64
5.1.2 Boundary 67
5.2 AIII topological insulator model 69
5.2.1 Surface Dirac approximation 71
5.2.2 Detaching and characterizing surface bands 71
5.3 Field theory of the AIII topological insulator 74
5.3.1 Field theory at $E = 0$ 74
5.3.2 Field theory of the AIII insulator at the surface 77

5.4 Surface Hall conductance 78
5.5 Conclusion 80
A Appendix A 83
A.1 Replica Trick 83
A.2 Self consistent Born approximation 84
B Appendix B 87
B.1 Derivation of the topological action 87
B.2 Derivation of the gradient action 88
B.3 Derivation of Eq. (3.42) 90
B.4 Derivation of the Smrcka-Streda coefficients 91
C Appendix C 93
C.1 Topological invariance of the magnetoelectric polarizability 93
C.2 Derivation of the non-linear σ model action for the HOTI 94
D Appendix D 99
D.1 Saddle point for the AIII model 99
D.2 Derivation of the AIII non-linear σ model 99

Bibliography 103

1

INTRODUCTION

The relevance of topology in condensed matter started with the discovery of the integer quantum Hall effect [1]. It was found that the mechanism behind the quantization of the Hall conductance had a topological origin and therefore its value was protected against any perturbations [2, 3]. This discovery also opened the door to phases of matter beyond the Landau-Ginzburg paradigm. The proposal of having the phenomenology of the integer quantum Hall effect without magnetic fields and in translational invariant systems was put forward by Haldane [4], where the topological invariant was defined using the eigenstates of the electronic band. Years later, after the discovery of the quantum spin Hall effect, it was clear that topological invariants could be defined using the bands of the system. This class of non-interacting phases of matter with topological bands were called *topological insulators*.

Topological insulators are phases of matter that, like ordinary insulators, have an energy gap between the highest occupied band and the lowest empty band. The difference is that they posses gapless states propagating at the boundaries. The integrity of the boundary gapless modes is guaranteed by the powerful principle of *bulk-boundary correspondence*, where the topological invariant defined from the bulk bands is directly related to the properties of the boundary modes. With the help of the 10-fold way [5], which classifies Hamiltonians into ten different symmetry classes, it was possible to classify topological insulators in all symmetry classes and in all dimensions.

This discovery motivated a vast amount of work both in the theoretical and in the experimental directions. From the theoretical side it was clear that it was possible to go beyond the 10-fold way classification if crystalline symmetries were included. The addition of crystalline symmetries allowed for the possibility of realizing higher order gapless boundary modes propagating (or residing) along the higher order boundaries of the systems. These systems are called *higher order topological insulators*.

On the other hand, we know that disorder is unavoidable and it is present in all real materials. In 1-*d* and in some 2-*d* systems we know that states localize in the presence of disorder [6]. However, gapless states are resilient towards localization because of topological protection. It was clear from the quantum Hall effect case that disordered samples were needed to match the experimental data. Disorder localized all states in the sample except for one. This sole state was the responsible for all the transport of states from boundary to boundary as well as for the edge modes observed at the boundaries. Disordered electron

systems, and in particular the low energy degrees of freedom in the scale of the mean-free path, can be described from the point of view of field theory using a non-linear σ model [7]. In the field theory setting the description of the integer quantum Hall effect is given by a non-linear σ model augmented with a topological θ term [8, 9]. For topological insulators it was clear that symmetry preserving disorder must not destroy the topological phases and that their description when disorder is added must be of a non-linear σ model with a topological term [10]. The type of topological term that can be added depends on the topological properties (homotopy groups) of the low energy manifold of the effective degrees of freedom. However, one must take into account that the definition of the topological invariants in terms of electronic bands is only valid in the limit of no disorder. That is due to the fact that disorder destroys translational invariance. This is why when disorder is added to a translational invariant system some concepts must be rethought, for example, spectral gaps are to be replaced with mobility gaps. In the limit of very strong disorder the topological phase gets compromised and a phase transition to a trivial phase is expected.

Therefore the study of the effect of disorder on topological insulators is an exciting task on its own. An analytical study and characterization of the effect disorder in (quasi-) one dimensional topological insulators was accomplished in [11] where it clear that depending on the amount of dirt on the system there could be phase transitions between different topological sectors of the theory.

The purpose of this thesis is then to study and characterize some disordered topological insulators in two and three dimensions. In chapter 3 we completely characterize the two band disordered Chern insulator where we draw a complete phase diagram in terms of energy, disorder strength and a microscopic parameter from the clean Hamiltonian. We also determine the position in energy of the delocalized state in the bulk. This state is the responsible for the quantized Hall response of this system. We do this by deriving a non-linear σ model from a microscopic lattice Hamiltonian where the coupling constants of the theory depend on the microscopic parameters. The derivation of this effective model does not rely on any Dirac approximation.

In chapter 4 we turn our attention to disordered higher order topological insulators and the effect of disorder on them. This is an interesting problem since higher order topological phases usually rely on crystalline symmetries and disorder breaks them. We focus on symmetries preserved on the average. In this way we identify the conditions under which higher order boundary modes are protected and look at their topological invariants. We do this by studying two examples, a three dimensional inversion symmetry second order topological insulator and a two dimensional chiral and mirror symmetric second order topological insulator.

In chapter 5 we turn our attention to surface states of 3 dimensional chiral topological insulators. In previous works it was established that this type of systems showed spectrum wide criticality, where for example, topological insulators in class AIII showed class A integer quantum Hall effect criticality at energies different from zero when disorder was added. We show that these states are fragile,that they are not topologically protected and that they can Anderson localize. The only state that does not Anderson localize is the topologically protected state at zero energy. This is accomplished by identifying a mechanism for detaching the surface and bulk states. In the bulk this mechanism is related to the possibility of Wannier localizing all the states without changing the topological properties of the whole system. In this chapter we determine the processes behind these phenomena by studying a minimal model of a class AIII topological insulator with topological number $\nu = 1$.

2

LOCALIZATION AND DISORDER

In condensed matter physics, it is often customary to work with perfectly translationally invariant systems. Band theory, along with Bloch's theorem, has proven successful in describing the motion of electrons in crystalline solids and predicting observable quantities. It allows to describe the physics of crystalline materials in the Brillouin zone. However, in real materials, disorder is ubiquitous, manifesting as impurities, defects, dislocations, and other imperfections. The presence of disorder leads to new and interesting phenomena that cannot be explained within the scope of Bloch's theorem.

In this chapter, we explore how disorder can affect the electrons and how through the presence of random disorder electrons can localize and drive, for example, a conductor into an insulator through the process of Anderson localization, we explore the phenomenon of Anderson localization by presenting several theoretical developments such as the one parameter scaling as well as a field theory of the free electron gas in a disordered environment, from this point of view we elucidate some of the physical processes involved in Anderson localization. In the second part of the chapter, we study the physics of the integer quantum Hall effect and how the underlying topology of these systems help some states to avoid Anderson localization in the presence of disorder. Moreover, we will see how disorder is essential for understanding the experimental observations in 2D electron gases subjected to a magnetic field.

2.1 EFFECT OF IMPURITIES ON ELECTRONIC SYSTEMS

Let us first consider the simple example of a free electron in a solid. According to Bloch's theorem this systems develops energy bands, and the states satisfy the Schrödinger equation, $\hat{H}(\mathbf{p})\psi_0(\mathbf{x}) = E(\mathbf{p})\psi_0(\mathbf{x})$, with $\hat{H}(\mathbf{p}) = \frac{\hat{\mathbf{p}}^2}{2m}$.

Now, we consider the limit in which disorder is quenched or static, meaning the electron dynamics are much faster than the dynamics of the impurities. To model disorder, we introduce a potential $\hat{V}(\mathbf{x})$ and examine its effect on the states. We obtain a new equation,

$$\left(\hat{H}(\mathbf{p}) + \hat{V}(\mathbf{x})\right)\psi_\alpha(\mathbf{x}) = E_\alpha\psi_\alpha(\mathbf{x}). \tag{2.1}$$

We can focus on the case of a single impurity with potential $\hat{V}(\mathbf{x}) = -\mathcal{Z}e^2/\kappa|\mathbf{x}|$, where $\mathcal{Z}e$ is the charge and κ the dialectric constant. In this case,

the energies of the system are $E_\alpha = -E_0\alpha^{-2}$, where $E_0 = m\mathcal{Z}^2e^4/2\kappa^2\hbar^2$. We note that the ground state wavefunction is localized and decays exponentially into the bulk,

$$\psi_0(|\mathbf{x}|) = (\pi a^3)^{-1/2}\exp\left(-|\mathbf{x}|/a\right), \tag{2.2}$$

where $a = \kappa^2\hbar^2/m\mathcal{Z}^2e^2$ is the effective Bohr radius for the impurity state. The fact that this state is localized means that the system should be an insulator at sufficiently low temperatures. Let us consider now a finite concentration of impurities, N_{imp}, in this case there might be an overlap of wavefunctions which in principle can delocalize the wavefunctions and render the system metallic. For a small impurity concentration N_{imp}, we can write the total wavefunction as a linear combination of states localized around the impurity centers $\mathbf{x}_\alpha$, with effective radius a,

$$\Psi(\mathbf{x}) = \sum_\alpha A_\alpha\psi(\mathbf{x}-\mathbf{x}_\alpha), \tag{2.3}$$

where there might be small but finite overlap among states. To quantify the amount of overlap let us consider the following: We approximate the concentration of impurities as a superlattice with spacing $b = N_{\text{imp}}^{-1/d}$, and together with radius of impurities we can define the dimensionless parameter, $N_{\text{imp}}a^d = (a/b)^d$, where $N_{\text{imp}}a^d \gg 1$ indicates a high degree of overlap between states. In the case taken here (small overlap) it is enough to consider nearest neighbour overlap and the effective Hamiltonian can be constructed as a tight-binding model written in second quantization in the following way,

$$H_{\text{eff}} = E_0\sum_i c_i^\dagger c_i + I\sum_{\langle ij\rangle} c_i^\dagger c_j, \tag{2.4}$$

where $I \propto e^{-b/a}$ is the overlap integral. Upon the calculation of the spectrum of this Hamiltonian we find $E(\mathbf{p}) = E_0 + 2I\sum_{i=1}^d \cos(bp_i)$. That means that the width of the impurity band is proportional to I, which decreases exponentially with $N_{\text{imp}}a^d$. On the other hand the effective mass is calculated as $m_{\text{eff}} = 1/2b^2I$ and it increases as the dimensionless parameter decreases. For one electron per impurity, the resulting band is half filled and metallic. However, this metallic phase can be fragile for several reasons. One reason could be that, due to the exponentially narrow size of the band, the tunneling time between impurity centers becomes exponentially long, causing the electron motion to quickly dephase. Another reason could be that a strong Coulomb interaction could give rise to a Mott-Hubbard metal insulator transition. The last reason can be due to random disorder in the sample [12], which is the case us interest to us.

Let us consider a variant of the previous tight binding model where we consider the on-site energy depending on the position i,

$$H = \sum_i W_i\, c_i^\dagger c_i + \sum_{\langle ij\rangle} I_{ij}\, c_i^\dagger c_j, \tag{2.5}$$

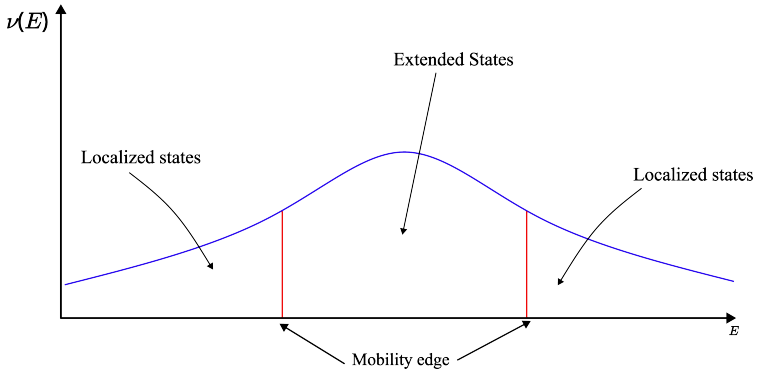

FIGURE 2.1: A schematic density of states where we see a separation between localized and extended states. The two regions are seprated by the mobility edge

where W_i and I_{ij} are both random. Anderson [6] proposed as a first approach a model where W_i is random and drawn from a box distribution $W_i \in [-W/2, W/2]$ and $I_{ij} = I$ is constant. The energy scales W and I in the Anderson model can be combined into a dimensionless parameter W/I. Anderson proposal is that for values of the parameter bigger than a critical value $(W/I) > (W/I)_c$ all states are localized. Below this value there is a mobility edge and the states are extended.

A remarkable aspect of this model is that the density of states shows no critical behavior at the edge of the band. Instead, the density of states develops tails, called Lifshitz tails [13], and the conductivity quickly falls to zero near the mobility edge. The mobility edge separates the localized states from the delocalized states in the band (see figure 2.1). Therefore, for a given chemical potential, we find that the system is either metallic or insulating. In order to study the fate of physical observables, in particular of the conductivity of the sample as disorder is present, we present in the next section the idea behind the scaling theory of localization.

2.2 SCALING THEORY OF LOCALIZATION

Following ideas by Thouless and Edwards [14, 15] regarding the conductivity on long thin wires '*the gang of four*' Abrahams, Anderson, Licciardello and Ramakrishnan [16] proposed a scaling theory for the conductance in d-dimensions. Let us consider a small block of linear size L. In this block, Edwards and Thouless defined a dimensionless parameter g as the ratio of two energies, the Thouless energy and the mean level spacing. The Thouless energy is defined as

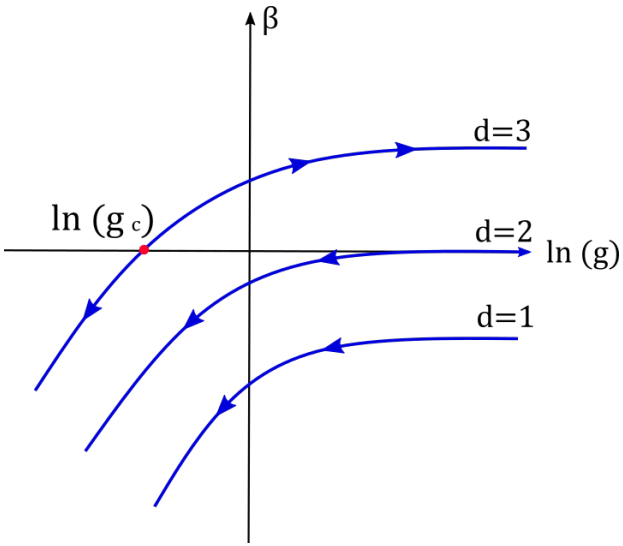

FIGURE 2.2: $\beta(g)$ function of the one parameter scaling hypothesis. In 1-d systems always localize, while in 2-d it depends on the Hamiltonian. In 3-d we find a metal insulator transition

the inverse of the time it takes an electron to reach the boundary of the block and it gives the broadening of the energy levels in the block. When $g < 1$ the states are localized and when $g > 1$ the states are extended. The parameter g is also dependent on the linear size of the block L. If we assume that a state has a localization length l, then $l > L$ implies $g > 1$ on the other hand if $l < L$ then $g < 1$. It was also shown that the parameter $g(L)$ is proportional to the conductance of the block $G(L)$. Abrahams *et al*. hypothesized that the conductance of a system of size bL is a function of $g(L)$ only, that is, $g(bL) = f_b(g(L))$. The previous statement is captured in the scaling function β defined as,

$$\beta(g) \equiv \frac{d \ln g}{d \ln L}. \tag{2.6}$$

The form of the scaling function is obtained by analyzing two limiting cases. When $g \gg 1$, the system behaves as an Ohmic conductor, therefore, $g \sim L^{d-2}$ and $\beta(g) = d - 2$. When $g \ll 1$, the system is in the insulating regime and we have localized states, therefore, $g \sim g_0 e^{-L/\xi}$ and $\beta(g) = \ln(g/g_0)$. The form of the scaling function is obtained by smoothly interpolating between the limiting cases. As we can see in figure (2.2), in 1D there is no metallic behaviour, the system always flows towards smaller values of g. In 2D the scaling function approaches zero for very large values of g. There it becomes

important to consider quantum corrections to the scaling function. The quantum corrections depend on the symmetry class of the Hamiltonian (see section 4.1). In the AI symmetry class the corrections push the scaling function down in a process called weak localization, meaning that all states are localized. In the AII symmetry class (systems with spin-orbit coupling) the corrections push the scaling function up in a complementary process called weak anti-localization, where we encounter a metal-insulator transition. The transition due to weak anti-localization is also realized in class D and DIII. In the chiral classes BDI, AIII and CII, metal-insulator transitions are also found. Unlike class AII, the metal-insulator transition is driven by non-perturbative contributions, i.e, vortex-like excitations [17].

In 3D, there is a critical conductance g^* in which $\beta(g^*) = 0$, representing an unstable fixed point, marking the metal-insulator transition. Close to the transition and on the conducting side the conductivity takes the form,

$$\sigma \sim \frac{g^*}{\ell} \left(\frac{g_0 - g^*}{g_*} \right)^{\nu}, \tag{2.7}$$

where ℓ is the mean free path and g_0 the conductance in the scale of the mean free path. The conductivity vanishes with critical exponent ν. In the insulating side of the transition, and at sufficient long length scales the states are insulating and g adopts the form,

$$g(L) = g_c \, e^{-L/\xi}, \quad \xi \approx \ell \, |(g_0 - g^*)/g^*|^{-\nu}, \tag{2.8}$$

where ξ is the localization length which diverges as we approach the fixed point.

2.3 FIELD THEORY APPROACH TO THE DISORDERED ELECTRON GAS

In this section we give a quick overview of the field theory approach to the disordered electron gas using the replica trick [7]. We first consider perturbation theory approach to the problem where we are able to compute corrections to observables like the conductivity. By considering these corrections we make contact to the previous section and see that for $d \leq 2$ the free electron gas localizes due to disorder and we identify the underlying physical mechanism for Anderson localization. The (not yet replicated) action we are going to consider is the following ,

$$S[\psi, \bar{\psi}] = \int \mathrm{d}^d x \, \bar{\psi}(\mathbf{x}) \left(E + i0^+ \tau_3 - H_0 - V(\mathbf{x}) \right) \psi(\mathbf{x}), \tag{2.9}$$

where $\psi(\mathbf{x}) = \psi^s(\mathbf{x})$ is a space dependent fermionic field with structure in the retarded/advanced space $s = \pm$, H_0 is the free particle Hamiltonian, $V(\mathbf{x})$ is the

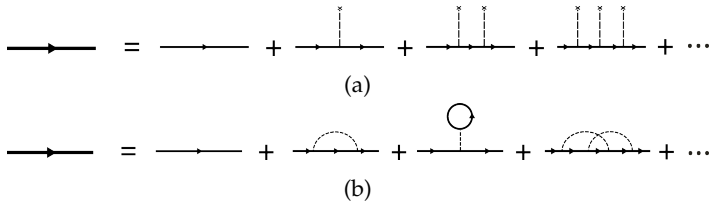

FIGURE 2.3: a) Pictorial representation of the full Green's function without disorder average. b) Pictorial representation of the averaged over disorder Green's function. The bold solid lines represent the full Green's function, the thin solid lines represent the free Green's functions and in a) the cross represent the insertion of the disorder potential $V(\mathbf{x})$.

disorder potential and τ_3 is the 3rd Pauli matrix acting in the retarded/advanced space. The propagator for this problem is written as the sum of the following scattering processes of the free propagator G_0 with the disorder potential V,

$$G(\mathbf{x},\mathbf{x}';E) = G_0(\mathbf{x},\mathbf{x}';E) + \int \mathrm{d}x''\, G_0(\mathbf{x},\mathbf{x}'';E)V(\mathbf{x}'')G(\mathbf{x}'',\mathbf{x}';E). \tag{2.10}$$

Pictorically the full Green's function can be represented as in figure (2.3a). Where the bold line indicates the full Green's function G, the thin line the free one G_0 and the cross the potential $V(\mathbf{x})$. The full Green's functions is therefore depicted as free propagation of the electron followed by scattering events due to the disorder potential. The disorder potential can be chosen to be drawn from an statistical ensemble, we chose such ensemble to be a Gaussian one and additionally we ask for a mean value of $\langle V(x)\rangle_{dis} = 0$ over the ensemble. The second moments of the disorder potentials are described by $\langle V(x)V(x')\rangle_{dis} = \gamma^2 K(x-x')$, where γ^2 is the disorder strength and $K(x-x')$ dictates the spatial correlation of the disorder potential. Now and for the rest of this thesis we are going to consider spatially uncorrelated disorder (white noise), $K(x-x') = \delta(x-x')$.

From the point of view of the disorder potential V as a random variable, we can calculate average of observables with respect to the ensemble of disordered potentials. To date, there are 3 ways of accomplishing this, *i*) The replica trick [18], *ii*) The supersymmetry method [19], *iii*) Keldysh formalism [20]. In this thesis we are going to use the replica trick to calculate of the observables and in general to compute the low energy theories of the systems studied here. A review of the replica trick is presented in appendix A.

Let us compute the averaged-over-disorder Green's function, $\langle G(x,x')\rangle_{dis}$. Intuitively we can think of this as joining the interaction lines in pairs, as depicted in figure (2.3b). In practice upon averaging the (replicated) partition function,

$\mathcal{Z} = \int D(\psi, \bar{\psi}) \exp(-S[\psi, \bar{\psi}])$ over disorder, we obtain a quartic interaction term, where the replicated fields interact with each other,

$$S_{int}[\psi, \bar{\psi}] = -\frac{\gamma^2}{2} \int \mathrm{d}^d x \, \bar{\psi}^a(\mathbf{x}) \psi^a(\mathbf{x}) \bar{\psi}^b(\mathbf{x}) \psi^b(\mathbf{x}), \tag{2.11}$$

where a, b are replica indices. According to the replica trick, to compute the averaged over disorder Green's function we do the following,

$$\langle G_{\mathbf{p},\mathbf{p}'} \rangle_{dis} = \lim_{R \to 0} \frac{1}{R} \sum_{a=1}^{R} \langle \psi^a_{\mathbf{p}} \bar{\psi}^a_{\mathbf{p}} \rangle_{\psi} \delta_{\mathbf{p},\mathbf{p}'}, \tag{2.12}$$

where we have gone to the momentum space and the average over ψ in the right hand side means average over the action with the interacting term. We notice that the averaged Green's function is diagonal in momentum space, this is due to the fact that the spatial dependence of the second moments has translational symmetry. We evaluate the Green's function by considering an expansion in the interacting term (eq. 2.11). To compute the full Green's function we calculate the self-energy operator Σ_p. The starting point is the free Green's function

$$G_{0,\mathbf{p}} \delta^{ab} = \frac{\delta^{ab}}{E + i0^+ \tau_3 - \epsilon(\mathbf{p})}, \tag{2.13}$$

where the indices a, b belong to replica space and $\epsilon(\mathbf{p}) = \mathbf{p}^2/2m$. To first order we need to consider the diagrams shown in figures (2.4a), (2.4b), we notice however that fermion loops vanish in the replica limit as their replica structure is such that,

$$\sum_{a=1}^{R} \sum_{b=1}^{R} \sum_{c=1}^{R} \delta^{ab} \delta^{ba} \delta^{cc} = R^2 \tag{2.14}$$

where the Kronecker deltas come from the Green's function (2.13) . Higher order fermion loops vanish under the same argument. The only first order contribution is then the one shown in figure (2.4a), which reads as,

$$\begin{aligned} \Sigma^{(1)}_{\mathbf{p}} = \gamma^2 \int \mathrm{d}^d p \, G_{0,\mathbf{p}'} &\approx \gamma^2 \int \mathrm{d}\epsilon \frac{\nu(\epsilon)}{E + i0^+ \tau_3 - \epsilon} \\ &\approx \gamma^2 P \int \mathrm{d}\epsilon \frac{\nu(\epsilon)}{E - \epsilon} - i\pi\gamma^2 \nu \tau_3. \end{aligned} \tag{2.15}$$

We only consider $\mathrm{Im}\, \Sigma^{(1)}_{\mathbf{p}} = -i\pi\gamma^2\nu\tau_3$, since the real part can be absorbed in the definition of E. The imaginary part of the self energy operator quantifies the attenuation of the Green's function due to impurity scattering.

Upon going to higher order corrections to the self-energy we encounter crossing diagrams, let us argue why these contributions will be negligible

FIGURE 2.4: Self energy diagrams. a) First order correction to the self energy. b) First order correction to the self energy with a fermion loop. c)Second order correction to the self energy, non crossing diagram. d) Second order correction to the self energy, crossing diagram

with respect to the non-crossing ones. The non-crossing contribution to the self-energy (figure 2.4c) has roughly the structure, $\Sigma^{(2)}_{n.c} \sim \sum_{\mathbf{p_1},\mathbf{p_2}} (G_{\mathbf{p_1}})^2 G_{\mathbf{p_2}}$, while the contribution from the crossing diagrams (figure 2.4d) reads, $\Sigma^{(2)}_{c} \sim \sum_{\mathbf{p_1},\mathbf{p_2}} G_{\mathbf{p_1}} G_{\mathbf{p_2}} G_{\mathbf{p_2}-\mathbf{p_1}+\mathbf{p}}$. The Green's functions are peaked around $|\mathbf{p}| = \sqrt{2mE}$ and due to this fact the crossing diagram has only one free sum, let us say $\mathbf{p_1}$, while the sum over $\mathbf{p}_2$ is highly constrained due to the condition $\mathbf{p_2} - \mathbf{p_1} + \mathbf{p}$ in the third Green's function. The relative weight of the non-crossing diagram to the crossing one is calculated as, $p^{2(d-1)}/(p\ell^{-1})^{d-1}$, where ℓ is the elastic mean free path. In the limit of weak disorder $p\ell \gg 1$ and $d > 1$, the contribution from crossing diagrams is negligible. This fact allows us to evaluate the self-energy under the self-consistent Born approximation (SCBA),

$$\Sigma_{\mathbf{p}} = \gamma^2 \int_{\mathbf{p}'} \mathrm{d}^d p' \, (E - \mathbf{p}'^2/2m - \Sigma_{\mathbf{p}'})^{-1}. \tag{2.16}$$

To solve this self-consistent equation we make the following Ansatz, $\mathrm{Im}\,\Sigma_{\mathbf{p}} = -\frac{1}{2\tau}\tau_3$, such that,

$$-\frac{1}{2\tau}\tau_3 \approx \gamma^2 \,\mathrm{Im} \int \mathrm{d}\epsilon \frac{\nu(\epsilon)}{E - \epsilon + \frac{i}{2\tau}\tau_3} \approx -\gamma^2 \pi \nu \tau_3, \tag{2.17}$$

where the elastic scattering rate is given by, $\tau^{-1} = v_F \ell = 2\gamma^2 \pi \nu$. The averaged over disorder Green's function is momentum space reads,

$$\langle G_{\mathbf{p}} \rangle_{dis} = \frac{1}{E - \frac{\mathbf{p}^2}{2m} - \frac{i}{2\tau}\tau_3}, \tag{2.18}$$

where in real space, after a Fourier transform, it looks like,

$$\langle G(\mathbf{x}, \mathbf{y}; E) \rangle_{dis} = G_0(\mathbf{x}, \mathbf{y}; E) e^{-|\mathbf{x}-\mathbf{y}|/2\ell}. \tag{2.19}$$

Here we see that the Green's function decays on the scale of the mean free path.

Using this formalism we can also calculate the effect of disorder in quantities like the conductivity, where we can elucidate the interference effects due to scattering off impurities. According to the Kubo-Greenwood formula the conductivity tensor is given by,

$$\sigma_{\alpha\beta} = \frac{e^2}{2\pi\omega} \int \frac{\mathrm{d}^d p}{(2\pi)^d} \int \mathrm{d}E \left[n_F(E) - n_F(E+\omega) \right] \left\langle v_\alpha G^A(\mathbf{p}; E) v_\beta G^R(\mathbf{p}; E+\omega) \right\rangle_{dis}, \tag{2.20}$$

where $v_\alpha = p_{F,\alpha}/m$, $p_{F,\alpha}$ is the Fermi momentum in the direction α and $n_F(E)$ is the Fermi-Dirac distribution. Diagramatically it can be described as the bubble diagram shown in figure 2.5a. As a first approximation we take the average in (2.20) to be the product of two averaged Green's functions (2.18), which after integration yields,

$$\sigma_{\alpha\beta} = \frac{e^2 D \nu}{1 - i\omega\tau} \delta_{\alpha\beta} \tag{2.21}$$

the classical Drude formula. We can consider corrections to the Drude formula if we consider the vertex corrections to the bubble diagram. Before doing that we first consider a related quantity to the one appearing in the conductivity (2.20), the density correlator $R(\mathbf{q}, \omega)$,

$$R(\mathbf{q}, \omega) = \left\langle G^A(\mathbf{p}; E) G^R(\mathbf{p}+\mathbf{q}; E+\omega) \right\rangle_{dis}. \tag{2.22}$$

The diagrammatic expression for $R(\mathbf{q}, \omega)$ is again a bubble. Considering the diagrammatic expansion we ignore all kind of crossings and we solve for the vertex Γ shown in figure 2.5d. The equation for the vertex is,

$$\Gamma_{\mathbf{p}_1, \mathbf{p}_2, \mathbf{q}} = \frac{1}{2\pi\nu\tau} + \frac{1}{2\pi\nu\tau} \int \mathrm{d}^d p \, G_{\mathbf{p}+\mathbf{q}} G_{\mathbf{p}} \Gamma_{\mathbf{p}, \mathbf{p}_2, \mathbf{q}}, \tag{2.23}$$

which is solved to give,

$$\Gamma_{\mathbf{q}} = \frac{1}{2\pi\nu\tau} \frac{1}{-i\omega + D\mathbf{q}^2}. \tag{2.24}$$

adding the external Green's functions, the density correlator is,

$$R(\mathbf{q}, \omega) = \frac{2\pi\nu}{-i\omega + D\mathbf{q}^2} \tag{2.25}$$

With these results we could calculate the correction to the conductivity from the ladder diagrams, for this we would need to integrate over energies (times the difference of the Fermi-Dirac distributions), over momenta, add the v_α, v_β and set $\mathbf{q} = 0$. This results in a contribution of zero [12]. We conclude that the quantum contributions do not come from the ladder diagrams.

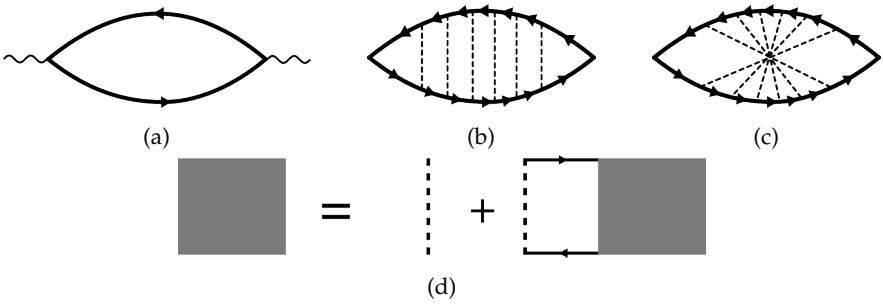

FIGURE 2.5: a) Diagram corresponding to the computation of the conductivity. The solid lines represent the Green's functions while the wavy lines represent $v_{\alpha,\beta}$. b) One of the ladder diagrams contributing to the computation of the density correlator. c) One of the maximally crossed diagrams contributing to the quantum corrections to the conductivity. d) Equation for the diffuson vertex, leading to the ladder diagrams.

There are another class of diagrams which can render corrections to the conductivity and those are the maximally crossed diagrams (see figure 2.5c). The reason to consider to consider the maximally crossed diagram despite of the crossings (which amount to a small contribution) is that so many small contributions from the crossing can make up something that is not negligible and serves as a correction to the classical conductivity.

The maximally crossed diagrams can be obtained from the ladder diagrams previously considered if we reverse the momenta of one of the Green's function $\mathbf{p} \to -\mathbf{p}$, now instead of considering the difference of momenta $\mathbf{q}$, (which is set to zero in the conductivity formula), we consider the sum of the two momenta $\mathbf{Q}$. Using diagrams we look at maximally crossed diagrams with the vertex Γ_C given by,

$$\Gamma_C = \frac{1}{2\pi\nu\tau}\frac{1}{-i\omega + D\mathbf{Q}^2} \tag{2.26}$$

and the quantum correction to the conductivity is [12],

$$\delta\sigma = -D\nu e^2\tau^2 \int \frac{\mathrm{d}^d Q}{(2\pi)^d}\,\Gamma_C \tag{2.27}$$

Integration over the vertex correction taking into account the sample size L, leads to the results,

$$\delta\sigma \sim \begin{cases} -\frac{e^2}{\pi\hbar}\left(L-\ell\right), & d=1 \\ -\frac{e^2}{\pi\hbar}\ln\left(\frac{L}{\ell}\right), & d=2 \\ \frac{e^2}{2\pi\hbar}\left(\frac{1}{L}-\frac{1}{\ell}\right), & d=3 \end{cases} \tag{2.28}$$

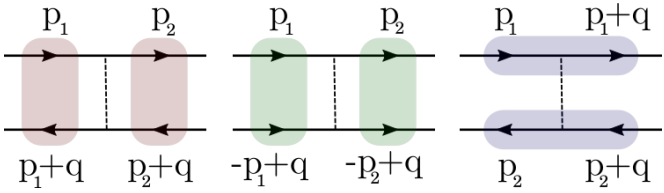

FIGURE 2.6: Exchange, Cooper and direct low momentum decoupling channels.

where in 2-d the quantum correction to the scaling function is,

$$\beta(g) = -\frac{1}{\pi^2 g} \tag{2.29}$$

with g the parameter defined in section 2.2. This equation implies the localization of all states. One can arrive at the same conclusion without using perturbation theory but using a Hubbard Stratonovich decoupling to eventually develop a field theory in terms of the low energy modes of the system [21–24]. From the previous discussions we can easily see that the ladder and the maximally crossed vertex corrections satisfy a diffusion equation and that they can in principle propagate in the system without decaying (unlike the Green's function). We call this contribution the diffuson and the Cooperon respectively and they are identified as the (massless) excitations of the low energy theory.

In the following we obtain an effective low-energy field theory for this massless degrees of freedom starting from the averaged-over-disorder partition function. We consider the quartic term induced by the disorder averaging process (2.11), in momentum space there are three channels in which we can decouple the quartic term. Those are, the exchange, Cooper and direct channel (see figure 2.6). In here, following the previous discussion, we decouple in the exchange and Cooper channels. To avoid having two Hubbard-Stratonovich fields, we perform the following trick. First we consider the action prior to disorder average written in the retarded/advanced sectors $s = \pm$,

$$\begin{aligned} S[\bar{\psi},\psi] &= -\sum_{s=\pm}\int \mathrm{d}^d x\, \bar{\psi}_s \hat{G}_s^{-1}\psi_s = -\frac{1}{2}\sum_{s=\pm}\int \mathrm{d}^d x \left[\bar{\psi}_s \hat{G}_s^{-1}\psi_s + (\bar{\psi}_s \hat{G}_s^{-1}\psi_s)^T\right] \\ &= -\sum_{s=\pm}\frac{1}{2}\int \mathrm{d}^d x \left[\bar{\psi}_s \hat{G}_s^{-1}\psi_s - \psi_s^T \hat{G}_s^{-1}\bar{\psi}_s^T\right] \equiv -\frac{1}{2}\sum_{s=\pm}\int \mathrm{d}^d x \overline{\Psi}_s \hat{G}_s^{-1}\Psi_s, \end{aligned}$$

where we have made the following definitions,

$$\Psi_s \equiv \begin{pmatrix} \psi_s \\ \bar{\psi}_s^T \end{pmatrix}, \ \overline{\Psi}_s \equiv (\bar{\psi}_s, -\psi_s^T),$$

as new fermionic fields acting in the newly introduced time-reversal space, in advanced/retarded space and in replica space. We call it time reversal space since the system belongs to the symmetry class AI where the Hamiltonian (and therefore the Green's function) posseses a time reversal symmetry according to $H = H^T$ (see section 4.1). Under this redefinition, the fields $\bar{\Psi}_s$ and Ψ_s are not independent from each other and they are related by the following transformation,

$$\overline{\Psi}_s = -\Psi_s^T (i\sigma_2^{tr}), \tag{2.30}$$

where σ_i^{tr} are the Pauli matrices acting on the time reversal space. We can further combine the advanced and retarded fields into one field,

$$\Psi \equiv \begin{pmatrix} \Psi_+ \\ \Psi_- \end{pmatrix}, \ \overline{\Psi} \equiv (\overline{\Psi}_+, \overline{\Psi}_-).$$

One may now proceed and take the average over the disorder to obtain the effective action,

$$\begin{aligned} S[\bar{\Psi}, \Psi] = -\frac{1}{2} \int \mathrm{d}^d x \, \overline{\Psi} \left(E + \omega + i0^+ \tau_3 + \frac{\nabla^2}{2m} \right) \Psi \\ + \frac{1}{16\pi\nu\tau} \int \mathrm{d}^d x (\overline{\Psi}\Psi)(\overline{\Psi}\Psi). \end{aligned} \tag{2.31}$$

where we have introduced a source field ω from which we can obtain correlations via derivatives of the partition function and the fields $\Psi = \{\Psi^{a,s,\sigma}\}$ have structure in replica a, advanced/retarded s and time reversal space σ. Let us take a closer look at the contributions from the Cooper and the exchange channels,

$$S_{dis} \approx \frac{1}{16\pi\nu\tau} \int \mathrm{d}^d x \big(\overline{\Psi}^{(1)} \Psi^{(2)} \overline{\Psi}^{(1)} \Psi^{(2)} + \overline{\Psi}^{(1)} \Psi^{(2)} \overline{\Psi}^{(2)} \Psi^{(1)} \big), \tag{2.32}$$

where fields with the same upper index form a slowly varying bilinear (see figure 2.6). Exploiting the symmetry condition (2.30) we find,

$$\overline{\Psi}^{(1)} \Psi^{(2)} = \left(\overline{\Psi}^{(1)} \Psi^{(2)} \right)^T = -\Psi^{(2)T} \overline{\Psi}^{(1)T} = \Psi^{(2)T} (i\sigma_2)(i\sigma_2) \overline{\Psi}^{(1)T} = \overline{\Psi}^{(2)} \Psi^{(1)}, \tag{2.33}$$

and therefore both channels give the same contribution. Effectively, we have only one channel. Rewriting this contribution using components $\alpha \equiv (a, s, \sigma)$, where a is the replica index, $s = \pm$ is the advanced/retarded index and $\sigma = 1, 2$ is the index in the time reversal space

$$S_{dis} = -\frac{1}{8\pi\nu\tau} \int \mathrm{d}^d x \, \Psi^{(1)\beta} \, \overline{\Psi}^{(1)\alpha} \Psi^{(2)\alpha} \, \overline{\Psi}^{(2)\beta}. \tag{2.34}$$

We decouple the interaction by introducing a matrix field $Q = \{Q^{\alpha\beta}(\mathbf{r})\}$ slowly varying in space. The new introduced matrix Q has the same structure as the product $\Psi\overline{\Psi}$ and therefore the following symmetry condition holds,

$$Q = (i\sigma_2^{tr})Q^T(i\sigma_2^{tr})^{-1}, \tag{2.35}$$

where in this notation we have omitted the tensor product of σ_2^{tr} with the identities in the other spaces. Inspired by the similarity in structure between $\Psi\overline{\Psi}$ and Q, we define the following *bar* operation on any matrix A as, $\bar{A} \equiv (i\sigma_2^{tr})A^T(i\sigma_2^{tr})^{-1}$. From the definition, it is clear that $\bar{Q} = Q$. We multiply the action by the unity, $\int DQ \exp\Big(-(\pi\nu/8\tau)\int \mathrm{d}^d x \,\mathrm{tr}\, Q^2\Big)$ and we perform the following shift $Q \to Q + i\Psi^{(1)}\overline{\Psi}^{(1)}/\pi\nu$. This procedure changes the disorder contribution of the action as,

$$e^{-S_{dis}[\Psi,\overline{\Psi}]} = \int DQ \exp\left[-\frac{\pi\nu}{8\tau}\int \mathrm{d}^d x \;\mathrm{tr}\, Q^2 - \frac{i}{4\tau}\int \mathrm{d}^d x\, \overline{\Psi} Q \Psi\right], \tag{2.36}$$

where we have used $\mathrm{tr}\big(Q\Psi\overline{\Psi}\big) = -\overline{\Psi}Q\Psi$ and we have dropped the superscripts. Adding this result to the whole partition function and integrating over Ψ, we obtain,

$$\left\langle \mathcal{Z}^R \right\rangle_{dis} = \int DQ \exp\left[-\frac{\pi\nu}{8\tau}\int \mathrm{d}^d x \,\mathrm{tr}\, Q^2 + \frac{1}{2}\,\mathrm{tr}\ln G^{-1}[Q]\right], \tag{2.37}$$

where $G[Q] \equiv (E + \omega\tau_3 + \nabla^2/2m + iQ/2\tau)^{-1}$. The effective action reads,

$$S[Q] = \frac{\pi\nu}{8\tau}\int d^d x \,\mathrm{tr}\, Q^2 - \frac{1}{2}\,\mathrm{tr}\ln G^{-1}[Q]. \tag{2.38}$$

Varying the action with respect to Q, we obtain the mean field equation,

$$Q = \frac{i}{\pi\nu}\,\mathrm{tr}\, G[Q]. \tag{2.39}$$

A solution of the mean field equation is given by the diagonal Ansatz $Q \equiv \Lambda = \sigma_3^{RA} \otimes \mathbb{I}_2^{tr} \otimes \mathbb{I}_R$. It turns out that this solution is not unique, if T is a transformation such that it is a symmetry of the problem then,

$$Q = T\Lambda T^{-1}, \tag{2.40}$$

is also a solution of the mean field equation (2.38). To find what kind of symmetry is found in this problem, we use the fact that $\bar{Q} = Q$, and that $\overline{Q_1 Q_2} = \bar{Q}_2\bar{Q}_1$ for any matrices Q_1 and Q_2 to obtain,

$$\bar{T}^{-1}\Lambda\bar{T} = T\Lambda T^{-1}.$$

The previous relation implies, $\bar{T} = (i\sigma_2^{tr})T^T(i\sigma_2^{tr})^{-1} = T^{-1}$, which is the defining relation for the unitary symplectic group $\mathrm{Sp}(4R)$. As advertised before, the transformations $\Psi \to T\Psi$ and $\overline{\Psi} \to \bar{T}\overline{\Psi}$ leave the action (2.31) invariant. Nevertheless, the diagonal Ansatz breaks the symmetry. There are however certain set of transformations T from the group $\mathrm{Sp}(4R)$ which commute with Λ leaving the diagonal Ansatz invariant. It is easy to see that the set of transformations that leave Λ invariant belong to the group $\mathrm{Sp}(2R) \times \mathrm{Sp}(2R)$. Based on these observations the theory describing the low energy degrees of freedom takes its values on the coset space $\mathrm{Sp}(4R)/(\mathrm{Sp}(2R) \times \mathrm{Sp}(2R))$, also known as the Goldstone manifold.

A straightforward expansion in gradients of the action (2.38) around the mean field solution yields the non-linear σ model,

$$S[Q] = \frac{\pi\nu}{4} \int \mathrm{d}^d x \, \mathrm{tr}(D\, \partial_i Q \partial_i Q - 2\omega Q\Lambda) \tag{2.41}$$

which is the low-energy model of diffusive dynamics in a disordered environment. This model can be used to derive the same conclusions obtained from the diagramatic perturbation expansion. In particular, a straightforward renormalization group analysis of this action in dimensions $2 + \epsilon$ leads to the β-function (2.29) [21]. This model and modifications of it will be the main theoretical tool to analyze different types of disordered topological insulators throughout this thesis.

2.4 QUANTUM HALL EFFECT

From the previous discussion on localization, it is clear that an electron gas in $2d$ localizes in the presence of arbitrary disorder. However, for certain special systems, we can sidestep the localization argument and find at least one delocalized state in the system. This is achieved by introducing an additional element: a perpendicular magnetic field. This field breaks time-reversal symmetry otherwise attained by a $2d$ electron gas. This scenario corresponds to the physics of the Hall effect. In such a system, we not only find a delocalized state but also discover conducting egde states at the boundaries of the sample. The presence of this delocalized state depends solely on the topological properties of the system and accurately describes the physics of the integer quantum Hall effect (IQHE). To understand this phenomenon better, we first review the physics of the IQHE. We explore the main topological concepts underlying the quantum Hall effect and, finally, examine the interplay between topology and Anderson localization.

The setup of a QHE experiment is shown in figure (2.7). A voltage difference in the x-direction induces a current in the same direction while the Lorentz force induces a difference of voltage in the y-direction. This voltage is called

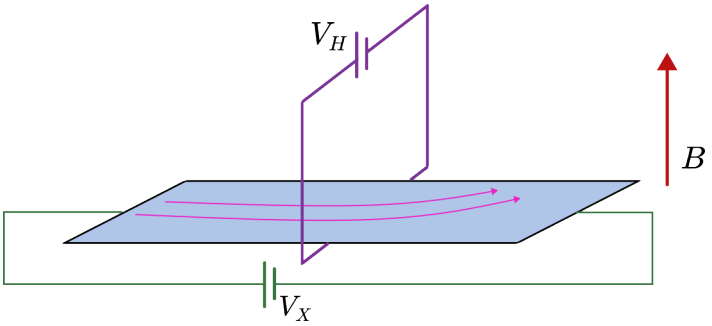

FIGURE 2.7: A $2d$ electron gas subject to a perpendicular magnetic field B and a voltage difference V_x in the longitudinal direction. Under this conditions there is a voltage difference V_H in the transversal direction due to the Lorentz force.

the Hall voltage. Due to the appearance of a new voltage on the y-direction, the conductance σ is best written as a tensor,

$$\sigma = \begin{pmatrix} \sigma_{xx} & \sigma_{xy} \\ -\sigma_{xy} & \sigma_{xx} \end{pmatrix}, \tag{2.42}$$

and the resistivity is just defined as the inverse of the conductivity tensor, $\rho = \sigma^{-1}$. An interesting feature of 2-dimensional samples is that the conductance g and the conductivity σ coincide, i.e, the conductance does not depend on the geometry of the sample.

In 1980, von Klitzing, Dorda and Pepper found experimentally [1, 25] that when the sample is subject to low temperatures and strong magnetic fields the transverse resistance ρ_{xy} displays plateaus with values $h/\nu e^2$ while the longitudinal resistance vanishes everywhere except at the transition between two plateaus (see figure 2.8). To a very high precision, ν is found to be an integer. This interesting effect goes by the name of integer quantum Hall effect. We shall see shortly that the origin of the quantum Hall phenomenon is topological and and its observation depends highly on the presence of disorder on the sample. But first, let us review the physics in the clean case.

We consider a non-interacting electron subject to a magnetic field. The Hamiltonian of the electron reads [1],

$$H = \frac{1}{2m}(\mathbf{p} - \mathbf{A})^2, \tag{2.43}$$

where the vector potential is chosen to be in the symmetric gauge, $\mathbf{A} = (B/2)\epsilon_{ij}x^j$. We define the following quantity $\boldsymbol{\pi} = \mathbf{p} - \mathbf{A}$ such that the Hamil-

1 We have set $\hbar = 1$ and $e = 1$.

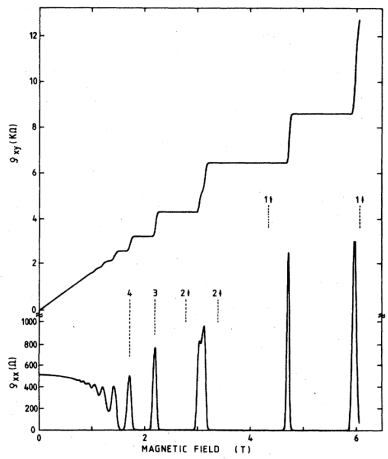

FIGURE 2.8: Experimental curves for the transverse resistance ρ_{xy} (upper part of the figure) and the longitudinal resistance ρ_{xx} (lower part of the figure) for varying magnetic field and fixed density. The transverse resistance is quantized in plateaus, while the longitudinal resistance is zero everywhere except at the transition between plateaus. Taken from [25]

tonian takes a simpler form, $H = \frac{1}{2m}\boldsymbol{\pi}^2$. The new momentum $\boldsymbol{\pi}$ satisfy the following commutation relation,

$$\left[\pi_x, \pi_y\right] = iB. \tag{2.44}$$

Inspired by the harmonic oscillator, we introduce the following ladder operators,

$$\begin{aligned} a &= \frac{1}{\sqrt{2B}}(\pi_y - i\pi_x), \\ a^\dagger &= \frac{1}{\sqrt{2B}}(\pi_y + i\pi_x), \end{aligned} \tag{2.45}$$

satisfying $\left[a, a^\dagger\right] = 1$. In terms of the ladder operators the Hamiltonian takes the form,

$$H = \omega_B(a^\dagger a + \frac{1}{2}), \tag{2.46}$$

where $\omega_B = B/m$ is the cyclotron frequency. The Hilbert space is constructed in the same way as in the harmonic oscillator. We define our ground state $|0\rangle$ as $a|0\rangle = 0$. The rest of the states are obtained by acting with the operator $a^\dagger$. The state $|n\rangle$ has energy $E_n = \omega_B(n + 1/2)$, where n is a positive integer. All energy levels are equally spaced and the separation between levels increases

linearly with the magnitude of the magnetic field applied. These energy levels are called Landau levels and each level hosts not one but many states, in fact the degeneracy of each level is quite large. To study the large degeneracy of the Landau levels, we introduce a new type of *momentum*, $\tilde{\boldsymbol{\pi}} = \mathbf{p} + \mathbf{A}$. It fulfills the commutation relation,

$$\left[\tilde{\pi}_x, \tilde{\pi}_y\right] = -iB \tag{2.47}$$

And in the symmetric gauge it satisfies,

$$\left[\pi_x, \tilde{\pi}_y\right] = 0. \tag{2.48}$$

By analogy with the previous construction we introduce a new set of ladder operators,

$$\begin{aligned} b &= \frac{1}{\sqrt{2B}}(\tilde{\pi}_y + i\tilde{\pi}_x), \\ b^\dagger &= \frac{1}{\sqrt{2B}}(\tilde{\pi}_y - i\tilde{\pi}_x), \end{aligned} \tag{2.49}$$

where they, too, satisfy $[b, b^\dagger] = 1$. We define the ground state as the state annihilated by both b and a: $a\,|0,0\rangle = b\,|0,0\rangle = 0$. The rest of the states are constructed by acting with $a^\dagger$ and $b^\dagger$ on the ground state. It is worth noting that the energy of a general state $|n, m\rangle$, does not depend on the quantum number m. This quantum number m is the one accounting for the huge degeneracy. We can find the wavefunctions in the lowest Landau level (LLL), i.e, we want to find the wavefunction corresponding to the state $|0, m\rangle$ by converting both sets of ladder operators into their differential form. Using complex coordinates $z, \bar{z}$ we obtain,

$$\begin{aligned} a &= -\sqrt{2}\left(\ell_B\bar{\partial} + \frac{1}{4\ell_B}z\right) \ , \ a^\dagger = \sqrt{2}\left(\ell_B\partial - \frac{1}{4\ell_B}\bar{z}\right), \\ b &= \sqrt{2}\left(\ell_B\partial + \frac{1}{4\ell_B}\bar{z}\right) \ , \ b^\dagger = -\sqrt{2}\left(\ell_B\bar{\partial} - \frac{1}{4\ell_B}z\right) \end{aligned} \tag{2.50}$$

where $\ell_B = 1/\sqrt{B}$ is the magnetic length. We first find the LLL when $m = 0$, and using $b^\dagger$ we construct the rest of the states in the LLL. The LLL has the following form,

$$\psi_{LLL,m} \sim \left(\frac{z}{\ell_B}\right)^m e^{-\frac{|z|^2}{4\ell_B^2}} \tag{2.51}$$

To see the degeneracy of the LLL, we notice that the previous equation is peaked around the radius $r = \sqrt{2m}\ell_B$. In a disk shaped region with area $A = \pi R^2$, the number N of possible states is,

$$N = \frac{R^2}{2\ell_B^2} = \frac{AB}{2\pi},$$

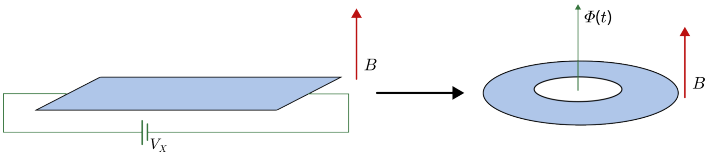

FIGURE 2.9: Hall bar continuously deformed to an annulus. The voltage difference V_x is replaced by an e.m.f generated by a time dependent flux threading the annulus.

which indicates the large degeneracy of the Landau levels. We can also define the flux quantum as, $\Phi_0 = 2\pi$ [2], and the degeneracy is also interpreted as the total flux $\Phi = AB$ in units of the flux quantum, $N = \frac{\Phi}{\Phi_0}$.

To study the topological aspects underlying the integer quantum Hall effect, we begin with a Hall bar and continuously deform it into an annulus, as illustrated in figure (2.9). The external voltage is replaced by the electromotive force generated by a weakly time-dependent flux threading the annulus [2]. According to the results of Byers and Yang [26], and Bloch [27], the observables of this system depend on the flux through the annulus, exhibiting periodicity with a period of Φ_0, the flux quantum. This implies that, when an integer number of flux quanta $\phi = n\Phi_0$ is inserted, the system's Hamiltonian is gauge equivalent to the Hamiltonian without flux.

As the flux gradually increases from $\phi = 0$ to $\phi = \Phi_0$, both the system's spectrum and the eigenstates evolve. However, at $\phi = \Phi_0$, the spectrum appears identical to that at $\phi = 0$, although the states themselves differ. For instance, if the system starts in the state $|n\rangle$, after the insertion of a flux quantum, it ends up in the state $|n+1\rangle$. This phenomenon is known as spectral flow.

Let us consider, without loss of generality, a situation where the Fermi level E_F is positioned between the first and second Landau levels. The edges of the annulus create a confining potential, resulting in chiral edge states propagating along both the inner and outer rings. Upon the slow insertion of a full flux quantum, these states shift from their initial positions: the edge state at the inner ring rises above the Fermi level, while the one at the outer ring drops below it, causing all the intermediate states to adjust accordingly. To regain equilibrium, the system needs to transfer one electron from the inner ring to the outer ring.

In the presence of disorder[3] in the bulk, the states are expected to be localized, making it seemingly impossible to transfer an electron from one edge to the other. To address this issue, Halperin [28] proposed that, despite the disorder,

2 Recovering the constant $\hbar$ and e the flux quantum is $\Phi_0 = \frac{2\pi\hbar}{e}$

3 The strength of the disorder should be smaller than the separation between levels, i.e., $\omega_B\tau \gg 1$, where τ is the scattering time.

there must be at least one delocalized state in the bulk. This delocalized state establishes a connection between the edges and facilitates the transfer of electrons from the inner edge to the outer edge. The edge modes, which propagate along the inner and outer rings, remain unaffected by the disorder due to their chiral nature; since there is no mechanism for back-scattering, hence they do not localize. Similarly, the delocalized state in the bulk is also chiral, making it resilient to disorder.

The presence of disorder in the sample is actually necessary to observe the plateaus in the experimental data of the quantum Hall effect and it is indeed curious that such universal effect is obtained because of random disorder in the sample. Let us imagine for a moment that the sample is clean, i.e, the system is translationally invariant and therefore no preferred frame of reference exists. We can go for example to a frame which moves with velocity $-\mathbf{v}$ (in the $x-y$ plane) relative to the lab frame. In this frame the electrons appear to be moving with velocity $+\mathbf{v}$ and carrying current density $\mathbf{j} = -ne\mathbf{v}$, where n is the surface density. The $\mathbf{E}$ and $\mathbf{B}$ fields in the lab frame are,

$$\mathbf{E} = 0, \quad \mathbf{B} = B\hat{\mathbf{z}}. \tag{2.52}$$

while in the moving frame they take the form,

$$\mathbf{E} = -\frac{1}{c}\mathbf{v} \times \mathbf{B}, \quad \mathbf{B} = B\hat{\mathbf{z}} \tag{2.53}$$

and using the expression for the current $\mathbf{j}$, the electric field can be written as $\mathbf{E} = \frac{1}{nec}\mathbf{j} \times \mathbf{B}$. Noticing that $\mathbf{B}$ points in the z direction we can write it in components as,

$$\mathbf{E}_\alpha = \frac{B}{nec}\epsilon_{\alpha\beta}\,\mathbf{j}_\beta, \tag{2.54}$$

where we define the resistivity tensor as,

$$\rho \equiv \frac{B}{nec}\epsilon_{\alpha\beta} = \frac{B}{nec}\begin{pmatrix} 0 & 1 \\ -1 & 0 \end{pmatrix}, \tag{2.55}$$

this matrix is easily inverted and from the off-diagonal elements we read the Hall conductivity $\sigma_{xy} = nec/B$. We note that ρ_{xy} is a linear function of the magnetic field where the slope only tells us about the density. We cannot account for the plateaus observed in the experimental data. Once we add disorder translation invariance is broken and a frame of reference is chosen, thus the argument presented before fails and we observe the quantum Hall plateaus.

If the the Fermi level E_F is placed between the ν and $\nu+1$ Landau levels, when we insert a flux quantum, ν electrons are transported from the inner edge to the outer edge. Let us suppose that this process takes time t, the current is $I = \nu/t$ and the voltage $\dot{\phi} = 2\pi/t$, the Hall conductance is then, $\sigma_{xy} = \nu/2\pi$ [4].

4 or $\sigma_{xy} = \nu e^2/h$ in physical units.

Later, it was realized by Thouless, Kohmoto, Nightingale, and den Nijs [3] that the Hall conductance is a topological invariant, the first Chern class of the $\mathrm{U}(1)$ principal bundle over the torus $\mathbb{T}^2$. In practice it is better to consider the Chern number c_1, the integral over $\mathbb{T}^2$ of the Chern class,

$$c_1 = -\frac{1}{2\pi}\int_{T^2}\mathcal{F}, \tag{2.56}$$

where the 2-form $\mathcal{F}$ is the Berry curvature. We will describe in more detail the Berry curvature and its relation to topological invariants in the next chapter. From this simple but powerful example we have seen that topology helps $2d$ systems to avoid Anderson localization at the center of the Landau band at arbitrary disorder, while at the same time we discover that it is disorder and Anderson localization of states not in the center of the Landau band combined with the phenomenon of spectral flow the responsible for the observation of the integer quantum Hall effect.

2.4.1 *Field theory of the quantum Hall effect*

In section (2.2), we discussed how the scaling theory of localization predicts localization for a 2D electron gas. In this section, we explore how the scaling theory of localization is modified when a magnetic field is introduced. Instead of focusing solely on the scaling of the longitudinal conductance $\sigma_{xx} \equiv g$, we also consider the scaling of the transverse conductivity σ_{xy}. By examining the scaling behavior of this new parameter, we uncover the unique properties of the quantum Hall effect.

The field theory for this theory can be constructed using the replica formalism, there are a couple of differences with respect to the previous construction. First of all, due to the presence of a magnetic field time reversal invariance is lost. The (replicated) action with impurity potential $V(\mathbf{x})$ is,

$$S[\bar{\psi},\psi] = \int \mathrm{d}^2x\, \bar{\psi}^{a,s}\left(E + i0^+\tau_3 - \boldsymbol{\pi}^2 - V(\mathbf{x})\right)\psi^{a,s} \tag{2.57}$$

where $\boldsymbol{\pi} = \mathbf{p} - \mathbf{A}$ and $\psi^{a,s}$ is a fermionic field with indices in replica space (a) and in retarded/advanced space s. The action is invariant under the group of unitary transformations $\mathrm{U}(2R)$ acting on the fields $\bar{\psi}$ and ψ. When averaged over (white noise) disorder, the action acquires a quartic interacting term as in the previous section. To decouple the quartic term a Hubbard-Stratonovich field P should be added. This field is likewise invariant under the action of $\mathrm{U}(2R)$. The resulting action in terms of only the fields P looks like,

$$S[A] = \int \mathrm{d}^2x\, \mathrm{tr}\, P^2 - \mathrm{tr}\log\left(E + i0^+\tau_3 - \boldsymbol{\pi}^2 - iP\right). \tag{2.58}$$

A saddle point analysis of the previous action, reveals that the mean-field configuration $\bar{P}$ breaks the symmetry of the action down to $\mathrm{U}(2R)/(\mathrm{U}(R) \times \mathrm{U}(R))$. This is the manifold in which the massless excitations around the saddle point $\bar{P}$ live, we therefore expect that the low-energy theory has the shape of a non-linear σ model. Interestingly due to the topological properties of the manifold $\mathcal{M} = \mathrm{U}(2R)/(\mathrm{U}(R) \times \mathrm{U}(R))$, in particular due to the non-triviality of its second homotopy group[5],

$$\pi_2(\mathcal{M}) = \mathbb{Z} \tag{2.59}$$

an extra topological term, which counts the windings of $\mathcal{M}$ around the sphere S^2, could be present in the low-energy theory. An expansion in gradients of the mean field action results in the following low energy action first derived by Pruisken [8, 9],

$$S[Q] = \frac{\sigma_{xx}}{8} \int \mathrm{d}^2x \ \mathrm{tr}\left(\partial_i Q \partial_i Q\right) + \frac{\sigma_{xy}}{8} \int \mathrm{d}^2x \, \epsilon_{ij} \, \mathrm{tr}\left(Q \partial_i Q \partial_j Q\right) \tag{2.60}$$

where the first term is the usual diffusive term and the second term is the topological term counting the windings around S^2. The coefficients of the action are σ_{xx} and σ_{xy} and they are the longitudinal and transverse conductivities in the scale of the mean free path ℓ. In particular $\sigma_{xy} = \sigma_{xy,\mathrm{I}} + \sigma_{xy,\mathrm{II}}$ is found as the sum of two terms called the Streda-Smrcka coefficients [30]. The second coefficient is interesting in the sense that is the non-classical contribution to the transverse conductivity,

$$\sigma_{xy,\mathrm{II}}(B) = \int_{-\infty}^{E} \mathrm{d}E \, \frac{\partial}{\partial B} \nu(E), \tag{2.61}$$

since it considers the contribution from all states below the Fermi energy, and moreover it probes the sensitivity of the density of states $\nu(E)$ to changes in the magnetic field.

Armed with a field theory for the quantum Hall effect we would like to explore its fate upon going to larger and larger system sizes. The scaling theory of localization in $2d$ predicts the coefficient σ_{xx} to vanish upon going to larger system sizes, but the scaling theory of localization cannot answer for σ_{xy}. Pruisken, Khmelnitskii and collaborators [8, 31] conceptualized and derived the diagram 2.10 for the two coefficients of the theory. Whenever the bare value of σ_{xy} is not a half-integer, the theory flows to the fixed points $(\sigma^*_{xx}, \sigma^*_{xy}) = (0, n)$, where n is the closest integer to the bare value σ_{xy}. When σ_{xy} is a half-integer the theory flows to the unstable fixed point $(\sigma^*_{xx}, \sigma^*_{xy}) = (g^*, n + 1/2)$, where n is again an integer. The former fixed point correspond to the plateaus and

5 Recall that the second homotopy group $\pi_2(\mathcal{M})$ of a manifold $\mathcal{M}$ is the group of equivalence classes that classify all the maps $f : S^2 \to \mathcal{M}$ [29].

the latter to the plateau transition where the longitudinal conductance attains a finite values of the order of 1.

The non-linear σ model describes accurately the physics of the quantum Hall effect, in particular, it captures the quantization of the transversal conductance and the vanishing of the longitudinal conductance in the plateaus. The non-linear σ model description breaks down at the plateau transition and another theory is needed to describe accurately the critical behavior of the theory. To date there are proposals of the theory having the shape of a conformal field theory [32, 33] but there is no full agreement among the scientific community.

2.5 MULTIFRACTALITY

At a critical point, due to the divergence of the localization length ξ, we observe strong fluctuations at all length scales. One way to analyze and characterize the critical point is through multifractal analysis. Multifractal structures, where they exist, are characterized by an infinite set of critical exponents that describe the scaling of the moments of some distribution [34–36]. In this context, we examine the square of the wavefunction $|\psi(x)|^2$ and its moments,

$$P_q = \int \mathrm{d}^d x \, |\psi(\mathbf{x})|^{2q}, \tag{2.62}$$

known as the inverse participation ratios (IPRs). At criticality, the IPRs exhibit anomalous scaling with the system size N as follows,

$$\langle P_q \rangle \sim N^{\tau_q}, \tag{2.63}$$

where τ_q represents a continuous set of exponents. These exponents are defined as $\tau_q = D_q(q-1)$, where $D_q = 0$ in an insulator and $D_q = d$ in a metal [34]. At criticality, however, the exponent is a non-trivial function of q, which can be expressed as the sum of a normal part plus an anomalous part, $\tau_q = d(q-1) + \Delta_q$.

Let us consider the case of weak multifractality, which means the critical point is close to a metal. This is particularly applicable for the Anderson model in dimension $2+\epsilon$, with $\epsilon \ll 1$. For weak multifractality, the anomalous part of the exponent is approximately parabolic,

$$\Delta_q = \gamma q(q-1), \tag{2.64}$$

where $\gamma \ll 1$. In the case of the quantum Hall effect, it has been observed that the multifractal spectrum is parabolic with $\gamma = 0.25$ [37].

Multifractal analysis is thus a powerful tool to probe the metallicity or insulating character of states in a sample via the analysis of the IPRs. Moreover, it is a robust method to analyze systems at criticality. Depending on the form of the

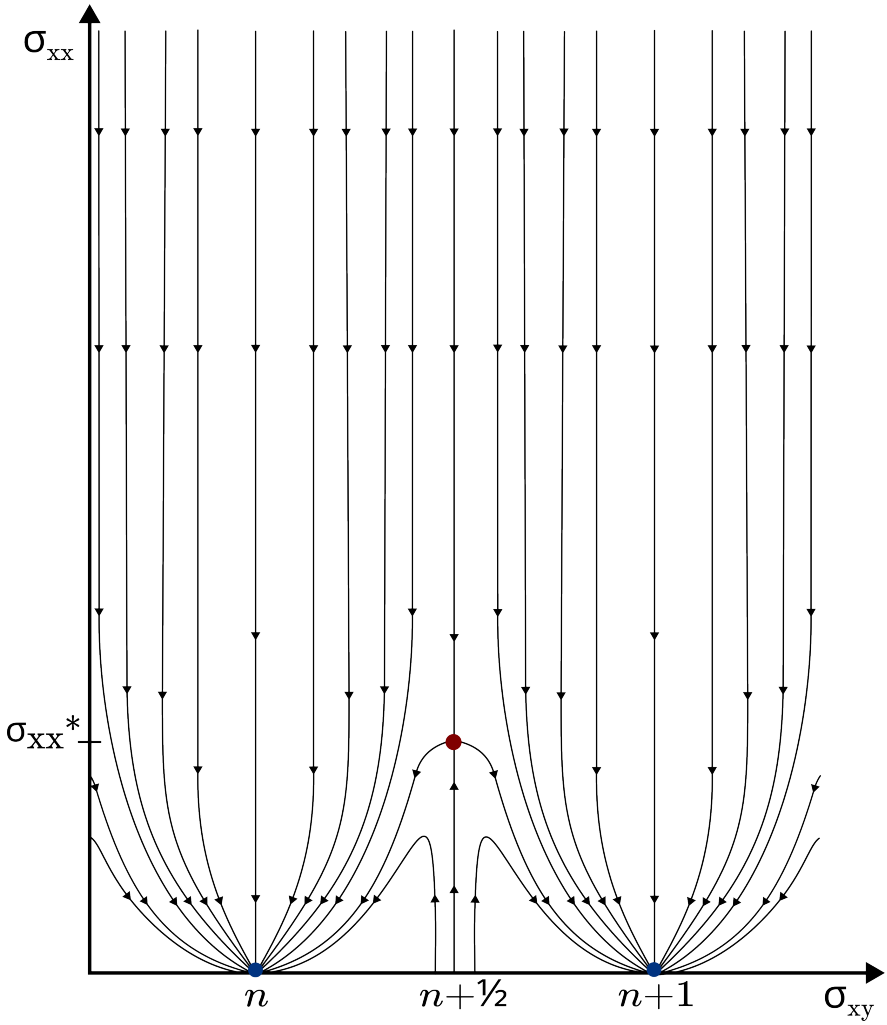

FIGURE 2.10: Two parameter phase diagram for the quantum Hall effect. This diagram predicts that for values of $\sigma_{xy} \notin \mathbb{Z} + \frac{1}{2}$ the theory flows towards an insulating phase $\sigma_{xx} = 0$ with $\sigma_{xy} \in \mathbb{Z}$ quantized. On the other hand for half integer values of σ_{xy} the theory flows towards a fixed point with non-vanishing longitudinal conductance σ^*_{xx} describing the plateau transition.

anomalous part of the multifractal spectrum, multifractal analysis can distinguish between different critical systems and categorize them into universality classes.

2.6 SUMMARY

In this chapter, we have discussed various phenomena associated with the presence of disorder in electron systems. We have seen that disorder can localize electrons through a process known as Anderson localization. In one-dimensional ($1d$) systems, electrons always localize regardless of the strength of the disorder. In two-dimensional ($2d$) systems, localization depends on the symmetry class of their Hamiltonian, while in three-dimensional ($3d$) systems, some states will localize while others remain metallic. Within a band, states near the band edge localize more easily. The point in the band that separates localized from delocalized states is called the mobility edge, where we observe a metal-insulator transition.

In a $2d$ electron gas subject to a perpendicular magnetic field, a transverse conductivity appears when a voltage difference is applied across the sample, a phenomenon known as the Hall effect. At low temperatures, this conductance is quantized in integer steps, known as the integer quantum Hall effect. Interestingly, the presence of disorder is crucial for observing the quantization plateaus. This might seem paradoxical because, according to the one-parameter scaling hypothesis, all states should localize in 2D. The resolution lies in hypothesizing that at least one state remains delocalized in the center of the Landau bands and that the scaling is described by the scaling of $(\sigma_{xx}, \sigma_{xy})$. From a field-theoretical perspective, averaging over disorder potentials and using the replica trick reveals that the quantum Hall effect is described by a non-linear σ-model with an additional topological θ term.

In the rest of this thesis, we will study the effect of disorder on specific types of topological insulators and their boundary states. We utilize our understanding of localization (and delocalization) and the tools of field theory for disordered systems to investigate their properties.

3

CHERN INSULATORS AND DISORDER

The quantum Hall insulator discussed in the previous chapter is a quintessential example of a topological insulator in two dimensions. We observed that its defining feature is the induction of a transversal current, the Hall current, by an external magnetic field, resulting in quantized Hall conductance. In contrast, models of quantum Hall insulators that do not require an external magnetic field are known as *anomalous quantum Hall insulators* (AQH) [4]. These systems lack certain symmetries and are classified as class A in the Altland-Zirnbauer scheme. A key aspect of the integer quantum Hall effect (IQHE), as discussed earlier, is the crucial role of disorder in the quantization of Hall conductance. Unlike the IQHE, where Landau levels are present, the AQH insulator features electronic bands defined in the Brillouin zone, allowing for the definition of topological invariants. Introducing disorder in this system transforms the topological band insulator into a topological Anderson insulator [38, 39], where a mobility gap replaces the spectral gap. According to Laughlin's argument, even in the presence of disorder, some states remain delocalized, similar to the delocalized states at the center of the Landau bands in the quantum Hall insulator.

We investigate the physics of AQH insulators by examining the Chern insulator, a fundamental example. Initially, we provide a detailed description of its properties in the clean case. Subsequently, we investigate the disordered Chern insulator, focusing on how the position of the delocalized state varies with the disorder strength, denoted as W, and the parameter r, which governs the topological phase in its clean form. Our analysis involves deriving a non-linear σ model to serve as a low-energy field theory based on a microscopic theory of the Chern insulator.

3.1 BERRY PHASE

The concept of Berry phase [40] is a key ingredient in the study of topological insulators. For us, it helps us classify the different topological phases in the Chern insulator and also makes contact with physical observables (the quantized quantum Hall conductance σ_{xy}). To obtain the Berry phase we consider a system described by the Hamiltonian H that depends on some parameters $A = (a_1, a_2, \ldots, a_n)$ that will be changing adiabatically. We consider the evolution of the system along the path $\mathcal{C}$ in parameter space and introduce an

instantaneous orthonormal basis of the instantaneous eigenstates $|n(A)\rangle$ of $H(A)$, which is obtained by solving the equation, $H(A)\,|n(A)\rangle = E_n\,|n(A)\rangle$ along each point of the path A. The idea is to see what happens to an initial state $|n(A(0)\rangle$ as we vary the external parameters. As we are varying the parameters, in an adiabatic fashion, after a time t we end up in the instantaneous state of $H(A)$ times a phase α,

$$|\phi(t)\rangle = \exp(-i\alpha(t))\,|n(A(t)\rangle\,. \tag{3.1}$$

We consider the Schrödinger equation projected in the instantaneous eigenstate $|n(A)\rangle$, $\langle n(A)|\,i\partial_t\,|\phi(t)\rangle = \langle n(A)|\,H(A)\,|\phi(t)\rangle$ and using the orthonormality of the instantaneous basis $\langle n(A)|n(A)\rangle = 1$ we arrive at a first order differential equation for $\alpha(t)$ which has the solution,

$$\alpha(t) = \frac{1}{\hbar}\int_0^t E_n(A(t'))\mathrm{d}t' - i\int_0^t \langle n(A(t'))|\,\frac{\mathrm{d}}{\mathrm{d}t'}\,|n(A(t'))\rangle\,\mathrm{d}t'. \tag{3.2}$$

The first term of $\alpha(t)$ is the so-called *dynamical phase* and is related to the time evolution of the state. The second part is the *Berry phase* that accounts for the difference of the instantaneous basis between two points t and $t + \mathrm{d}t$ along the path $\mathcal{C}$. This is the phase that would be of interest to us,

$$\gamma_n = i\int_{\mathcal{C}} \langle n(A)|\,\mathrm{d}\,|n(A)\rangle\,. \tag{3.3}$$

The fact that the integrand measures the change of the instantaneous basis should be reminiscent of the concept of connections in differential geometry, and for that reason we define the quantity $\mathcal{A}_n = i\,\langle n(A)|\,\mathrm{d}\,|n(A)\rangle$ as the Berry connection which is the connection of the principal $U(1)$–bundle $P(U(1), \mathcal{M})$ [29], where $\mathcal{M}$ is the parameter space, with local coordinates $A = (a_1, a_2, \ldots, a_n)$.

We can perform a gauge transformation on the state $|n(A)\rangle \to \exp(i\xi(A))\,|n(A)\rangle$, which is translated into a gauge transformation in the Berry connection $\mathcal{A}_n \to \mathcal{A}_n - \mathrm{d}\xi$. Upon computing the phase we find that it gets shifted by a factor of $\xi(A(0)) - \xi(A(T))$, where T is the final time. One could argue that with a clever choice of gauge the Berry phase could be cancelled. This is in general not true. Let us take the case, for example, of closed loops in parameter space. This implies that $A(T) = A(0)$ and the factor coming from the gauge transformation gets cancelled, leaving a general non-zero Berrry phase γ_n.
For closed loops we can use Stoke's theorem in 3.3,

$$\gamma_n = i\oint_C \langle n(A)|\mathrm{d}\,n(A)\rangle = i\int_S \langle \mathrm{d}\,n(A)|\mathrm{d}\,n(A)\rangle = \int_S \mathcal{B}_n \tag{3.4}$$

where $\mathcal{B}_n$ is the Berry curvature and S is chosen such that its boundary is C.

In the case of the integer quantum Hall effect there is a particular link between the Berry phase and the value of the Hall conductivity σ_{xy}. This link reveals a deep connection between topology and the observables on a physical system.

Let us take the IQHE system and the annular geometry that we consider before in section (2.4). We are going to thread two fluxes, one in the x–direction ϕ_x and another one in the y–direction ϕ_y. The gauge potentials (in the Landau gauge) get changed to,

$$A_x = \frac{\phi_x}{L_x}, \quad A_y = \frac{\phi_y}{L_y} + Bx. \tag{3.5}$$

Accordingly the Hamiltonian gets the extra term,

$$\Delta H = -J_x \frac{\phi_x}{L_x} - J_y \frac{\phi_y}{L_y}.$$

Let us take the ground state of the unperturbed quantum Hall Hamiltonian $|\psi_0\rangle$. At first order in perturbation theory we obtain the correction for the ground state as,

$$|\psi_0'\rangle = |\psi_0\rangle + \sum_{n\neq\psi_0} \frac{\langle n|\,\Delta H\,|\psi_0\rangle}{E_n - E_0}\,|n\rangle\,, \tag{3.6}$$

and upon an adiabatic change of the flux we obtain that the new ground state changes as,

$$\left|\frac{\partial\psi_0'}{\partial\phi_i}\right\rangle = -\frac{1}{L_i}\sum_{n\neq\psi_0} \frac{\langle n|\,J_i\,|\psi_0\rangle}{E_n - E_0}\,|n\rangle\,. \tag{3.7}$$

With this expression it is possible to rewrite the Kubo formula for σ_{xy} in terms of the change of the ground state to external parameters, and then average over all possible values of the flux, to obtain,

$$\sigma_{xy} = i\int_{\mathbb{T}^2} \mathrm{d}\phi_x \mathrm{d}\phi_y \left(\left\langle \frac{\partial\psi_0'}{\partial\phi_y}\middle|\frac{\partial\psi_0'}{\partial\phi_x}\right\rangle - \left\langle \frac{\partial\psi_0'}{\partial\phi_x}\middle|\frac{\partial\psi_0'}{\partial\phi_y}\right\rangle\right). \tag{3.8}$$

On the other hand, since we have an adiabatic change of external parameters, the Berry curvature in terms of the angular coordinates $\theta_i = 2\pi\frac{\phi_i}{\phi_0}$ (with ϕ_0 equal to the flux quantum) is,

$$\mathcal{B}_{xy} = i\left(\left\langle \frac{\partial\psi_0'}{\partial\theta_y}\middle|\frac{\partial\psi_0'}{\partial\theta_x}\right\rangle - \left\langle \frac{\partial\psi_0'}{\partial\theta_x}\middle|\frac{\partial\psi_0'}{\partial\theta_y}\right\rangle\right), \tag{3.9}$$

and therefore the Berry phase is,

$$\gamma_0 = \int_{\mathbb{T}^2} \mathrm{d}\theta_x \mathrm{d}\theta_y\, \mathcal{B}_{xy}, \tag{3.10}$$

where $\mathbb{T}^2 = S^1 \times S^1$ is the 2-torus defined by the external parameters. It is well known that this integral is equal to $\gamma_0 = 2\pi\,\mathrm{Ch}$, where Ch is the first Chern number and takes only integer values. Upon averaging over all fluxes we find that the Hall conductance is equal to,

$$\sigma_{xy} = \frac{e^2}{h}\,\mathrm{Ch}, \tag{3.11}$$

a quantity that (as we have seen before) has a topological origin and is quantized.

3.2 CHERN INSULATORS

We can extend naturally all the concepts from the previous section to $2d$ translational invariant systems. In these systems we have a Brillouin zone corresponding to $\mathbb{T}^2$ and energy bands, on each of the bands we have states labeled by the momentum $|u_k\rangle$. Let us suppose there are gaps between the bands, and that our Fermi energy is located in one of gaps (insulator). We can define a Berry connection for such states on each band,

$$\mathcal{A}_k = i\,\langle u_k|\mathrm{d}u_k\rangle\,. \tag{3.12}$$

From here we can compute the curvature associated with this connection $\mathcal{B}_k = \mathrm{d}\mathcal{A}_k$. Additionally, we can compute the Berry phase γ around a closed loop as the integral of the connection around the Brillouin zone,

$$\gamma = \int_{\mathbb{T}^2} \mathcal{B}_k = 2\pi\,\mathrm{Ch}, \tag{3.13}$$

where in the last equation we have used the definition of the first Chern number $\mathrm{Ch} \in \mathbb{Z}$. This kind of topological invariants are known by the name of TKNN invariants [3]. We see clearly that we can associate an integer number to each band. Let us suppose we have n filled bands labeled by l, the Hall conductivity of the system is then,

$$\sigma_{xy} = \frac{e^2}{h}\sum_{l=1}^{n}\mathrm{Ch}_l, \tag{3.14}$$

where Ch_l is the Chern number of the l-th band. We have managed to define an intrinsic Hall conductivity for a translational invariant $2d$ system without the necessity of any external magnetic field (or any external parameter). This effect is dubbed the *anomalous quantum Hall effect*. Let us consider the example of two band insulators, the easiest example where we see a non-vanishing Hall conductance. In momentum space the Hamiltonian takes the form,

$$H_0(k) = h_1(\mathbf{k})\sigma_1 + h_2(\mathbf{k})\sigma_2 + h_3(\mathbf{k})\sigma_3 \tag{3.15}$$

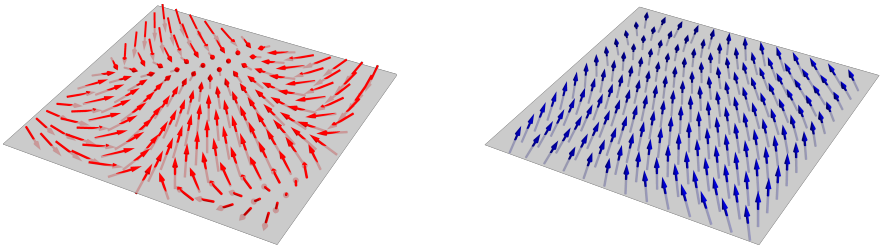

(a) (b)

FIGURE 3.1: a) Vector field $\hat{n}(k)$ corresponding to model 3.19 in the topological phase. Upon going around the Brillouin zone the vector winds one time around the sphere S^2. b) Vector field $\hat{n}(k)$ corresponding to model 3.19 in the trivial phase. There are no windings around S^2.

where the energy of the two bands is $E_{\pm}(\mathbf{k}) = \pm\sqrt{h_1^2 + h_2^2 + h_3^2} = \pm E(\mathbf{k})$. We have an insulator as long as $E(\mathbf{k}) \neq 0$ for all $\mathbf{k}$. We can compute then the Chern number of the lower band. We represent the lower (valence) band by $|-\rangle$, and therefore,

$$\begin{aligned} H(\mathbf{k})\,|-\rangle &= -E(\mathbf{k})\,|-\rangle\,, \\ \hat{n}(\mathbf{k})\cdot\sigma\,|-\rangle &= -\,|-\rangle\,, \end{aligned} \tag{3.16}$$

where $\hat{n}(\mathbf{k}) = \frac{H(\mathbf{k})}{E(\mathbf{k})}$ is an unit vector living in the sphere S^2. This unit vector represents a mapping from the Brillouin zone $\mathbb{T}^2$ to the sphere S^2 and therefore the Berry curvature in terms of this vector is given by [41],

$$\mathcal{B} = \frac{\epsilon_{ij}}{2}\,\hat{n}\cdot\left(\partial_i\hat{n}\times\partial_j\hat{n}\right)\mathrm{d}k_x\mathrm{d}k_y \tag{3.17}$$

The Hall conductivity is therefore,

$$\sigma_{xy} = \frac{e^2}{4\pi h}\int_{\mathbb{T}^2}\epsilon_{ij}\,\hat{n}\cdot\left(\partial_i\hat{n}\times\partial_j\hat{n}\right)\mathrm{d}k_x\mathrm{d}k_y = \frac{e^2}{h}\,\mathrm{Ch}_v\,. \tag{3.18}$$

This equation has a nice geometric interpretation as it counts the number of times that $\mathbb{T}^2$ wraps around the sphere S^2. This number is precisely the Chern number.

The first model of a Chern insulator with a Hall conductivity was proposed by Haldane [4], where he considered electrons moving on a honeycomb lattice with nearest neighbor and next to neareast neighbor hoppings. However, Qi,Wu and Zhang [42] introduced a simpler model of a Chern insulator in a square lattice with only nearest neighbor hoppings and periodic boundary conditions in the x and y–directions. In momentum space it takes the form,

$$H_0(k) = \sin k_x\sigma_1 + \sin k_y\sigma_2 + (r - \cos k_x - \cos k_y)\sigma_3, \tag{3.19}$$

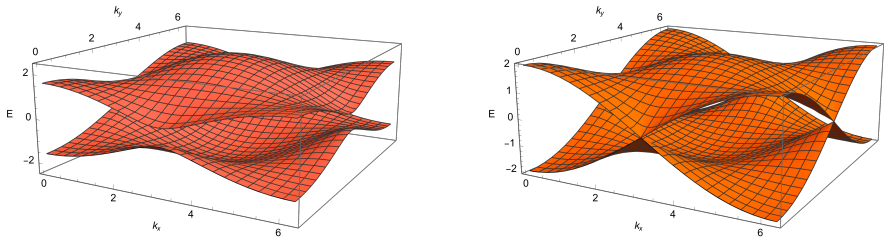

(a) (b)

FIGURE 3.2: a) Band of the Chern insulator model 3.19 at $r = 0.5$ with a gap between the valence and conduction band. b) Band of the Chern insulator model 3.19 at $r = 0$ showing the band closure. This is a critical point between the two topological phases.

with r a parameter controlling the topological phase. The model consists of an upper (conduction) band and a lower (valence) band (see figure 3.2). The dependence of the Chern number of the valence band with r is as follows (see figure 3.3),

$$\mathrm{Ch}_v = \begin{cases} 1 & -2 < r < 0, \\ -1 & 0 < r < 2, \\ 0 & r > |2|. \end{cases} \tag{3.20}$$

This model has 2 topological phases and one trivial phase. The points $r = -2, 0, 2$ are points where a topological phase transition takes place, this corresponds to band closures and openings.

Near these band openings and closures it is possible to approximate the Hamiltonian to,

$$H_D(k) = k_x\sigma_1 + k_y\sigma_2 + m_c\sigma_3 \tag{3.21}$$

where $m_c = r - c$ with $c = -2, 0, 2$ depending on which point we expand around. The last expression is a Dirac Hamiltonian in 2 dimensions. If we compute the Chern number of the Hamiltonian (5.7) we would obtain $\pm 1/2$, which is not an integer value. The reason is that in the Dirac approximation there is a not a well defined bandwidth. In fact the band extends over the whole UV. In systems on a lattice the bandwidth is finite and in the UV we have some curvature in the bands where the Chern number gets the additional $1/2$ to yield an integer. However the difference in Chern numbers between phases is well defined and is an integer. For that reason these kind of Hamiltonians are useful in describing some phenomena around the topological phase transitions, but they fail to describe the general physics of the Chern insulators and one often has to resort to regularization schemes to extract meaningful observables.

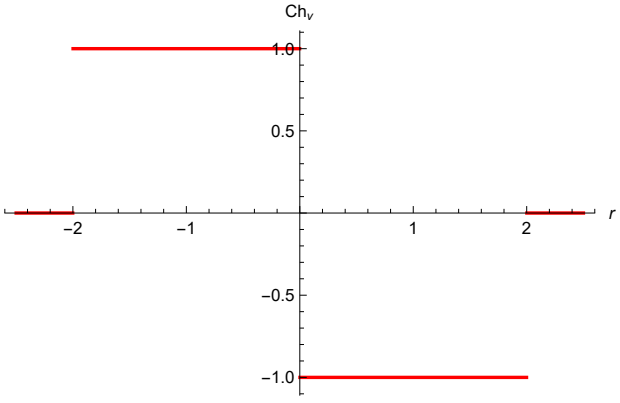

FIGURE 3.3: Dependence of the Chern number Ch_v on the parameter r.

This model, as the integer quantum Hall model, supports edge modes. The number of edge modes and the Chern number are related via the bulk-boundary correspondence. The absolute value of the Chern number $|\,\mathrm{Ch}_v\,|$ determines the number of modes propagating at the boundary of the system (given that we have a Chern insulator-vacuum interface). To see this we consider a Chern insulator with boundaries in the y–direction and periodic boundary conditions in the x–direction. In this setup k_y is no longer a good quantum number and we only have k_x. It is possible to plot the spectrum of the system as a function of k_x only, see figure 3.4. In there we can see (in blue) clearly gapped states that are confined to the bulk. In contrast, we also observe gapless modes (in red) that are localized entirely at the boundaries of our system. At $k_x = 0$ we see that the dispersion of the edge modes is linear for small k_x it is around these values where we can approximate our Hamiltonian to a Dirac Hamiltonian as discussed previously.

Using the Dirac approximation it is also easy to see the emergence of gapless modes at the boundary. Let us model the boundary by a y–dependent mass parameter $m_2(y)$. The mass has value $m_2(y) = -1$ inside the bulk $y > 0$ (topological phase) and changes suddenly to $m_2(y) = 1$ outside the bulk $y < 0$ (trivial phase). The following equation has a zero mode solution when $k_x = 0$,

$$\begin{aligned} &(i\partial_y\sigma_2 + m_2(y)\sigma_3)\,|\psi\rangle = 0, \\ &|\psi\rangle = \mathcal{N}\exp\left(\int^y \mathrm{d}y' m_2(y)\right)|{\rightarrow}\rangle\,, \end{aligned} \tag{3.22}$$

where $\mathcal{N}$ is a normalization factor and $|{\rightarrow}\rangle$ is a eigenstate of σ_1 with eigenvalue $+1$. This mode is localized at the interface between the topological and the trivial phase along the y–boundary, precisely the edge modes of the system.

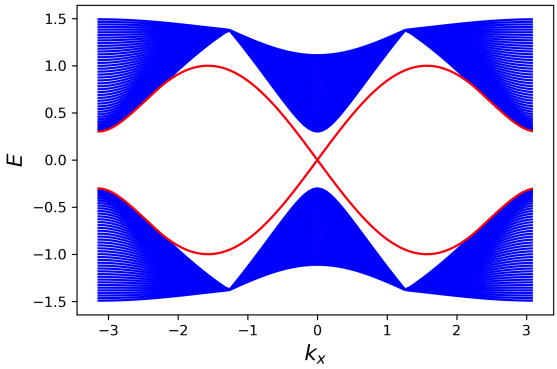

FIGURE 3.4: Spectrum of the Chern insulator with respect to k_x. In blue we have the gapped bulk states, while in red we see the gapless edge modes.

This highly localized solutions also known as solitons where already described by Jackiw and Rebbi [43] in the context of high energy physics.

3.3 DISORDER

In the clean case, we have seen that Chern insulators show really interesting physics. There is a topological number associated to them, they display edge modes and they also display the anomalous quantum Hall effect. As it happened with the integer quantum Hall effect, the quantization of the Hall conductivity and the existence of plateaus relies on the presence of disorder in the system. Nevertheless, we know that in 2-d in the presence of disorder states must localize via the mechanism of Anderson localization. In the instance of the (anomalous) quantum Hall effect, given that σ_{xy} is non-vanishing, we apply Laughlin argument and postulate that there must be at least one state that does not localize. This state is responsible for the quantization of σ_{xy} and the appearance of plateaus. It is also the state connecting the boundaries giving rise to chiral edge modes propagating along them. When we add disorder we find a tension forming between Anderson localization and topology. At the end if the disorder is strong enough all the states will localize.

As we add disorder we ought to ask the following questions for the Chern insulator: Is the Chern insulator resilient against disorder? If it is, how much disorder is needed to drive the Chern insulator into a trivial insulator? At which energies do we find the delocalized state? How do we define a topological invariant in this case? Does the delocalized state belong to the same class of the integer quantum Hall effect?. For the rest of the chapter we plan to answer

all these questions using the tools of replica field theory and numerical results available in the literature. The discussion here is based in Moreno-Gonzalez, Dieplinger and Altland [44].

The first thing to notice is that disorder breaks translational symmetry. Hence, Bloch states are to be replaced by states that usually Anderson localize, moreover, impurities can create states inside the spectral gap. This implies that for scattering rates off impurities τ^{-1} bigger than the band gap, the spectral gap gets filled by impurity states, therefore rendering the global spectral density gapless. All these new states inside the band gap are Anderson localized. Instead of the spectral gap (that is compromised due impurities), we considered the mobility gap, i.e, the gap between localized states in different bands. The analytical approach to tackle the problem of the disordered Chern insulator is an effective topological field theory in real space. The topological field theory describing its physics turns out to be the non-linear σ model with topological θ term,

$$S[Q] = \int \mathrm{d}^2x \left(g \,\mathrm{tr}(\partial_i Q \partial_i Q) + \frac{\theta}{16\pi} \epsilon_{ij} \,\mathrm{tr}\big(Q \partial_i Q \partial_j Q\big) \right), \tag{3.23}$$

where the two coupling constants $g = \sigma_{xx}/8$ and $\theta = 2\pi\sigma_{xy}$ are determined by the system's longitudinal and transverse Hall conductance, respectively (in units of the conductance quantum). It is no surprise that the same action describing the integer quantum Hall effect it is now describing the disordered Chern insulator since the physical phenomena are similar. Nevertheless, the difference lies in the dependence of g and θ with respect to the parameters of the model. In the next sections we derive this action from a microscopic model (3.19) and we give concrete expressions for the coupling constants g and θ in terms of the energy E, the topological parameter r and the disorder strength W.

3.3.1 *Effective field theory of the disordered Chern insulator*

In this section we present the derivation of the effective field theory of the disordered Chern insulator. The starting point is a disordered potential $V(\mathbf{x})\sigma_0$ taken from a Gaussian ensemble with zero mean and uncorrelated in space,

$$\begin{aligned} \langle V(\mathbf{x}) \rangle_{dis} &= 0, \\ \langle V(\mathbf{x}) V(\mathbf{x}') \rangle_{dis} &= \frac{W^2}{2} \delta(\mathbf{x} - \mathbf{x}'), \end{aligned} \tag{3.24}$$

where W^2 is the variance. The full Hamiltonian of the model is then $H = H_0 + V\sigma_0$, where H_0 is the two band Hamiltonian eq. (3.15) from the previous section . The action corresponding to the microscopic model is,

$$S[\bar{\psi}, \psi] = i \int \mathrm{d}^2x \, \bar{\psi}(\mathbf{x}) \left(E + i0^+ \tau_3 - H \right) \psi(\mathbf{x}), \tag{3.25}$$

where τ_3 acts on the retarded advanced space and $\psi(\mathbf{x}) = \{\psi(\mathbf{x})^{s,\sigma}\}$ is a fermionic field with indices in retarded/advanced space s and internal space σ. The next step is to average over all possible realization of disordered potentials $V(\mathbf{x})$. In order to access the averaged observables we use the replica trick, in which we consider R-copies of our system Z^R in order to compute the averaged observables (see section 2.3 and appendix A for a discussion),

$$S[\bar{\psi}, \psi] = i \int \mathrm{d}^2x \, \bar{\psi}^a(\mathbf{x}) \left(E + i0^+\tau_3 - H\right) \delta_{ab} \, \psi^b(\mathbf{x}).$$

From here we treat the action using the replica field theory:

- We average the partition function over all realizations of disorder V.
- We obtain a new quartic term in the action of the form

$$S_{dis} = \frac{W^2}{4} \int \mathrm{d}^2x \, \bar{\psi}^a(\mathbf{x})\psi^b(\mathbf{x})\bar{\psi}^b(\mathbf{x})\psi^a(\mathbf{x}), \tag{3.26}$$

  coupling different replica sectors.
- We decouple the quartic term by a Hubbard-Stratonovich transformation, yielding an action of the form [19, 45, 46],

$$S[A, \bar{\psi}, \psi] = \frac{1}{W^2} \int \mathrm{d}^2x \, A(\mathbf{x})^2 + i \int \bar{\psi}(E - H_0 + i\kappa A)\psi \tag{3.27}$$

- We integrate the fermions fields in the path integral to obtain the following effective action,

$$S[A] = \frac{1}{W^2} \int \mathrm{d}^2x \, A(\mathbf{x})^2 - \mathrm{tr} \ln \left(E - H_0 + i\kappa A\right). \tag{3.28}$$

This action is suitable to a saddle point analysis. A variation of the action with respect to A leads to the stationary phase equation

$$A(\mathbf{x}) = \tfrac{W^2}{2} \, \mathrm{tr}\big(E + i0^+\tau_3 - H - A\big)^{-1}(\mathbf{x}, \mathbf{x}), \tag{3.29}$$

i.e. a self consistent Born equation with 'impurity self energy', A. We parameterize a matrix-diagonal solution compatible with the symmetry of the causal increment $i0^+\tau_3$ as $A \to \Delta E + i\kappa\tau_3$. Plugging this Ansatz into the self-consistent equation we obtain expression for both ΔE and κ,

$$\Delta E + i\kappa\tau_3 = \frac{W^2}{2} \int_{BZ} \frac{\mathrm{d}^2k}{(2\pi)^2} \, \mathrm{tr} \left(\frac{1}{E - H(\mathbf{k}) - \Delta E - i\kappa\tau_3} \right).$$

The real part of the previous equation, ΔE, represents an overall shift in the energy E of the system. The imaginary part is the self energy due to impurity

scattering, which is proportional to the scattering rate off impurities and consequently defines another quantities of interest such as the elastic scattering time τ and the mean free path ℓ, (see appendix A.1).

This equation admits a continuous manifold of solutions, $A = \Delta E + i\kappa Q$, where $Q = T\tau_3 T^{-1}$ with unitary $T \in \mathrm{U}(2R)$ parameterizing the coset space $U(2R)/(U(R) \times U(R))$. Substituting these configurations into the action, and upgrading the constant T to a slowly varying Goldstone mode $T(x)$, we are left with the effective action

$$S[T] = -\mathrm{tr}\ln\left(E - h_a(\mathbf{k})\sigma_a + i\kappa T(\mathbf{x})\tau_3 T^{-1}(\mathbf{x})\right), \tag{3.30}$$

where we absorbed the energy shift ΔE into E, neglected the infinitesimal 0^+ in comparison to κ, and used a summation convention for repeated indices a. In the following we expand this action in slow T-fluctuations, first leaving the detailed form of the momentum-dependent coefficients $h_a = h_a(k)$ unspecified. This expansion will yield an effective action for the Goldstone modes.

We begin our analysis of the fluctuation action with a unitary rotation of the tr ln, leading to

$$S[T] = -\mathrm{tr}\ln\left(E - h_a\sigma_a + i\kappa\tau_3 - [T^{-1}, h_a\sigma_a]T)\right), \tag{3.31}$$

where the argument-dependence $h_a = h_a(\mathbf{k})$ and $T = T(\mathbf{x})$ is left implicit. Previous work performed this analysis for an effective Dirac Hamiltonian, $h_a = (k_1, k_2, m)$, for which the transformation of the logarithm is not innocent: It generates the chiral anomaly, and the need for UV regularization. Here, we need not worry, as we are working with a manifestly UV regular theory. In fact, working with the full lattice theory allows us to find the critical energies since in the Dirac approximation the UV details (and the details of criticality) are blurred by the UV divergences and subsequently by the UV regularization methods that cannot be justified from a condensed matter perspective.

Assuming variation of the fields T over scales much larger than the lattice spacing, we approximate the commutator up to second order in derivatives using the Moyal expansion as

$$[T^{-1}, h_a\sigma_a]T \simeq F_i\Phi_i - \tfrac{1}{2}J_{ij}\Phi_i\Phi_j,$$

with $F_i = i\partial_i h_a\sigma_a$, $J_{ij} = \partial_i\partial_j h_a\sigma_a$, $\Phi_i = (\partial_i T^{-1})T$, and the abbreviated notation $\partial_i v = \partial_{k_i} v$ and $\partial_i T = \partial_{x_i} T$. Our task now is to evaluate the formal second order expansion

$$\begin{aligned} S[Q] &= -\mathrm{tr}\ln\left(E - h_a\sigma_a + i\kappa\tau_3 - F_i\Phi_i + \frac{1}{2}J_{ij}\Phi_i\Phi_j\right) \\ &= \underbrace{\mathrm{tr}\left(GF_i\Phi_i - \frac{1}{2}GJ_{ij}\Phi_i\Phi_j\right)}_{S^{(1)}} + \underbrace{\frac{1}{2}\mathrm{Tr}(GF_i\Phi_i)^2}_{S^{(2)}}, \end{aligned} \tag{3.32}$$

with the Green function

$$G = (E + i\kappa\tau_3 - h_a\sigma_a)^{-1} = D(E + i\kappa\tau_3 + h_a\sigma_a),$$
$$D = [(i\kappa\tau_3 + E)^2 - h_a h_a]^{-1}. \tag{3.33}$$

In the following, we discuss how the two terms above yield the sum of a gradient term and a topological term for the effective action of the system. Both contributions are of second order in derivatives, the difference being is that one contains $\partial_i\partial_i$ derivative combinations, the other $\epsilon_{ij}\partial_i\partial_j$.

3.3.2 *Topological action*

In the construction of the topological action, we go fishing for antisymmetric derivative combinations $\epsilon_{ij}\partial_i\partial_j$. As detailed in the appendix B.1, these combinations arise from both terms $S^{(1)}$ and $S^{(2)}$. Building upon this point, we derive the topological action.

$$S_{\text{top}} = S^{(1)}_{\text{top}} + S^{(2)}_{\text{top}} = \frac{\theta_2 + \theta_1}{16\pi} \int \mathrm{d}^2x\, \epsilon_{ij}\, \mathrm{tr}\big(Q\partial_i Q\partial_j Q\big), \tag{3.34}$$

with coupling constants

$$\theta_1 = 8\kappa \int (\mathrm{d}^2k) D^+ D^- F_k,$$
$$\theta_2 = 4\pi i \int (\mathrm{d}^2k) \int_E^\infty d\omega\, (D_\omega^{+2} - D_\omega^{-2}) F_k \tag{3.35}$$

where $(\mathrm{d}^2k) = \frac{\mathrm{d}k_1 \mathrm{d}k_2}{(2\pi)^2}$ and

$$F_k = \epsilon_{abc} h_a \partial_1 h_b \partial_2 h_c = (\partial_1 h \times \partial_2 h)\cdot h. \tag{3.36}$$

Following standard conventions [8, 30], we associate the one/two derivative action $S^{(1/2)}$ with the two/one contribution to the topological action, $\theta_{2/1}$. Our final task thus is to compute the coefficients $\theta_{1,2}$. These integrals are straightforward for weak disorder, under a presumed hierarchy of energy scales

$$\kappa \ll E \lesssim 1. \tag{3.37}$$

We first represent the propagators D^s as

$$D^s = \frac{1}{E^2 - \epsilon^2 + is\gamma\tau_3}, \qquad \gamma = 2\kappa E, \quad \epsilon^2 = \sum_a h_a^2.$$

Under the stated conditions, this leads to the approximation

$$\kappa D^+ D^- = \frac{\kappa}{(E^2-\epsilon^2)^2+\gamma^2} \simeq \frac{\pi}{4E^2}\delta(E-\epsilon), \tag{3.38}$$

where here and throughout, $\epsilon > 0$ is the positive root of ϵ^2. Thus,

$$\theta_1 \simeq \frac{2\pi^2}{E^2}\int (\mathrm{d}k) F_k \delta(E-\epsilon),$$

which is an on-shell integral probing the density of states at E. Turning to θ_2, we note $D^{s2}_\omega \simeq \partial_{\omega^2} D^s_\omega$, and

$$D^+_\omega - D^-_\omega \simeq -\frac{\pi i}{\omega}\delta(\omega-\epsilon)$$

Entering these relations into the integral defining θ_1 and integrating by parts, it is straightforward to verify that

$$\theta_2 \simeq 2\pi^2 \int (\mathrm{d}^2k) F_k \left(\frac{\Theta(\epsilon-E)}{\epsilon^3} - \frac{\delta(\epsilon-E)}{\epsilon^2}\right).$$

We note that the second, on-shell term cancels against θ_1. To understand the meaning of the first, recall that $\epsilon = |h|$. We may thus define the unit sphere area element $S \equiv F/\epsilon^3 = n\cdot(\partial_1 n \times \partial_2 n)$ with unit vector $n = h/\epsilon$. Tidying up, we obtain the topological angle as,

$$\theta = \frac{1}{2}\int_{\epsilon_k > E} \mathrm{d}^2k\, n\cdot(\partial_{k_1} n \times \partial_{k_2} n)). \tag{3.39}$$

From this derivation we find that the topological angle is defined by the fraction of the full Berry flux $2\pi l$ carried by all states in the band above the reference energy E since only $\theta \bmod 2\pi$ matters, we may equally compute the flux of states below E. Criticality occurs for states for which $\theta(E) = \pi$.

3.3.3 *Gradient action*

The gradient term of the action is obtained by similar inspection of $S^{(1,2)}$, this time focusing on derivative combinations of the form $\sim F_i F_i$. As detailed in appendix B.2, this leads to

$$\begin{aligned} S_{\mathrm{grad}} &= g\int \mathrm{d}^2x\ \mathrm{tr}\,(\partial_i Q \partial_i Q)\,, \\ g &= I_+ + I_- + I_{+-}, \end{aligned} \tag{3.40}$$

with coupling constants given by

$$I_{+-} = \frac{1}{2}\sum_a \int (\mathrm{d}^2k)(E^2+\kappa^2-\epsilon^2+2h_a^2)D^+D^-\partial_i h_a \partial_i h_a,$$
$$I_{\pm} = \frac{1}{4}\sum_a \int (\mathrm{d}^2k)((E+i\pm\kappa)^2-\epsilon^2+2h_a^2)D^{\pm 2}\,\partial_i h_a \partial_i h_a. \tag{3.41}$$

We are left with the task to do the momentum integrals. For weak disorder, these integrals are analytically doable, if somewhat tedious. As a result, detailed in appendix B.2, we obtain

$$g = \frac{E^2-m^2}{2|E|\kappa}\Theta(E^2-m^2), \tag{3.42}$$

where $m = (r-c)$ and $c = 2, 0, -2$ depending on the Dirac cone around which we approximate. This result states that for weak disorder, diffusive quasiparticle propagation is limited to energies above the clean insulator band gap, m. For energies $E \gg m$, the coupling constant asymptotes to $\sim E/\kappa$ which is the characteristic scale for the conductivity of a weakly disordered two-dimensional conductor.

3.3.4 *Beyond the weak disorder limit*

Far from the weak disorder the fractional Berry flux becomes statistically distributed, and its mean value features as the topological angle θ. This value can be represented as the sum of two momentum space integrals over SCBA broadened Green functions, the Smrčka-Středa coefficients , $\theta_1 = 2\pi\sigma_{xy}^{\mathrm{I}}$ and $\theta_2 = 2\pi\sigma_{xy}^{\mathrm{II}}$. Odd integer values $\theta = \theta_1 + \theta_2 = (2n+1)\pi$ serve as markers for topological quantum criticality, as in the IQH context.

From equation (3.35) we may calculate angle θ for arbitrary two-band Hamiltonians H and for values (r, E, W) such that the self consistent Born approximation underlying our theory remains valid, $E\kappa \gtrsim 1$. However, outside the weak disorder regime $E\kappa \gg 1$ considered in the previous section the analytical computation of the integrals becomes cumbersome, or even impossible.

Progress can nevertheless be made, starting from the following representation of the coupling constants in terms of energy/momentum integrals:

$$\theta_1 = -\frac{i\pi}{2}\int (\mathrm{d}^2k)\,\epsilon_{ij}\,\mathrm{tr}\left(\tau_2 G_E \partial_i G_E^{-1}\tau_1 G_E \partial_j G_E^{-1}\right),$$
$$\theta_2 = \frac{\pi\epsilon_{\alpha\beta\gamma}}{3}\int_{-\infty}^{E}\mathrm{d}\omega\int(\mathrm{d}^2k)\times \tag{3.43}$$
$$\times\,\mathrm{tr}\left(\tau_3 G_\omega \partial_\alpha G_\omega^{-1} G_\omega \partial_\beta G_\omega^{-1} G_\omega \partial_\gamma G_\omega^{-1}\right),$$

where $G = G_E$ is the SCBA Green function Eq.(3.33). Latin indices take the values $i, j = 1, 2$ and the Greek indices the values $\alpha, \beta, \gamma = \omega, 1, 2$. Referring to appendix B.3 for the derivation of these representations from Eq.(3.35), we note that in the IQH context these integral representations are known as the Smrcka-Streda Hall coefficients, $\sigma^{\mathrm{I}}_{xy} = \theta_1/2\pi$, and $\sigma^{\mathrm{II}}_{xy} = \theta_2/2\pi$. These parameters describe the Fermi surface (σ^{I}_{xy}) and thermodynamic ($\sigma^{\mathrm{II}}_{xy}$, note the integral over all energies below the Fermi surface) contribution to the Hall response $\sigma_{xy} = \sigma^{\mathrm{I}}_{xy} + \sigma^{\mathrm{II}}_{xy}$.

We have derived a non-linear σ model for the disordered Chern insulator from which we have obtained the coupling constants (g, θ) which were to be identified with $(\sigma_{xx}, \sigma_{xy})$ (modulo proportionality factors). Their value corresponds to the conductivities of the system at scales compared to the mean free path ℓ. As we consider larger and larger length scales, the coupling constants (g, θ) will flow to either $(0, 2n\pi)$ (the insulating state) or to $(g^*, (n + \frac{1}{2})\pi)$ (the quantum Hall critical point) for $n \in \mathbb{Z}$ and $g^* = \mathcal{O}(1)$ as described by Pruisken and Khmelnitskii (figure 2.10). This implies that if we have $\theta = \pi$ for some values of (E, W, r), the theory will flow to criticality irrespective of the bare value of g. For the model (3.19) we have three stable fixed points $(0, -2\pi), (0, 0), (0, 2\pi)$ corresponding to the insulating phases and two unstable fixed points $(g^*, -\pi), (g^*, \pi)$ corresponding to the critical value that separates the insulating phases. This allows us to construct a phase diagram for the disordered Chern insulator in the space (E, W, r), where we have a critical surface separating different topological phases. As we can see in figure 3.5 inside the 'lobes' we have the topological phases, with Chern number 1 and -1 for the left and right lobes respectively. They are separated from the trivial phase by the critical surface.

For length scales longer than the localization length ξ, whenever $\theta \neq \pi$ our action consists only of the topological term,

$$S_{\mathrm{top}} = \frac{\theta}{16\pi} \int \mathrm{d}^2 x \, \mathrm{tr} \left(Q \partial_i Q \partial_j Q \right), \tag{3.44}$$

which can be written as a boundary term using Stoke's theorem and the parametrization $Q = T \tau_3 T^{-1}$,

$$S_{\mathrm{top}} = \frac{\theta}{4\pi} \oint \mathrm{d}\tilde{x} \, \mathrm{tr} \left(T^{-1} \tau_3 \partial_{\tilde{x}} T \right), \tag{3.45}$$

where $\tilde{x}$ is a one-dimensional boundary coordinate. This action describes the propagation of dissipationless chiral modes at the 1-d boundaries of the system. They propagate along the boundary and remain protected against disorder as long as the disorder is not too strong. It also can be noted that this action lacks gauge invariance. In order to cancel the term arising from this transformation we need to get the counter term from the bulk action in a mechanism known

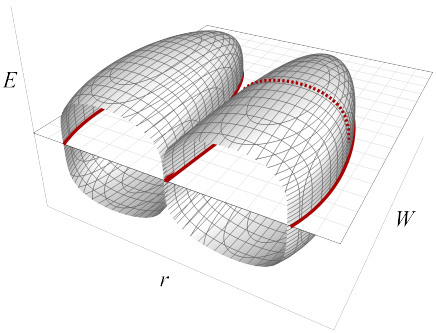

FIGURE 3.5: Schematic illustration of the critical surface of a Chern insulator. The clean system is defined in terms of different topological sectors realized as a function of a control parameter r, for example, $\mathrm{Ch}_1 = 0 \to 1 \to -1 \to 0$. For a given value of r and disorder strength, W, delocalized states exist at a critical energies $E_l(r, W)$, one for each band. The merging of these bands at the center of the spectrum marks the stability boundary of the TI; for larger disorder the system has become a trivial Anderson insulator. (For systems with high Chern indices, $\max|\mathrm{Ch}_l| > 1$, the destruction of topological order for increasing W occurs in the successive merging of multiple surfaces $E_l(r, W)$.). Figure taken from [44].

as anomaly inflow. In the language of quantum Hall physics this is also the mechanism behind spectral flow.

3.4 NUMERICAL MULTIFRACTAL ANALYSIS

In this section we summarize the multifractal analysis for the disordered Chern insulator. Multifractal analysis can helps us uncover the nature of the critical surface of the Chern insulator by studying the properties of the scaling of the IPRs [34, 47, 48] . The reason to study the multifractal analysis is that it will give us a second tool to find the critical surface and the chance to compare to the analytical approach. Additionally, it will uncover the nature of the transition, i.e, it will help us to put the criticality of the Chern insulator in the integer quantum Hall criticality class. We take the Hamiltonian (3.19) in the real space representation in a lattice with boundary conditions, and we consider its wavefunctions at energy E and consequently the IPRs,

$$P_q^E = \sum_{ij,\alpha} |\psi_{ij,\alpha}^E|^{2q}, \tag{3.46}$$

with $\psi^E_{ij,\alpha}$ the wavefunction at energy E, at the lattice site (i,j) and with internal degree of freedom α. The IPRs 3.46 should scale with the system size N in the following way,

$$P^E_q \propto N^{\tau_q}, \tag{3.47}$$

As mentioned already in section 2.5, $\tau_q = d(q-1)$ for a metal in d-dimensions and $\tau_q = 0$ for an insulator. The fluctuations of a critical wavefunction are captured by anomalous part of τ^E_q, $\Delta^E_q = \tau^E_q + d(q-1)$. For the quantum Hall transition it has been found that, $\Delta_q \approx 0.25\, q(q-1)$.

In practical terms we have finite system sizes and we compute the following quantity,

$$\tilde{\tau}(N)_q = \frac{\log\langle P^{E,W,r}_q(N)\rangle_{\text{dis,E}}}{\log N}, \tag{3.48}$$

where N is the system size, and it needs to be averaged over disorder configurations with disorder strength W and a window of energy around E. In the limit $\lim_{N\to\infty} \tilde{\tau}_q = \tau_q$ the scaling exponent is recovered. In [44] the scaling exponent τ_q and the critical exponent ν are found to be $\tau_q = 0.931 \pm 0.004$, $\nu = 2.73 \pm 0.16$, which is consistent with the values found in Chalker-Coddington networks and tight binding models [37, 49–51].

3.5 COMPARISON BETWEEN DIFFERENT APPROACHES

In figure 3.6 we compare the results obtained from numerical simulations done in [44] with the analytical predictions for the position of the extended state in the band of eigenstates. Numerically, these states are identified by calculating of the exponent $\tau_q = 2(1-q) + \Delta_q$, at quantum Hall criticality, $\Delta_q = 0.25 \times q(q-1)$, for the extremal value $q = 0.5$, i.e. $\Delta_{\min} = \Delta_{q=0.5} \approx -0.06$, and $\tau_{0.5} \approx 0.94$. The leftmost panel shows the system size dependent $\tau^N_{0.5}$ for $r = 1.2$, $W = 1.45$ as a function of E. At the above value $\tau^N_{0.5} \approx \tau_{0.5} \approx 0.94$ (green arrow) the data becomes system size independent, signifying criticality with an exponent matching the quantum Hall expectation.

To compare to the field theory predictions, we compute σ_{xy} by numerical evaluation of Eqs. (3.43) for the same values of r and W (blue curve). The crossing of the critical conductance $\sigma_{xy} = \frac{1}{2}$ is indicated by a blue arrow. The analytical and numerical predictions are not in perfect, but in reasonable agreement, given that there are no adjustable fitting parameters.

The center panel shows the energy of the extended state at $r = 1.7$ (left) and $r = 1.2$ (right) as a function of the disorder strength W. The green curves show the analytically computed longitudinal conductance, where $\sigma_{xx} \gtrsim 1$ is necessary for quantiative reliability of the field theory. As long as this condition is met, the analytical and numerical predictions for the value of the critical energy are

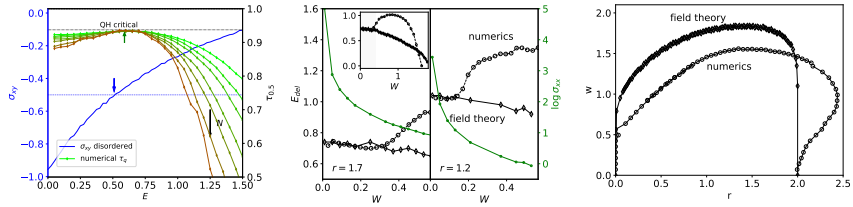

FIGURE 3.6: Analytical and numerical prediction for the position of the extended state. Left: the blue solid line shows the Hall conductivity calculated from Eq. (3.39), for different energies, at $(r, W) = (1.2, 1.45)$, while the blue dashed line shows the Hall conductivity for the clean Chern insulator at $r = 1.2$. Criticality is associated with the value $\sigma_{xy}(E) = 1/2 \bmod 1$, cf. blue arrow. On the right axis the numerical results for the effective dimensions $\tau_q(E)$ for different system sizes $N = 64$ (green) up to $N = 512$ (red) are shown (black arrow). The dotted horizontal line is the dimension $\tau_{0.5} \approx 0.94$ of the quantum Hall critical state. This condition is approximately met at the green arrow, which is reasonably, but not perfectly well aligned with the blue analytical marker. Center: prediction for the delocalized states taken from multifractal analysis and field theory at $r = 1.7$ and $r = 1.2$ as a function of disorder strength W. Additionally the analytically calculated σ_{xx} is shown (green). The inset shows the behavior of the delocalized state calculated with both analytical and numerical approaches for the full topological phase at $r = 1.7$. Right: phase diagram of the disordered Chern insulator in the r-W-plane at $E = 0$, calculated analytically and numerically. Figures taken from [44].

in good agreement. At larger values of the disorder, σ_{xy} is at its critical value, and $\sigma_{xx} = \mathcal{O}(1)$, so we are in proximity to the quantum critical point where the present theory is no longer applicable. In this regime, the numerical prediction for the critical energy shows a transient increase (cf. inset) for which we do not have a good explanation. Eventually, the numerical and analytical value for the critical energy approach zero — that they do so at roughly the same disorder concentration may be coincidental — thus signalling the breakdown of the topological phase due to disorder.

The right panel shows a cut through the critical surface at $E = 0$. Inside the lobe we have the Chern number $\mathrm{Ch}_c = -1$, outside it is vanishing. Broadly speaking, we again observe semi-quantitative parameter free agreement between field theory and numerics. However, there are some qualitative features which the former does not capture: Close to the clean critical value, $r = 2$, disorder stabilizes the topological phase in that the critical value gets pushed upwards (the bulge visible in the numerical data.) This feature does not show in the field theoretical calculation. We suspect that this is due to the fact that we

are in parametric proximity to a Dirac band closing at weak disorder and zero energy. For such configurations, the SCBA approximation produces incorrect estimates for self energies. However, a more detailed analysis of the latter beyond the SCBA approximation is beyond the scope of this work.

3.6 SUMMARY

In this chapter we described the physics of the anomalous quantum Hall insulator. We explored the physics of the clean AQHI where instead of Landau levels we have energy bands separated by (spectral) gaps described in the Brillouin zone. Using the geometric concepts of Berry curvature we see that it is possible to define a topological invariant, the Chern number, for each of the bands of the AQHI. This topological invariance manifests itself when computing the Hall conductance that is equal to the sum of the Chern numbers of the bands below the Fermi energy times e^2/h.

As a simple model we took the two-band insulator (3.19) defined on a square lattice and we characterized its topological properties, band structure and we saw the emergence of gapless edge states in systems with boundaries. The topological phases are characterized by Chern numbers $\mathrm{Ch}_v = -1, 1$ while the trivial insulating phase has a Chern number of zero, $\mathrm{Ch}_v = 0$. We can go between different phases by tuning the parameter r in the model.

In the disordered Chern insulator, the spectral gap of the clean insulator is replaced by a mobility gap: generic states inside the spectrum are Anderson localized, thus preventing bulk hybridization between the extended surface states of the system. However, this feature cannot extend to all states: there must exist bulk delocalized states establishing contact between the surface bands somewhere up in the spectrum. However, these consistency arguments do not tell us where the delocalized states lie in energy, nor what their critical properties are. Those questions where the purpose of this chapter.

Describing the Chern insulator in terms of the three parameters band energy, E, effective disorder strength, W, and a parameter, r, controlling its topological index $\mathrm{Ch}(r)$, we applied a combination of analytical and numerical methods to study the 'critical surface' of delocalized states in the Chern insulator. For generic parameter values, the critical states are buried deep in the band, meaning that these analyses had to operate outside the regime where 'Dirac' band linearlizations are an option. Perhaps unexpectedly, this generalization turned out to be a blessing, from various perspectives: The analytical derivation of an effective field theory building on the full microscopic band structure was no more difficult than the one starting from a lineraized spectrum. However, unlike that one, it was not plagued by spurious ultraviolet divergences, and it produced intuitive predictions for the identification of the critical states. Specifi-

cally, we found that, at least for weak disorder, criticality was tied to the integral Eq.(3.39): the energy of critical states in the weakly disordered system is such that the integrated Berry curvature of a all states above (or below) it equals π. The effective action describing the localization properties of these and of generic states was that of the quantum Hall insultator, confirming the expectation of bulk quantum Hall crtiticality in the system. However, for generic points in the parameter space (r, W, E) the weak disorder condition required for this description to be quantitatively reliable was violated, and quantitative errors ahead to be expected.

Comparing the analytical results with the numerical computation of the scaling dimensions of the anomalous exponent τ_q we were able to predict the position of the delocalized state in the parameter space and moreover we were able to study the critical properties of these delocalized states. This analysis confirmed the expectation of quantum Hall criticality, and for sufficiently weak disorder the results obtaind by the field theoretical computation. Outside that regime, the quality of the analytical predictions deteriorated, with errors up to $\mathcal{O}(1)$, but no parametric disagreement.

4

SURFACE STATES OF HIGHER ORDER TOPOLOGICAL INSULATORS

In this short chapter we go further into the exploration of non-interacting topological phases by considering more possibilities, that is, we take into account symmetries that might be present on the system. By only considering time-reversal, particle-hole and chiral symmetry the space of non-interacting single particle Hamiltonians can be classified into 10-classes, called the 10-fold way. From it, it is possible to further classify all the possible Hamiltonians displaying boundary states protected by topology and to define their topological invariants. Moreover, if we go further and consider crystalline symmetries the classification goes beyond the previous classification and even higher-order boundary states can appear. Below we take a quick look at the ten-fold way and how to go beyond it to get higher order boundary states. At the end we look at the effect of disorder in these phases. This is an interesting problem since disorder usually breaks the crystalline symmetries. Nevertheless, we look at the case where the crystalline symmetries are preserved on the average and see how the boundary states are affected by it.

4.1 THE TENFOLD WAY

In the previous chapter we considered the Chern insulator as an example of a topological insulator. The Chern insulator Hamiltonian is an example of a Hamiltonian with no symmetries. There are many more example of non-interacting Hamiltonian which display a topological character. Famous examples include, the quantum spin Hall insulator in $2d$ and $3d$ [42, 52–54], the SSH chain [55], the Kitaev chain [56], the chiral $p_x + ip_y$ superconductor [57] (in the BdG formalism), etc. The Hamiltonians supporting these topological phases cannot be deformed into each other and therefore they all describe different phases of matter. In order to classify the Hamiltonians and their topological phases we ought to look at their symmetries. Following the classification by Altland and Zirnbauer [5] of random Hamiltonians we see that there are 10 classes of Hamiltonians and they are labelled by the presence or absence of time reversal symmetry, particle-hole symmetry and chiral symmetry. There is a one-to-one correspondence between this classes of Hamiltonians and the set of symmetric spaces. We can therefore use the labelling introduced by Cartan to recognize them [58, 59]. For example, the Chern insulator belongs to the

class A type of Hamiltonians, the Hamiltonians with no symmetries. Let us present the three symmetries that give rise to the 10-fold way classification of Hamiltonians.

The first symmetry that we are going to consider is time reversal symmetry. The form of the operator acting on the Hilbert space is, $T = U_T K$, where U_T is an unitary transformation and K is the complex conjugation operator. On the level of the (first quantized) Hamiltonian H time reversal symmetry $\mathcal{T}$ acts in the following way,

$$\mathcal{T} \circ H \equiv T^{-1} H T = U_T^\dagger H^* U_T. \tag{4.1}$$

The square of the time reversal operator gives, $\mathcal{T}^2 = \pm 1$. A Hamiltonian H is said to be time-reversal invariant if, $\mathcal{T} \circ H = U_T^\dagger H^* U_T = +H$.

The next symmetry particle-hole symmetry. The form of the operator acting in the Hilbert space is $C = U_C K$, where U_C is an unitary operator and K is the complex conjugation operator. At the level of the Hamiltonian we have that,

$$\mathcal{C} \circ H \equiv C^{-1} H C = U_C^\dagger H^* U_C, \tag{4.2}$$

and we also have that $\mathcal{C}^2 = \pm 1$. A Hamiltonian is said to be particle-hole symmetric if, $\mathcal{C} \circ H = U_C^\dagger H^* U_C = -H$.

Finally the last symmetry, chiral (or sublattice) symmetry, is defined as the product of time reversal and particle-hole symmetry, $\mathcal{S} = \mathcal{T}\mathcal{C}$. A Hamiltonian is said to be chiral symmetric if,

$$\mathcal{S} \circ H \equiv U_S H U_S = -H \tag{4.3}$$

where U_S is an unitary operator. The chiral symmetry squares to one, $\mathcal{S}^2 = 1$.

Taking into account the possibilities of these operators we can count the number of possible combinations of the three symmetries. For time reversal symmetry we have 3 options, absence of symmetry, squaring to one or to minus one. By similar considerations we have three possibilities for particle-hole symmetry. The combination of time reversal symmetry and particle-hole symmetry defines the absence or presence of chiral symmetry. There is one more possibility, namely, no time-reversal symmetry, no particle hole symmetry but chiral symmetry. Taking into account this we have then $3 \times 3 + 1 = 10$ possible combinations of the symmetries, which give rise to the 10 different classes of Hamiltonians. We summarize all the possibilites and give their Cartan label in table (4.1).

So far we have seen how the Hamiltonians can be classified into ten classes, we would like to ask now, given a Hamiltonian in certain symmetry class and in certain dimension d how do we know if it is topological? How many topological insulators per dimension d do we find? And what topological invariant classifies them? Here we mention a way to classify these non-interacting Hamiltonians but readers who want a full in-depth discussion and different methods

Class	$\mathcal{T}$	$\mathcal{C}$	$\mathcal{S}$	G/H
A	0	0	0	$\mathrm{U}(2n)/(\mathrm{U}(n)\times\mathrm{U}(n))$
AI	1	0	0	$\mathrm{Sp}(4n)/(\mathrm{Sp}(2n)\times\mathrm{Sp}(2n))$
AII	-1	0	0	$\mathrm{O}(2n)/(\mathrm{O}(n)\times\mathrm{O}(n))$
AIII	0	0	1	$\mathrm{U}(n)$
BDI	1	1	1	$\mathrm{U}(2n)/\mathrm{Sp}(2n)$
C	0	-1	0	$\mathrm{Sp}(2n)/\mathrm{U}(n)$
CI	1	-1	1	$\mathrm{Sp}(2n)$
CII	-1	-1	1	$\mathrm{U}(n)/\mathrm{O}(n)$
D	0	1	0	$\mathrm{O}(2n)/\mathrm{U}(n)$
DIII	-1	1	1	$\mathrm{O}(n)$

TABLE 4.1: Cartan labelling of the ten symmetry classes. 0 represent the absence of the symmetry while +1 or -1 represent the presence and the value to which they square. In the last column the (fermionic) Goldstone manifold G/H for each class is indicated, where n is the number of replicas.

of classification should consult the references [10, 60, 61]. We use the fact that a topological insulator has states at the boundary which under arbitrary perturbations and weak disorder respecting the symmetries of the Hamiltonian do not localize. We have seen in the previous section that the disordered problem has an effective low energy theory in terms of a non-linear σ models. Depending on the symmetry class each of these non-linear σ models is defined over the Goldstone manifold G/H (see table 4.1). In the replicated fermionic theory this Goldstone manifold is compact. The non-triviality of the homotopy group in d or $d-1$ dimensions $\pi_d\left(G/H\right)$, $\pi_{d-1}\left(G/H\right)$, decides whether the effective low energy action admits a topological term. The options for a non-linear σ model to have a topological term are: a θ-term, (which appeared in the Chern insulator and the quantum Hall effect), a $\mathbb{Z}_2$ term and a Wess-Zumino-Witten (WZW) term [10]. For the θ-term, as we saw in the last chapter, delocalization is only assured whenever $\theta = \pi \mod 2\pi$ and for the rest of the values it indicates localization. This term alone would not be of help to classify the delocalized states at the surface of the topological insulators. For example, in the Chern insulator (or the quantum Hall effect) the topological term that classifies the different phases is equation (3.45), where θ there is properly quantized.

The $\bar{d} = d-1$ boundary of a topological insulator term allows for a $\mathbb{Z}_2$ term whenever $\pi_{\bar{d}}(G/H) = \mathbb{Z}_2$ and a WZW term whenever $\pi_{\bar{d}+1}(G/H) = \mathbb{Z}$. Looking at the ten symmetry classes and all possible dimensions we see that on each dimension there are always 5 possible topological insulators 2 $\mathbb{Z}_2$

insulators and 3 $\mathbb{Z}$ insulators and moreover it is periodic in dimension d mod 8 [61]. With all this information it is possible to construct a periodic table for topological insulators.

It should be noted that the disordered problem of topological insulators is not only useful to classify the possible topological phases but it is also an interesting problem on its own. As we saw in the last chapter disorder can also cause topological phases transitions and even at sufficiently strong disorder drive the whole system to a trivial phase. This kind of processes are not captured just by looking at the geometrical aspects of the manifolds G/H but also by looking at the microscopic parameters of each model.

4.2 HIGHER ORDER TOPOLOGICAL INSULATORS

The possibilities for non-interacting phases can be extended if one considers further symmetries, in this case crystalline symmetries [62, 63]. Not only crystalline symmetries can extend the classification of topological phases but also give rise to new forms of bulk-boundary correspondence, in the sense that we can have delocalized states at higher-order boundaries which are crystalline symmetric [64–67]. The extra-crystalline symmetries consider are usually mirror symmetry, inversion and rotation by a fixed angle.

The k-th order boundary is defined as the boundary of co-dimension k of a system. For example, typical topological insulators have a boundary of co-dimension 1. For 3-d systems we can have second-order boundary states propagating at the hinges or third order boundary states living in the corner.

Next we present two particular cases of higher order topological insulators with mirror symmetry and inversion symmetry respectively. In the first case we consider a 2-d HOTI with chiral symmetry and with corner modes. Here we do not rely on specific models and rather we study the topological invariants in the clean case and how they are affected when disorder is introduced in the system. It is worth mentioning that, in 2-d systems second-order boundary states live in the corners. These states are anomalous in the same sense that the boundary states of usual topological insulators are anomalous. In these crystalline phases there are also some other possibilities for which do not have anomalous boundary states but they may have a filling anomaly [68]. The filling anomaly is just a deviation of charge neutrality which manifests itself by the appearance of fractional corner charges. These phases are called obstructed atomic limits [69]. Nevertheless, there is also a possibility of obstructed atomic limits not to have a filling anomaly making the classification of topological crystalline phases a very involved endeavour [70, 71]. The second case is a 3-d model which realizes chiral hinge modes on opposite sides of the geometry

under consideration. After looking at the main properties of the clean case we introduce disorder on the surface and analyze the fate of the hinge modes.

4.2.1 *Mirror symmetric AIII HOTI*

For this class of systems we consider Hamiltonians with chiral symmetry,

$$\sigma_3 H(k_x, k_y)\sigma_3 = -H(k_x, k_y), \tag{4.4}$$

where σ_3 plays the role of the chiral symmetry operator. On the other hand we consider Hamiltonians with mirror symmetry in the following way,

$$\tau_3 H(k_x, k_y)\tau_3 = H(k_x, -k_y), \tag{4.5}$$

where τ_3 acts on different degrees of freedom other than the chiral symmetry operator. The eigenvalues of σ_3 and τ_3 are called chirality and mirror parity respectively. On the high mirror symmetric lines $k_y = 0, \pi$, due to mirror symmetry (4.5) the Hamiltonian is decomposed in blocks with definite mirror parity $\tau = \pm 1$. We can define the winding numbers of these blocks, $W_\tau(0/\pi)$ defining the topological invariants of the bulk, with the constraint, $W_+(0) + W_-(0) = W_+(\pi) + W_-(\pi)$. In here we focus in the case where $W_\pm(0) = 0$ and the bulk topological invariant is defined as,

$$Q_{\text{bulk}} = W_-(\pi). \tag{4.6}$$

On the other hand, if we consider a geometry with mirror symmetric corners, we expect corner modes localized on these corners [67, 70]. These corner modes have a defined chirality and mirror parity. We denote the number of corner modes with chirality σ and mirror parity τ as $n_{\sigma,\tau}$. The number $N_{\text{corner},\tau} = n_{+,\tau} - n_{-,\tau}$ is robust to local perturbations that respect both mirror symmetry and chiral symmetry. Nevertheless, it is not robust to addition of one dimensional AIII chains with edge modes along the boundaries. Therefore, the only well defined topological invariant is,

$$Q_{\text{corner}} = N_{\text{corner},+} - N_{\text{corner},-} \tag{4.7}$$

The bulk boundary correspondence asserts that $Q_{\text{bulk}} = Q_{\text{corner}}$ [71].

Upon addition of disorder that respects chiral symmetry and mirror symmetry on the average but not locally the mirror parity for the corner modes stops being a well defined quantity and therefore only the sum,

$$\bar{N}_{\text{corner}} = N_{\text{corner},+} + N_{\text{corner},-} \tag{4.8}$$

remains well defined. The fact that we can still add one dimensional AIII chains along the boundaries implies that the total number of corner modes can only be changed by two and,

$$\bar{Q}_{\text{corner}} = (N_{\text{corner},+} + N_{\text{corner},-}) \mod 2 \tag{4.9}$$

is the boundary invariant. Thanks to the bulk-boundary correspondence we know that two Hamiltonians having the same invariant $\bar{Q}_{\text{corner}}$ can be deformed into each other without closing the gap.

Given that the $\bar{Q}_{\text{corner}}$ is defined only modulo 2, the configurations with two corner states and zero corner states are equivalent. Therefore, it means that disorder can cause the mobility gap in the boundaries to close (while the bulk gap remains open) without changing the overall topology of the system. Disorder blurs the distinction between corner states of opposite mirror parity and hence, trivializes certain configurations that were topologically non-trivial in the absense of it. The classification of disordered AIII Hamiltonians with mirror symmetry is dictated by a $\mathbb{Z}_2$ invariant.

4.2.2 *Inversion-symmetric insulator with chiral hinge modes*

We take as a concrete model the clean version of an inversion symmetric Hamiltonian with no other symmetries (class A) supporting chiral hinge modes,

$$\begin{aligned} H(k) = &\left(M - \sum_{i=1}^{3} \cos k_i \right) \tau_1 \sigma_0 \\ &+ v \sum_{i=1}^{3} \sin k_i \tau_3 \sigma_i + m \sum_{i=1}^{3} \tau_0 \sigma_i, \end{aligned} \tag{4.10}$$

where τ_a and σ_a ($a = 0, 1, 2, 3$) are two sets of Pauli matrices plus the identity, M is the bulk mass, $m \ll 1$ is small parameter gapping out the surface states along the coordinate planes and v is the velocity. Inversion symmetry is implemented as $\mathcal{I} = \tau_1$, and acts on the Hamiltonian as,

$$\begin{aligned} H(k_x, k_y, k_z) &= \mathcal{I} H(k_x, k_y, k_z) \mathcal{I}^{-1} \\ &= \tau_1 H(-k_x, -k_y, -k_z) \tau_1. \end{aligned} \tag{4.11}$$

The topological phase occurs when $1 < |M| < 3$ and is characterized by two chiral hinge modes. These are located at inversion related hinges and propagate in opposite directions, see figure 4.1.

Plotting the spectrum of the Hamiltonian in the topological phase we find that this phase supports hinge modes (figure 4.2a), moreover if we plot the the magnitude of the wavefunctions of these hinge modes in a cross section (in the $x - y$ plane) of a infnitely long paralleliped, we find that they propagate along the hinges of the parallelipiped (figure 4.2b).

Given that this topological insulator has only inversion symmetry we can construct the topological invariant associated to it. It is the magnetoelectric polarization P_3 [72–74], which is quantized to $\mathbb{Z}_2$, and is defined as,

$$P_3 = \frac{1}{16\pi^2} \int \mathrm{d}^3 k \, \epsilon_{ijk} \, \mathrm{tr} \left[(f_{ij} - \frac{i}{3}[a_i, a_j]) a_k \right], \tag{4.12}$$

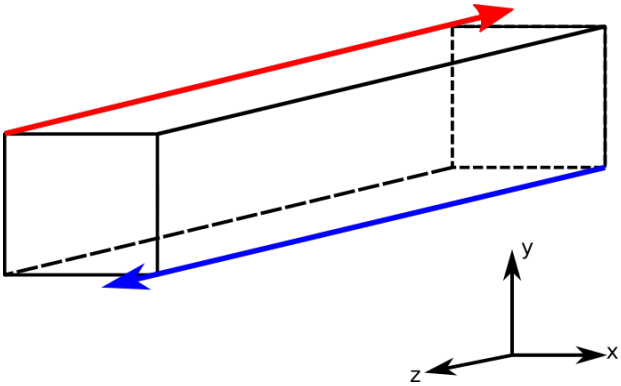

FIGURE 4.1: The model (4.10) in a parallelepiped geometry. In this geometry the model can host chiral modes propagating in two of the hinges.

where a_i is the non-abelian Berry connection and f_{ij} the non-abelian field-strength tensor. It is easy to see that this quantity is quantized. We define the sewing matrix as,

$$|u_i(-\mathbf{k})\rangle = B_{ij}\mathcal{I}\,|u_j(\mathbf{k})\rangle\,, \tag{4.13}$$

the matrix relating the states in the occupied band with the inversion symmetric partners in the same occupied band. The non-abelian Berry curvature $\mathbf{a}$ and the field strength-tensor $\mathbf{f}$ at the inversion momentum $-\mathbf{k}$ are related to the ones at momentum $\mathbf{k}$ by the following transformations,

$$\begin{aligned}\mathbf{a}(-\mathbf{k}) &= -B\mathbf{a}(\mathbf{k})B^\dagger + i\left[B\partial B^\dagger\right]\\ \mathbf{f}(-\mathbf{k}) &= B\mathbf{f}(\mathbf{k})B^\dagger\end{aligned} \tag{4.14}$$

And the magnetoelectric polarization can be expressed in terms of the sewing matrix as,

$$P_3 = -\frac{1}{48\pi^2}\int \mathrm{d}^3k\,\epsilon_{ijk}\,\mathrm{tr}\left[(B(\mathbf{k})\partial_i B^\dagger(\mathbf{k}))(B(\mathbf{k})\partial_j B^\dagger(\mathbf{k}))(B(\mathbf{k})\partial_k B^\dagger(\mathbf{k}))\right] \tag{4.15}$$

which in units of 2π can only take the values: 0 corresponding to the trivial phase and $\frac{1}{2}$ corresponding to the topological phase. In a field theory, including the presence of electric and magnetic fields, P_3 couples to the term proportional to $\mathbf{E}\cdot\mathbf{B}$ in the action. In this type of actions P_3 takes the role of the axion field [72]. This coupling leads to interesting responses in the system, for example, a half-integer quantum Hall effect at the surface. Let us take as an example the surface whose normal vector points in the x–direction (see figure 4.1) and P_3 changing values between $1/2$ and 0 at an interface between the

higher order topological insulator and the vacuum. This renders a x–dependent magnetoelectric polarization $P_3(x)$. The 4-vector current-density is given by [75],

$$j^\mu = \partial_x P_3 \epsilon^{\mu\nu\rho} \partial_\nu A_\rho, \tag{4.16}$$

where μ are space-time indices and A_ρ is the 4-vector potential. In the case of a uniform electric field in the z direction E_z, the current-density in the y-direction is expressed as,

$$j_y = \partial_x P_3 \, E_z, \tag{4.17}$$

and the Hall conductivity at the surface of the HOTI in the $y-z$ plane is given by, $\sigma_{yz} = \int \mathrm{d}P_3 = \Delta P_3$, the change in P_3 at an interface topological insulator–vacuum which is equal to $1/2$. This means that at the surface of the HOTI we have a half-integer quantum Hall effect.

From the boundary perspective it means that only the parity of the number of hinge modes Q_{hinge} propagating in the $+z$–direction N_+ plus the number of hinge modes propagating in the $-z$–direction N_- divided by 2, is a topological invariant,

$$Q_{\text{hinge}} = \frac{1}{2}\left(N_+ + N_-\right) \mod 2 \tag{4.18}$$

We can see that by adding perturbations respecting inversion symmetry at the surface. For example we can add a Chern insulator in half of the surface and its inversion symmetric counterpart on the other half. The addition of the Chern insulators at the surface will change the overall number of hinge modes by a multiple of four (by a multiple of 2 on each hinge), thus preserving parity and leaving Q_{hinge} unchanged.

We construct an effective surface Hamiltonian for a system that is infinitely long in the z-direction but finite in the x and y-directions. We take (4.10) in the topological phase and project onto zero-energy surface states. This yields an effective low energy Hamiltonian for each of the 4 surfaces. These can be combined into a single surface theory describing a plane is infinite in the z-direction but periodic in a second coordinate x' (topologically a cylinder). The resulting $2d$ effective surface Hamiltonian [64, 66] takes the form,

$$H_0 = v k_{x'} \sigma_1 + v k_z \sigma_3 + m(x') \sigma_2, \tag{4.19}$$

where the parameter m acquires a spatial dependence. On half of the surface $m > 0$ while the other half $m < 0$. Therefore, at the two hinges where this parameter changes sign we have chiral hinge modes propagating in the y-direction as seen in figure 4.3. The modulus $|m|$ is the surface spectral gap. The use of the effective Hamiltonian (4.19) requires that the surface gap $|m|$ is much smaller than the bulk gap of the full three-dimensional lattice Hamiltonian (4.10).

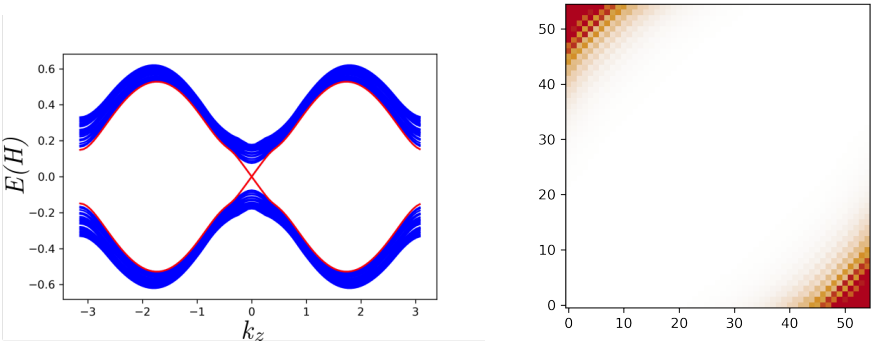

(a) (b)

FIGURE 4.2: a) Spectrum of the inversion symmetric HOTI with periodic boundary conditions in the z–direction. In red we see the appearence of gapless modes. b) Cross section in the plane $x - y$ of the geometry in figure 4.1 showing the modulus of the wavefunction of the gapless modes. They are highly localized around two hinges.

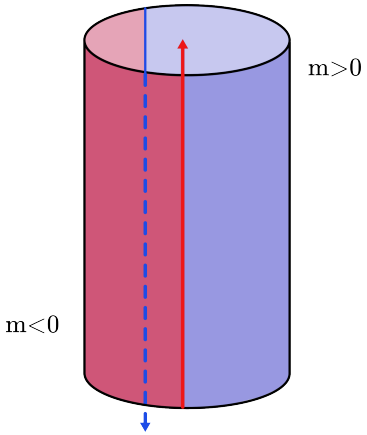

FIGURE 4.3: Inversion symmetry higher order topological insulator in a cylindrical geometry. At the level of the surface theory we have the parameter m changing sign at two hinges where we find gapless modes propagating.

4.2.2.1 *Disordered case*

We next evaluate the effect of surface disorder, in particular, we would like to see the stability of the hinges modes under the influence of random disorder. We take the effective surface Hamiltonian (4.19) and model the disorder by a scalar Gaussian distributed potential $V(\mathbf{x})$,

$$\begin{aligned} \langle V(\mathbf{x})\rangle_{\text{dis}} &= 0, \\ \langle V(\mathbf{x})V(\mathbf{x}_0)\rangle_{\text{dis}} &= \frac{\gamma_0^2}{2}\delta(\mathbf{x}-\mathbf{x}_0). \end{aligned} \tag{4.20}$$

with $\mathbf{x} \equiv (x', y)$. The Hamiltonian for the surface of the higher-order topological insulator with the disorder is

$$H_S = H_0 + V(\mathbf{x})\sigma_0. \tag{4.21}$$

where $H_0 = H_0 = vk_{x'}\sigma_1 + vk_y\sigma_2 + m(x')\sigma_3$ is the same Hamiltonian as (4.19) after a π-rotation in the $y-z$ plane. This Hamiltonian breaks inversion symmetry since the disordered potential $V(x)$ is not necessarily inversion symmetric. One could argue that since the symmetry is broken there are no hinge modes, but since we are considering the conditions (4.20) inversion symmetry is preserved on the average. The Hamiltonian (4.19) can be treated by the same methods discussed in the previous chapter, it is however important to add a regulator because the Hamiltonian alone suffers from UV divergences, the effective action in terms of Q and an external gauge field $\mathbf{a}$ is given by,

$$\begin{aligned} S[Q,\mathbf{a}] &= S_0[Q,\mathbf{a}] - S_\eta^M[Q,\mathbf{a}] \\ &= -\operatorname{tr}\ln\left(\epsilon - v(\mathbf{k}\cdot\boldsymbol{\sigma}) + v(\mathbf{a}\cdot\boldsymbol{\sigma}) - m\sigma_3 + i\kappa Q\right) \\ &\quad + \operatorname{tr}\ln\left(-v(\mathbf{k}\cdot\boldsymbol{\sigma}) + v(\mathbf{a}\cdot\boldsymbol{\sigma}) - \tilde{M}\sigma_3 + i\eta Q\right), \end{aligned} \tag{4.22}$$

where we have used a Pauli-Villars regularization [76] in order to avoid the UV divergences mentioned before, with $\tilde{M} \to \infty$ and $\eta \to 0$, κ is the scattering rate off impurities, which is found self-consistently as,

$$\kappa = \gamma_0^2 \operatorname{Im}\left[\int \frac{d^2k}{(2\pi)^2} \operatorname{Tr}\left(\frac{1}{\epsilon - i\kappa - H_0}\right)\right]. \tag{4.23}$$

We expand the action (4.22) in gradients of T (appendix C.2) to construct a low energy action that takes the form of a nonlinear σ model [77, 78],

$$\begin{aligned} S[Q] =& \frac{1}{8}\Big(\sigma_{xx}\int d^2x \operatorname{tr}(\nabla Q)^2 \\ &+ \sigma_{xy}\int d^2x \varepsilon^{ij3}\operatorname{tr}(Q\nabla_i Q\nabla_j Q) \\ &- \frac{1}{2}\int d^2x \varepsilon^{ij3}\operatorname{tr}(Q\partial_i Q\partial_j Q)\Big), \end{aligned} \tag{4.24}$$

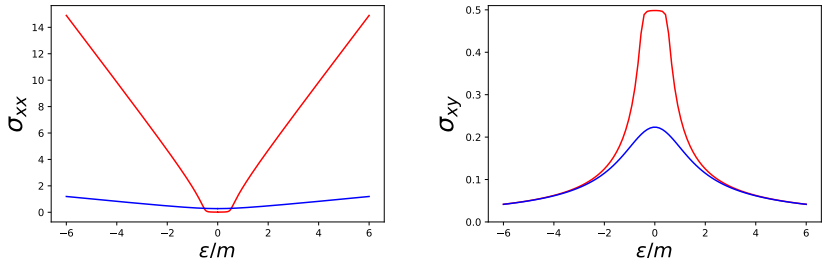

FIGURE 4.4: Longitudinal and transverse conductivities σ_{xx} and σ_{xy} for weak (red, $\kappa/m = 0.2$) and strong (blue, $\kappa/m = 2.6$) disorder. The value of the surface gap is set to $m = 0.5$. Without disorder, the surface spectrum is gapped for $|\varepsilon| < |m|$. For $m < 0$, σ_{xy} changes sign, while σ_{xx} remains the same.

where $Q = T^{-1}\tau_3 T$, $\nabla_i = \partial_i - i[a_i, \quad]$ is the covariant derivative,

$$\sigma_{xx} = \frac{1}{2\pi}\left(1 + \frac{\epsilon^2 + \kappa^2 - m^2}{2\kappa} f(\epsilon, m)\right)$$

and

$$\sigma_{xy} = \frac{m}{2\pi}(f(\epsilon, m) + f(m, \epsilon))$$

with

$$f(x, y) = \frac{1}{x}\left(\arctan\left(\frac{x+y}{\kappa}\right) + \arctan\left(\frac{x-y}{\kappa}\right)\right)$$

and we have set $v = 1$. The θ angle of the nonlinear sigma model is therefore given by $\theta = 2\pi\left(\sigma_{xy} - (1/2)\right) \bmod 2\pi$. In the large system size limit, this parameter renormalizes to an integer multiple of 2π [8, 31], $\theta \to 2\pi\lfloor\sigma_{xy} - \frac{1}{2}\rceil$, where $\lfloor . \rceil$ is the nearest integer function ($\lfloor 2.6 \rceil = 3$, $\lfloor 1.2 \rceil = 1$, etc). This implies that σ_{xy} asymptotically assumes a half integer quantized value — the half integer quantum Hall effect occurring at topological insulator surfaces.

Our model has a space dependent mass-like parameter $m(x')$, with $m(x') > 0$ in one half of the space, $m(x') < 0$ the other, and a smooth interpolation in-between. The scaling behavior outlined above then implies that $\sigma_{xy} = (1/2)\,\mathrm{sgn}(m)$ in the two half regions, asymptotically. The quasi-one dimensional interface region supports one propagating quantum Hall edge channel, corresponding to the hinge mode in the three-dimensional crystal described by Eq. (4.10).

How does this scenario respond to increases in the disorder strength, from values $\kappa < |m|$ to $\kappa > |m|$? In Fig. 4.4, the two 'bare' transport coefficients σ_{ij}

corresponding to these regimes are shown as functions of the energy ϵ, in red and blue respectively. These coefficients define the short-distance starting values for the renormalization described above. For weak disorder, the longitudinal conductance σ_{xx} at increasing distance scales stays low inside the gap $|\epsilon| < |m|$ but grows quickly if $|\epsilon|$ exceeds $|m|$ due to the spectral weight present outside the gap. At the same time, σ_{xy} diminishes with $|\epsilon|$, so that the bare value of θ is close to $-\frac{1}{2}$. For strong disorder and intra-gap energies, σ_{xx} exceeds its weak-disorder limit due to impurity states smearing the gap. Outside the gap, we observe qualitatively similar behavior as in the weak-disorder case, be it that the reaching of a high conductance regime is much slower than in the clean case. Despite the very different bare values for the weak and strong disorder regimes, in both cases, the surfaces will approach an insulating state in the thermodynamic limit upon taking into account the renormalization described by the nonlinear sigma model (4.24). This means that, asymptotically, the existence of hinge states is granted for all energies inside the bulk gap (including energies larger than the surface spectral gap $|m|$ in the absence of disorder). However, surface states may have a large localization length for large energies or for weak disorder, so that for finite system size hinge states may be compromised because of backscattering via surface-state intermediaries if the surface localization length exceeds the system size.

The model (4.10) corresponds to an intrinsic second-order topological insulator: The presence of chiral hinge states is required by the nontrivial topology of the bulk. Formally, the addition of a Pauli-Villars regulator in the surface theory breaks inversion symmetry and it could be argued that the regularized model corresponds to an extrinsic second-order topological insulator. In both cases, the boundary phenomenology is the same, since the breaking of crystalline symmetry by the Pauli-Villars regulator does not close the bulk or the surface gaps. For the same reason, the (quantized) response to external sources and the fate of the hinge states upon the addition of disorder is the same in the intrinsic and extrinsic scenarios.

This construction, that was aimed at the case of the inversion symmetric HOTI, can be also done for any other type of 3-d higher order topological insulators with hinge modes, topological invariant $\mathbb{Z}_2$, and effective low energy surface Hamiltonian of the form (4.19) with a effective surface mass m changing sign at two or more hinges.

4.3 CONCLUSION

In this chapter we explored the role of symmetries of the Hamiltonians. We see that considering time-reversal symmetry, particle-hole symmetry and chiral symmetry we can classify the Hamiltonians into 10 different classes. Depending

on the spatial dimension and the class of the Hamiltonians we can determine whether they are topological or not. Classifications of topological insulators tell us that for each dimension we have 5 types of topological insulators, 3 $\mathbb{Z}$ insulators and 2 $\mathbb{Z}_2$ insulators.

The inclusion of further symmetries, in the form of crystalline symmetries augments the possibility for different types of topological insulators and their classification. One notable aspect of the addition of crystalline symmetries is that they enhance the possibilities of boundary modes. With crystalline symmetries it is possible to define higher-order boundary states.

The addition of disorder to the system usually breaks the crystalline symmetries. However, one may still ask for the fate of the boundary modes when the symmetry is preserved on the average. For 2-d higher order topological insulators with mirror symmetry disorder simplifies the classification where just a $\mathbb{Z}_2$ is needed to describe the distinct topological phases. In the topological phase the corner modes are resilient against Anderson localization.

In the case of 3-d higher order topological insulator with inversion symmetry we developed an effective low energy field theory for the surface. The theory turns out to be a non-linear σ model with a θ-term. The observable coefficients σ_{xx} and σ_{xy} are given in terms of the microscopic parameters of the system and are defined in the scale of the mean free path. In this surface theory σ_{xy} is not quantized to integer values but rather to half-integer values yielding a manifestation of the half-integer quantum Hall effect. For half of the surface σ_{xy} renormalizes to $1/2$ while the other half renormalizes to $-1/2$, in the hinges where the two halfs of the surfaces meet we find one dimensional channels where the hinge modes propagate without Anderson localizing.

In summary, we find that although disorder breaks the crystalline symmetries locally when preserved on average it can remain topological with boundary modes resilient against Anderson localization and on the other hand they can ease the classification of topological crystalline phases.

5

FRAGILITY OF SPECTRAL FLOW IN CLASS AIII TOPOLOGICAL INSULATORS

In chapter 3, we thoroughly characterized the disordered Chern insulator. Through field theory methods, we determined the positions of delocalized states for given disorder strengths (W) and parameters (r). The existence of these delocalized states hinged on the principle of spectral flow. When subjected to an external magnetic field in the longitudinal direction, the Chern insulator exhibits a current in the transverse direction. These delocalized states within the bulk are responsible for this phenomenon, with bridges in the bulk connecting the surfaces to facilitate anomalous transport of spin and heat, among other phenomena. Moreover, they offer topological protection against Anderson localization.

While the principle of spectral flow was believed to be universal among all topological insulators, at least in the Wigner-Dyson classes (class A, AI, AII), we will see in this chapter that this principle is not general. For instance, $3d$ topological insulators in the non-Wigner-Dyson classes (AIII, CII, DIII) may exhibit an absence of spectral flow due to its fragility. In these classes, surface states could detach from the bulk. Consequently, the transport characteristics of these topological insulators in the presence of disorder differ from those in the usual insulators of the Wigner-Dyson classes.

The absence of spectral flow from the bulk perspective occurs when the bulk admits a complete basis of exponentially localized Wannier states. From the surface perspective, it means that almost all surface states can undergo Anderson localization in the presence of disorder, except for the chiral symmetric state at $E = 0$, which enjoys topological protection as long as the bulk remains topological [79, 80]. Wannier localizable phases which are topological are not as rare as one might initially think. As a matter of fact, one dimensional topological phases are Wannier localizable; examples include the SSH chain [55] and the Kitaev chain [56]. On the other hand 2-d topological phases are not Wannier localizable. As we saw in the chapter 3, Chern insulators have a delocalized state above and below the Fermi energy which connects the boundaries, rendering these phases Wannier non-localizable. In the case of the quantum spin Hall insulator and the 3-d topological insulator similar arguments can be made [81].

Analyzing the situation of Wannier localizability at the boundaries can be tricky, especially since there may be a temptation to use Dirac approximations at

the surface states. The detachment (in energy) from the bulk takes place at 'high' energies (close to the band), where Dirac approximations lose effectiveness since they primarily focus on energies very close to the gap closing energy. Therefore it is neccesary for the time being to abandon the Dirac approximations since they can oversimplify and miss the essential mechanisms behind these phenomena.

Furthermore, we will discuss how this absence of spectral flow may not always occur. In fact, previous numerical studies in classes AIII, CII, and DIII [82–85] have found a continuum of critical states at the surface for energies $E \neq 0$ in the presence of disorder, a phenomenon termed spectrum-wide criticality.

In the upcoming sections, we examine the conditions under which surface states localize or remain delocalized in the presence of disorder. We accomplish this by studying a minimal model of a class AIII topological insulator with winding number $\nu = 1$. Utilizing field theory, we demonstrate that whether a surface state localizes or not is tied to the presence of (surface) Berry curvature (equation (3.39)). Specifically, when the Berry curvature is non-zero, states at energies $E \neq 0$ localize. However, it is crucial to note that the definition of the Berry curvature requires detachment between the bulk and surface; otherwise, the Berry curvature remains ill-defined. This chapter is based on the reference [86].

5.1 FRAGILITY OF THE SPECTRAL FLOW

We now see two perspectives for the absence of the spectral flow, from the bulk and from the boundary. From the bulk the absence of it comes from the Wannier localizability of the bulk states, since these localized states cannot form a "bridge" connecting the two surfaces. While from the boundary the absence of spectral flow comes from the possibility of detaching bulk and boundary states at all momenta.

5.1.1 *Bulk*

A free fermion insulator is considered Wannier localizable if the subspaces defined by valence and conduction bands can be described by bases of states $|\Psi_{R,\alpha}\rangle$, which are exponentially localized around specific centers R, with α representing an additional index. These Wannier localized states are unaffected by flux insertions, hence preventing any spectral flow within the system. It is important to note that Wannier localizability does not imply the *atomic limit*, where the insulator becomes topologically trivial. Thus Wannier localizability is a weaker condition than retractability to the atomic limit [87–94]. The presence

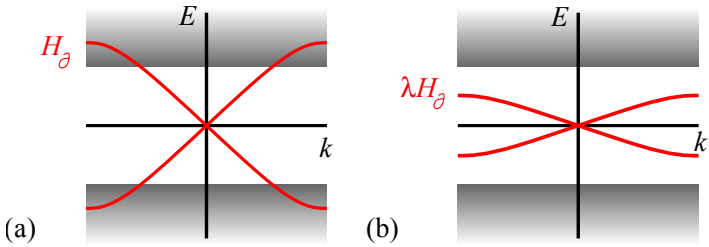

FIGURE 5.1: Schematic picture of the spectrum of the Hamiltonian $H' = H_\partial \oplus H_{\text{bulk}}$. In red the surface spectrum and in black the bulk spectrum. a) and b) show the before and after the rescaling of the surface spectrum by a factor of λ. Taken from [86].

of small but finite overlaps between neighboring unit cells remains crucial for maintaining the topological non-triviality [95]. The Wannier states are generally not eigenstates of the original Hamiltonian. Nevertheless, we can perform the following deformation to obtain a topologically equivalent one: the first step is to deform the Hamiltonian such that the bands are individually flat. Secondly we apply unitary transformations (commuting with the Hamiltonian) to the Wannier basis on each band subspace, and lastly we can deform back to a Hamiltonian where the bands are not necessarily flat. The deformed Hamiltonian is then,

$$H' = \sum_{R,\alpha} \epsilon_{R,\alpha} \left|\Psi_{R,\alpha}\right\rangle \left\langle\Psi_{R,\alpha}\right|, \tag{5.1}$$

where $\epsilon_{R,\alpha}$ assume the role of state energies. Using this protocol, let us consider a system with boundaries which is Wannier localizable in directions transverse to them. We can decompose the Hamiltonian as [96],

$$H' = H_\partial \oplus H_{\text{bulk}}, \tag{5.2}$$

where H_∂ is the contribution of Wannier states within a Wannier localization radius of the surface, and H_{bulk} its complement. With this separation we can re-scale $H_\partial \to \lambda H_\partial$ to shrink the surface band until it can be dettached from the bulk bands at all momenta.

As an example we can take a look at the AIII insulator in 3 dimensions. This is one of the simplest examples of a topological insulator which is Wannier localizable. Hamiltonians H obey the chiral symmetric condition $\{H, \Gamma\} = 0$. Where Γ is the chiral operator. In a basis where $\Gamma = \tau_3$ we have,

$$H = \begin{pmatrix} 0 & A \\ A^\dagger & 0 \end{pmatrix}, \tag{5.3}$$

where A is a complex matrix. We assume H (and therefore A) is a local Hamiltonian. The matrix elements of A, in the Wannier basis, between orbitals α and α' and sites R, R' is given by $\langle R\alpha|A|R'\alpha'\rangle$ and it decays exponentially with the distance $|R - R'|$.

In a system with periodic boundary conditions the spectrum is gapped. In this case we can deform the Hamiltonian (without closing the gap) in a way that we send all positive eigenvalues to $+1$ and the negative ones to -1. The fact that this deformation does not close the gap, and consequently preserves the bulk topology, implies that the locality condition remains unchanged. The new Hamiltonian H_f is written as,

$$H = \begin{pmatrix} 0 & U \\ U^\dagger & 0 \end{pmatrix}, \tag{5.4}$$

where U is a local unitary matrix. It is straightforward to construct the eigenstates of H_f [95],

$$\left|\Psi^{\pm}_{R,\alpha}\right\rangle = \begin{pmatrix} |R,\alpha\rangle \\ \pm U^\dagger |R,\alpha\rangle \end{pmatrix}, \tag{5.5}$$

which is localized around R, given that $|R,\alpha\rangle$ is a Wannier function and $U^\dagger$ a local unitary matrix. The ground state of H and H_f are the same, showing that this phase albeit localized is still topological. The Wannier functions are not unique. With a choice of a local unitary matrix V we could obtain as well another set of eigenstates of H_f, namely, $\left|\Psi^{\pm,V}_{R,\alpha}\right\rangle = (\mathbf{1}\otimes V)\left|\Psi^{\pm}_{R,\alpha}\right\rangle$. This implies that the bulk–boundary decomposition is also not unique. In the next sections we are going to see that we can define a surface Chern number and that its parity should match the parity of the topological invariant of the bulk. At the level of the eigenstates of the Hamiltonian this means that for different Wannier basis, $\left|\Psi^{\pm}_{R,\alpha}\right\rangle, \left|\Psi^{\pm,V}_{R,\alpha}\right\rangle$ the surface Chern number could be different but with the same parity [97],

$$\delta\,\mathrm{Ch} = 2\nu[V], \tag{5.6}$$

where ν is the winding number of V expressed as an integral in momentum space.

The ability of topological phases to be Wannier localizable without altering their intrinsic topological properties implies that the 10-fold classification of topological insulators remains unchanged. However, it allows for further classification of topological phases into those that are Wannier localizable and those that are non-localizable.

For classes A, AI, and AII (Wigner-Dyson classes) in a topological phase, they are always Wannier non-localizable. The reason is that one always has the freedom to choose a reference energy inside the bulk gap. The existence

of a topologically protected state at some energy implies its existence at all energies inside the gap. On the other hand, for the rest of the symmetry classes, particle-hole or chiral symmetry forces the spectrum to be mirror symmetric around $E = 0$. The condition of equivalence of all energies no longer holds, and the presence of a band of delocalized states inside the gap cannot be assured. To establish if a phase in these classes is Wannier localizable, we ultimately need to consider if the chiral and particle-hole symmetries are *spectator symmetries*. Symmetries are referred to as spectator symmetries if the topological properties of the system, such as boundary states, remain unaltered even after the (chiral or particle-hole) symmetries are removed. Examples include 2-*d* topological insulators in classes C and D, as well as 3-*d* class DIII topological insulators with an odd topological invariant.

In summary, we have established that Wannier localizability indicates the potential for a gap to form between bulk and surface states through the introduction of a localized surface perturbation. Similarly, the introduction of disorder results in the Anderson localization of all states at energies other than zero. We refer to the occurrence of both these scenarios as the *fragility of surface states*. It is essential to emphasize that these scenarios represent mere possibilities and there are cases where they do not occur. In the following sections, we will explore the mechanism behind the fragility of surface states within a minimal model of a class AIII topological insulator with a winding number $\nu = 1$.

5.1.2 *Boundary*

The 2-*d* gapless surface states of 3-*d* topological insulators are effectively described by Dirac Hamiltonians of the form,

$$H_D = k_x \Gamma_x + k_y \Gamma_y, \tag{5.7}$$

where k_x and k_y represent momenta near the closing point, and the Gamma matrices satisfy $\{\Gamma_i, \Gamma_j\} = 2\delta_{ij}$. One notable observation is that the Hamiltonian (5.7) exhibits ultraviolet divergence. Furthermore, it cannot be represented as a low-energy limit of a lattice model; in other words, under the Dirac approximation, it is not feasible to describe the surface of a topological insulator as a standalone entity.

From this perspective, the spectral flow can be understood as governed by an anomaly. To illustrate this, we introduce an external vector potential A into the Hamiltonian (5.7). However, in adopting a regularization scheme, we inevitably sacrifice gauge invariance. The consequence of this loss is the breakdown of particle number conservation. This is exemplified by the adiabatic insertion of a flux quantum through the bulk, resulting in the upward displacement of states

in energy. States above the cutoff energy (defined by the regularization) simply vanish. However, by reality, these high-energy states undergo transformation into bulk states, while bulk states are simultaneously transformed into states occupying the lowest energy levels. This mechanism enables the observation of states being transported along the bulk from one boundary to the other, thereby giving rise to the quantized transverse transport of charge, spin, or heat.

However, what about the case of a topological insulator where spectral flow might be absent? From our previous discussion, we inferred that in such cases, the bulk behaves as a sink for states pushed upward in energy. In a topological insulator lacking spectral flow, where the bulk and boundary are disconnected, the states pushed above must remain confined within the surface. In the subsequent discussion, we explore this scenario in more detail for a class AIII topological insulator.

The Dirac description of the surface of a class AIII topological insulator is given by the following two band Hamiltonian,

$$H_d = k_x \tau_x + k_y \tau_y, \tag{5.8}$$

where τ_i, are Pauli matrices. The chiral symmetry operator is given by $\Gamma = \tau_z$, such that, $\Gamma H_d \Gamma = -H_d$. No deformation of the Hamiltonian can open a gap without violating chiral symmetry, since the only term opening a gap is proportional to τ_z.

We introduce a band of localized states, and in order to maintain chiral symmetry, we position them at energies $\pm\epsilon_c$. The Hamiltonian describing this situation is given by,

$$H_d' = \begin{pmatrix} k_x \tau_x + k_y \tau_y & \gamma \tau_- \\ \gamma^* \tau_+ & \epsilon_c \tau_x \end{pmatrix}, \tag{5.9}$$

where $\tau_\pm = \tau_x \pm i\tau_y$, and γ represents the interband coupling, causing avoided crossings between the newly introduced localized bands and the linearly dispersive bands. The introduction of these bands induces a global gap in the spectrum. Nevertheless, despite the presence of this gap, the Hamiltonian (5.9) still exhibits ultraviolet divergence.

When we introduce an external vector field while respecting chiral symmetry, we observe the following mechanism: states are pushed up in energy upon the insertion of flux quanta. However, due to the global gap in the energy bands, states cannot reach the upper energy cutoff. As a result, there is no conversion of surface states to bulk states, and consequently, no transversal transport of charge occurs. All the observed phenomena are confined to the surface. Figure 5.2 shows pictorially the situation that we described.

From the boundary perspective, we also observe a detachment between the bulk and the boundary. This detachment allows us to define a surface Chern

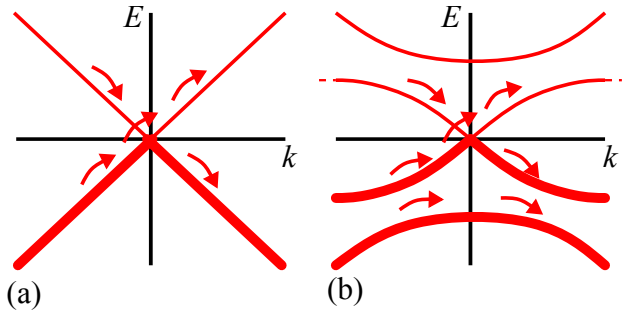

FIGURE 5.2: a) The Dirac spectrum at the surface of a 3-d AIII topological insulator along some axis k. Upon insertion of a flux, states are pushed up and down in energy. b) Inserting bands at energies $\pm\epsilon_c$ effectively cuts the flow of states towards higher energies when a flux is inserted. Taken from [86]

number [97, 98]. The states used to define the Berry curvature are $|\alpha_k\rangle$, with k belonging to the surface Brillouin zone, which represent the positive energy states of the finite band. The Berry curvature and Chern number are given by:

$$\begin{aligned} \Omega_k &= i \langle d\alpha_k | d\alpha_k \rangle , \\ \text{Ch} &\equiv \frac{2}{2\pi} \int_{BZ} \Omega_k . \end{aligned} \tag{5.10}$$

The factor of 2 accounts for the identical contributions of the positive and negative-energy surface bands, which are related by chiral symmetry. As mentioned earlier, the value of the Chern number can vary, but its parity must match the parity of the bulk winding number.

5.2 AIII TOPOLOGICAL INSULATOR MODEL

In this section, we apply the concepts discussed previously to explore a specific model of a three-dimensional AIII topological insulator. We consider a prototypical and minimal model in k-space, described by the Hamiltonian [10],

$$H(k) = \left(M - \sum_{a=x,y,z} \cos k_a \right) \tau_y \sigma_0 + \sum_{a=x,y,z} \tau_x \sigma_a \sin k_a , \tag{5.11}$$

where M is a parameter that controls the topological phase, and we have assumed unit hopping strength. The model involves two sets of Pauli matrices: τ_i acting on the chiral subspace and σ_j on another set of degrees of freedom. The

topological invariant ν for translationally invariant AIII topological insulators is calculated as follows,

$$\nu = \frac{1}{48\pi^2}\int \mathrm{d}^3k\epsilon^{abc}\,\mathrm{Tr}\left(H^{-1}\tau_3\partial_a H H^{-1}\tau_3\partial_b H H^{-1}\tau_3\partial_c H\right), \tag{5.12}$$

yielding the values,

$$\left.\begin{array}{ll}\nu = 1 & \\ \nu = -2 & \text{for} \\ \nu = 0 & \end{array}\right\} \quad \left.\begin{array}{l} 1 < |M| < 3 \\ |M| < 1 \\ \text{else} \end{array}\right\}.$$

In the literature, this model has been classified within class AIII, characterized solely by chiral symmetry. However, by introducing particle-hole symmetry, represented by $U_C = \tau_y\sigma_y$, and defining the time-reversal operator as $U_T = i\tau_x\sigma_y$, we can reclassify it into class DIII, since $U_C H^T(k) U_C = -H(-k)$, $U_T H^T(k) U_T = H(-k)$ and time reversal symmetry squares to -1.

To ensure that we have a model belonging to class AIII, particle-hole symmetry must be broken while preserving chiral symmetry. This is achieved by introducing disorder potentials that respect only chiral symmetry. For practical implementation, we employ the real space representation of the Hamiltonian in a tight-binding model on a cubic lattice,

$$H = M\sum_{\mathbf{R}} |\mathbf{R}\rangle\,\tau_y\sigma_0\,\langle\mathbf{R}| + \frac{1}{2}\sum_{\mathbf{R}}\left(t^a_{\mathbf{R}}\,|\mathbf{R}+e_a\rangle\,(\tau_y\sigma_0 - i\tau_x\sigma_a)\,\langle\mathbf{R}| + h.c.\right), \tag{5.13}$$

where $\mathbf{R}$ are the lattice vectors, e_a are the unit vectors along the lattice directions, and $t^a_{\mathbf{R}}$ are now modified to include static random phase variables,

$$t^a_{\mathbf{R}} \to t\, e^{-i\phi^a_{\mathrm{R}}}, \tag{5.14}$$

where $a \in \{x, y, z\}$ specifies the direction of the nearest-neighbor bond, and the $\{\phi^a_{\mathrm{x}}\}$ are static random phase variables with variance

$$\langle \phi^a_{\mathbf{R}}\phi^{a'}_{\mathbf{R}'}\rangle = W^2\delta_{\mathbf{R}\mathbf{R}'}\delta_{aa'}. \tag{5.15}$$

In subsequent sections, we will investigate the effects of disorder on the properties of this topological insulator model, especially focusing on the topologically non-trivial phase $\nu = 1$. We will begin with a discussion on the properties of the clean version of this insulator.

5.2.1 *Surface Dirac approximation*

According to the bulk-boundary correspondence, a topological invariant ν (or winding number) in bulk corresponds to $|\nu|$ species of gapless Dirac fermions at the boundary. Let us consider a realization of the previous model with a termination in the x-direction at $x = 0$ and let us choose $1 < M < 3$ such that our model's topological invariant is tuned to $\nu = 1$. In going from the bulk of the topological insulator ($x < 0$) to the vacuum at ($x > 0$) we neccesarily close the bands at $x = 0$. Such closure is found at $(k_y, k_z) = (0, 0)$ in the surface Brillouin zone. In the vecinity of the point (k_y, k_z) we can approximate $\sin(k_a) \approx k_a$ and $\cos(k_a) \approx 1 - \frac{k_a^2}{2}$ and we can do the substitution $k_x \to -i\partial_x$. The resulting Hamiltonian is,

$$H \approx \left(-\frac{1}{2}\partial_x - \mu\right) \tau_y\sigma_0 + \tau_x\sigma_x\,(-i\partial_x) + \left(\frac{k_y^2 + k_z^2}{2}\right) \tau_y\sigma_0 + k_y\,\tau_x\sigma_y + k_z\,\tau_x\sigma_z, \tag{5.16}$$

where $\mu = 3 - M$. Given that the closure of the gap occurs at $(k_z, k_y) = 0$ we set them to these values and to find the zero mode,

$$H\big|_{k_{y,z}=0}\,|0, m\rangle = 0 \tag{5.17}$$

where, $|0, m\rangle \equiv |m_z\rangle_\tau\,|m_x\rangle_\sigma\,|\psi\rangle$ with $m \in \{\uparrow, \downarrow\}$ the polarization of the surface state, $|m_z\rangle_\tau$ and $|m_x\rangle_\sigma$ eigenspinors of τ_z and σ_x respectively and $|\psi\rangle$ an envelope function highly localized at $x = 0$ and decaying exponentially into the bulk. To find an effective Hamiltonian for the surface, we project into the space of zero modes,

$$H_{surf} = k_z\sigma'_x + k_y\sigma'_y \tag{5.18}$$

where σ'_a is a set of Pauli matrices acting on the space of zero modes. This particular Hamiltonian was already described in the previous section where we found that it has a fragile obstruction to localization, which is lifted adding extra degrees of freedom to the surface Hamiltonian (5.18).

5.2.2 *Detaching and characterizing surface bands*

In the model outlined by equation (5.13), the surface band is intrinsically connected to the bulk bands. To explore the effects of localized perturbations, a potential is introduced specifically on the surface layers of the system. This potential, while maintaining chiral symmetry, deliberately breaks both particle-hole and time-reversal symmetries. The potential is expressed as,

$$U_{\mathrm{f}} = \sum_{\mathbf{R}\in\text{surface}} \sum_{a=x,y,z} u_{\mathrm{f},a}\,|\mathbf{R}\rangle\,\tau_y\,\sigma_a\,\langle\mathbf{R}|\,, \tag{5.19}$$

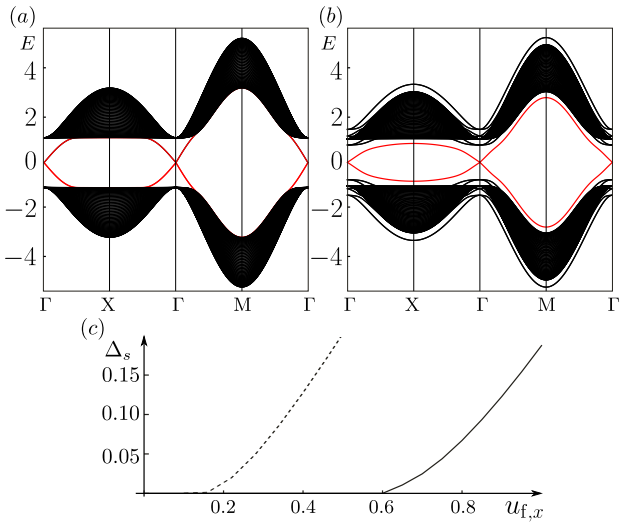

FIGURE 5.3: a) Spectrum of the AIII insulator with M=2 and open boundary conditions in the x–directions. The bulk (surface) spectrum is shown in black (red). There is a single Dirac cone at the Γ point and surface and bulk states merge at high energies. b) Same plot as a) but with the introduction of a fragmenting potential U_f with $n = 3$. Surface and bulk bands dettach. c) Minimal value u_f^c of the fragmenting potential required for the dettachment of bulk and surface bands for only one layer $n = 1$ (solid line) and for 3 layers $n = 3$ (dashed line). Taken from [86].

where $\mathbf{R}$ runs over the outermost n surface layers.

The introduction of the *fragmenting surface potential* has an impact when the magnitude of $u_{f,x}$ exceeds a certain threshold, u_f^c. Beyond this threshold value, an indirect gap emerges between the surface band along the x-direction and the adjacent bulk bands. This gap effectively separates the surface from the bulk, disrupting the spectral flow. The critical magnitude u_f^c that induces this separation is dependent on the number of surface layers included in the definition of U_f (see figure 5.3).

Since we have isolated surface bands it makes sense to define surface Chern numbers defined by its Berry curvature using the equation (5.10). The parity of the Chern number must be the same as the parity of the winding number ν. One way to see this is to consider two Hamiltonians H and H' with winding numbers ν and $-\nu$, and surface Chern numbers Ch and $-\mathrm{Ch}'$ respectively. We construct a new Hamiltonian $\delta H = H \oplus H'$ with vanishing winding number $\nu = 0$ and surface winding number $\mathrm{Ch} - \mathrm{Ch}'$. Since the Hamiltonian δH is trivial, we can deform the surface band and separate the band on positive and

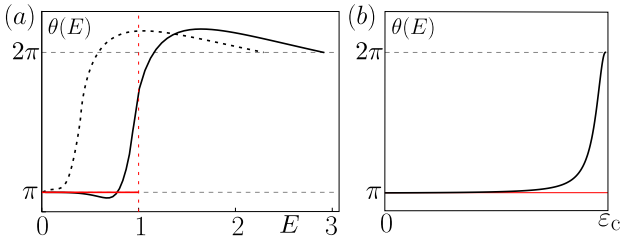

FIGURE 5.4: a) Integrated Berry curvature of the model 5.11 against energy for the case of fragmenting potential $u_{f,x} = 0$(red line),$u_{f,x} = -0.3$ (black solid line) and $u_{f,x} = -0.3$ (black dotted line). The fragmenting potential is applied to $n = 3$ layers and the vertical red line marks the position of the bulk gap. b) Integrated Berry curvature for the Dirac surface model (red line) and for the extended Dirac model with localized bands at $\pm\epsilon_c$ (black line). Taken from [86].

energy band contributions opening a gap at $E = 0$ without closing the gap between the surface and the bulk. The full Chern number of the surface is two times the Chern number of the positive energy band because of the chiral symmetry.

For the particular fragmenting potential consider here, the Chern number takes the values,

$$\mathrm{Ch} = -\operatorname{sgn}(u_{f,x}) \tag{5.20}$$

where the different signs correspond to different choices of gauge, and as we just discussed the difference between the Chern numbers is an even number. From chapter 3 we know that the question of Anderson localization in the presence of weak disorder can be answered by looking at the integrated Berry curvature carried by the states with energy ϵ_k below a reference energy E. For our particular surface band we define the θ angle,

$$\theta(E) = \pi + \int_{0 \leq \epsilon_k \leq E} \Omega_k, \tag{5.21}$$

and the states are delocalized at an energy E, whenever $\theta(E) = \pi \mod 2\pi$. At $E = 0$, $\theta(0) = \pi$ which is consistent with the claim that at zero energy the state is delocalized. Apart from zero energy the θ angle takes values different from π which indicates that this states localize in the thermodynamic limit.

In figure 5.4(a) we see $\theta(E)$ as a function of the reference energy E for a strength on the fragmenting potential $u_{f,x} = -0.3, -1$ applied on the three outermost layers. For energies close to $E = 0$, the fragmenting potential has no effect. However as we increase the strength of the fragmenting potential more and more energies get affected by it. As we approach the bulk gap the value

of $\theta(E)$ differs from π significantly. From the discussion in chapter 3 we know that those states will localize when weak disorder is added to the AIII insulator.

5.3 FIELD THEORY OF THE AIII TOPOLOGICAL INSULATOR

In this section, we explore the impact of disorder on the AIII topological insulator model outlined previously. Specifically, we examine how disorder influences the topological properties and interacts with Anderson localization. To achieve this, we utilize field theory tools to develop theories for both the bulk and the boundary of the system. Following the development of the field theory, we will compare the information that we can extract from them with the results discussed earlier, thereby contextualizing the effects of disorder in AIII topological insulator. As we have seen before the case at $E = 0$ and $E \neq 0$ behave differently and we will discuss them separately.

5.3.1 *Field theory at $E = 0$*

To develop a theoretical framework at zero energy, $E = 0$, we begin by defining the Hamiltonian H_0 as shown in equation (5.11). Within the basis where the chiral symmetry operator Γ is represented as τ_3, the Hamiltonian takes a fully off-diagonal form,

$$H_0 = \begin{pmatrix} 0 & h \\ h^\dagger & 0 \end{pmatrix}, \tag{5.22}$$

with h given by:

$$h = \sum_{a=x,y,z} \sigma_a \sin k_a - i \left(M - \sum_{a=x,y,z} \cos k_a \right) \sigma_0 \tag{5.23}$$

We then introduce a disorder potential $\hat{V}$, which anticommutes with Γ,

$$\hat{V} = \begin{pmatrix} 0 & V_+ \\ V_- & 0 \end{pmatrix}, \tag{5.24}$$

where $V_- = V_+^\dagger$. This random potential $\hat{V}$ is assumed to originate from a Gaussian ensemble and is spatially uncorrelated,

$$\begin{aligned} \langle V_+(x) \rangle &= 0 \\ \langle V_-(x) \rangle &= 0 \\ \langle V_+(x) V_-(x') \rangle &= \frac{\gamma^2}{2} \mathbb{1} \delta(x - x'). \end{aligned} \tag{5.25}$$

To address the disordered system, we explore the problem using the replica formalism by considering R copies of the zero-energy partition function Z^r. The partition function at zero energy is expressed as,

$$Z = \int D\psi D\bar{\psi} \exp\left\{ \left(i \int \mathrm{d}^3x \, \bar{\psi}(-\mathcal{H})\psi \right) \right\} \tag{5.26}$$

and the action for the replicated system is,

$$S[\psi, \bar{\psi}] = i \int d^3x \, \left(\bar{\psi}_+^a \, (h + V_+) \, \psi_-^a + \bar{\psi}_-^a (h^\dagger + V_-) \psi_+^a \right). \tag{5.27}$$

This action remains invariant under certain transformations, maintaining symmetry under the group $U(2R) \times U(2R)$,

$$\begin{aligned} \bar{\psi}_+ \to \bar{\psi}_+ T_L, \quad \bar{\psi}_- \to \bar{\psi}_- T_R, \\ \psi_+ \to T_R^{-1} \psi_+, \quad \psi_- \to T_L^{-1} \psi_-, \end{aligned} \tag{5.28}$$

Upon averaging the replicated partition function over the disorder, a quartic interaction term in the fermionic fields emerges in the effective action,

$$S[\bar{\psi}, \psi] = i \int \mathrm{d}^3x \, \left(\bar{\psi}_+^a h \psi_-^a + \bar{\psi}_-^a h^\dagger \psi_+^a - i\gamma^2 \, \psi_-^a \bar{\psi}_-^b \psi_+^b \bar{\psi}_+^a \right). \tag{5.29}$$

We decouple this quartic term by considering two new matrix fields A_+, A_- and we integrate over fermions, where we obtain the following effective action,

$$S[A_+, A_-] = \frac{1}{\gamma^2} \int \mathrm{d}^3x \, \mathrm{tr}(A_+ A_-) - \mathrm{tr} \log \begin{pmatrix} A_+ & -h \\ -h^\dagger & A_- \end{pmatrix}. \tag{5.30}$$

As we did previously with the Chern insulator we perform a saddle point analysis of this action where we obtain, mean field equations for A_+ and A_-. We notice that this solutions break the $U(2R) \times U(2R)$ group down to $U(2R)$. The mean field solution $\bar{A}_+$ can be parametrized by a matrix $i\kappa\tau_3 M$ belonging to $U(2R)$ and accordingly $\bar{A}_- = i\kappa M^{-1}\tau_3$. Details of this analysis can be found in appendix D. We can write an effective action in terms of a spatially dependent M,

$$S[M] = -\,\mathrm{tr} \log \begin{pmatrix} i\kappa\tau_3 & -h - M^{-1}[h, M] \\ -h^\dagger & i\kappa\tau_3 \end{pmatrix} \tag{5.31}$$

The term with the commutator can be expanded up to second order in derivatives of space and momentum using the Moyal expansion,

$$M^{-1} * [h*, M] \approx \Phi_i(x) \partial_{p_i} h + \frac{1}{2} \Phi_i(x) \Phi_j(x) \, \partial^2_{p_i, p_j} h \tag{5.32}$$

where $\Phi_i = \partial_{x_i} M^{-1} M$. We can expand this action up to third order in Φ to obtain,

$$S[\Phi] = -\operatorname{tr}(G_0 F) - \operatorname{tr}(G_0 J) + \frac{1}{2}\operatorname{tr}(G_0 F G_0 F) - \frac{1}{3}\operatorname{tr}(G_0 F G_0 F G_0 F), \quad (5.33)$$

with,

$$\begin{aligned} G_0 &= \begin{pmatrix} i\kappa\tau_3 & -h \\ -h^\dagger & i\kappa\tau_3 \end{pmatrix}^{-1} = \frac{-1}{\kappa^2 + |h|^2}\begin{pmatrix} i\kappa\tau_3 & h \\ h^\dagger & i\kappa\tau_3 \end{pmatrix}, \\ F &= \begin{pmatrix} 0 & -\Phi_i(x)\partial_{p_i} h \\ 0 & 0 \end{pmatrix}, \\ J &= \begin{pmatrix} 0 & -\frac{1}{2}\Phi_i(x)\Phi_j(x)\,\partial^2_{p_i,p_j} h \\ 0 & 0 \end{pmatrix}. \end{aligned} \quad (5.34)$$

For example, taking as a particular model the Dirac version of the action 5.11 yields the following action (see appendix D.2), a non-linear σ model with a topological term counting the windings of unitary matrices over S^3 [10, 99, 100] is obtained,

$$S[M] = g\int \mathrm{d}^3x\ \operatorname{tr}\left(\partial_i M \partial_i M^{-1}\right) + \frac{\vartheta}{24\pi^2}\int \mathrm{d}^3x\,\epsilon^{ijk}\operatorname{tr}\left(M^{-1}\partial_i M M^{-1}\partial_j M M^{-1}\partial_k M\right) \quad (5.35)$$

where g is the conductivity and ϑ a topological parameter. For energies away from zero an additional term appears, $S_E[M] = E\nu\int \mathrm{d}^3x \operatorname{tr}(M + M^{-1})$, which is often called the mass term.

At $E = 0$, in the limit of increasingly large distances we expect the parameters to renormalize to $(g, \vartheta) = (0, 2\pi n)$, where n is an integer. In this case we say that we have a topological Anderson insulator. In this limit the topological term can be transformed into a boundary term, which takes the well-know form of $\Gamma[M]/12\pi$ a Wess-Zumino-Witten [101] term of the surface action. Close to the boundary we might then obtain an action,

$$S_\partial = g_s\int \mathrm{d}^2x\,\partial_i \tilde{M}\partial_i \tilde{M}^{-1} + \frac{\Gamma[M]}{12\pi}, \quad (5.36)$$

where $\tilde{M}$ are the same matrix fields but restricted to the surface and g_s the surface conductivity. At large scales it renormalizes to a conformally invariant action with $g_s = 1/8\pi$ [101, 102] representing a two-dimensional Dirac point at zero energy.

At $E \neq 0$, the strongly relevant (in the renormalization group sense) mass term $S_E[M]$, only admits configurations $M \equiv Q = T\tau_3 T^{-1}$, implying the vanishing of the terms $S_E[Q]$ and $\Gamma[Q]/12\pi$. This configuration breaks the symmetry

from $U(2R)$ down to $U(2R)/(U(R)\times U(R))$, the Goldstone manifold of a class A system. The action is reduced to a usual non-linear σ model describing a 3-d metal below the Anderson transition point, meaning that in this limit the system behaves as a Anderson insulator. There is another case that one might consider, the limit of small energies, i.e, energies close to 0. We may use the surface action (5.36) where the Wess-Zumino-Witten term is reduced to the θ term of the Pruisken action tuned into criticality, $\theta=(2n+1)\pi$, with $n\in\mathbb{Z}$ [101]. Close to zero energy the surface states close to $E=0$ show a tendency to delocalization, away from it we need to analyze the situation using what we have learned from the previous sections.

5.3.2 *Field theory of the AIII insulator at the surface*

The theory of the surface of the disordered AIII insulator can be obtained with the theory we devised for $2-d$ systems in the last chapter. In particular we might start from equation (3.30), where $Q(x)=T(x)\tau_3T^{-1}(x)$ is the projection onto the surface of the matrix fields defined in the previous section. To describe the Hamiltonian on the surface we first must notice that *i*) a Dirac description of the Hamiltonian might be incomplete, specially since the interesting phenomena might happen close the the bulk bands and a Dirac approximation totally washes away this information, *ii*) there is no lattice representation of the surface of the AIII insulator. With this in mind we consider a spectral decomposition of the AIII surface Hamiltonian,

$$H_s(k)=\sum_\alpha |\alpha_k\rangle\,\epsilon_{\alpha_k}\,\langle\alpha_k|\,, \tag{5.37}$$

where $\{|\alpha_k\rangle\}$ are the systems eigenstates at a given transverse momentum, however it must be noticed that the decomposition does not include all eigenstates at a given k. Only states that have a finite spatial overlap with $Q(x)$ contribute to the tr log expansion described in section (3.3.1). The usual candidates are the two chiral eigenstates on the surface band. Nevertheless, given the internal structure of the spinor, 4 states per momentum k are needed and just 2 states are insufficient. To avoid looking into the bulk to get the rest of the states, we consider eq. (5.37) as a formal complete sum. Furthermore, we considered a flattened version of the Hamiltonian (5.11) with a fragmenting surface potential. The consequence would be that there is a finite spectral gap between the surface and bulk bands. As mentioned before, applying a field theoretical analysis to the surface we find once more an effective non-linear σ model with a Pruisken θ- term. The coefficient accompanying the θ term takes on the form (at small disorder strengths),

$$\theta=\frac{1}{\pi}\int \mathrm{d}^2k\,\Omega_k\Theta(\epsilon_\alpha-E) \tag{5.38}$$

which is the equation used in the last section to determine the topological properties of the surface states. One big difference from the Chern insulator described in the previous chapter is that the contribution from the upper and lower surface bands does not need to add to zero, this is possible due to the system being the surface of a $3d$, i.e, at the surface we have effectively one isolated band.

We have discovered that, away from zero energy and in a disordered AIII insulator where the surface and bulk bands are detached, the phenomenology resembles that of the integer quantum Hall effect (IQHE). Remarkably, according to the renormalization flow diagram for the IQHE (see figure 2.10), the coefficient θ will flow to $2\pi n$, and the corresponding conductivity g will flow to zero in the limit of long scales, indicating localization. Consequently, for energies $E \neq 0$, the states are localized. However, in the special case when $\theta = \pi n$, we observe spectrum-wide criticality, which occurs when the surface and bulk bands are joined. It means that there is a delocalized state in the bulk connecting the boundaries.

5.4 SURFACE HALL CONDUCTANCE

In the previous sections we provided an explicit term that detaches the surface and the bulk. Moreover we found that once we do this, we can define a surface Berry curvature and therefore there is a well defined Chern number on the surface. Once we compute the integral of the Berry curvature up until some reference energy E we can elucidate the Anderson localization properties of the states at that given energy. The value of the Chern number depends on the sign of the fragmenting potential $u_{f,x}$. We could now ask what happens when we consider a situation when the fragmenting potential changes sign along the surface. For definiteness let us consider the example of two domain walls in the surface plane parallel to the $y-z$ plane. We assume periodicity in the y-direction which forces the surface to have two domain walls. Alternatively one could deform the slab geometry into a cylinder, converting the x–direction into a radial direction and the y–direction into the angular periodic direction (see figure (5.5)). We expect to find two 1-d counterpropagating chiral propagating modes along the z-direction at the points where the domain wall changes sign. Interestingly these chiral modes connect the surface and bulk bands as can be seen in figure (5.6).

In the clean model, these states are supported by only by states inside the high-lying band gap, below it, they hybridize with the surface states. As we discussed in the previous section, in the presence of disorder and at $E \neq 0$ surface states localize, however the chiral modes do not. In order for them to survive they extend their support over the whole surface spectrum (see figure

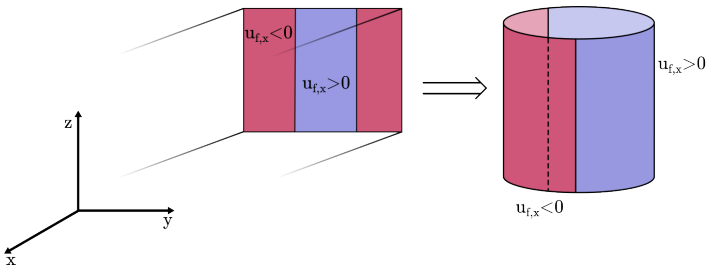

FIGURE 5.5: Description of domain walls placed at one of the surfaces of AIII insulator parallel to the y-z plane. Equivalently with periodic boundary condition in the y-axis we can deform the AIII insulator to a cylinder where at its surface we can place the domain walls.

5.6). They hybridize with the topologically delocalized states at $E = 0$ and with delocalized states in the bulk. The domain walls and thus the chiral modes propagating along them forbid a full localization of states at high energies.

At $E \neq 0$ the chiral symmetry is effectively broken so each surface might be treated as an effective 2-d system in class A. In this way the chiral modes propagating along the domain walls are to be identified with the edge states appearing in the quantum Hall insulator and we can apply the Laughlin's argument applies. These chiral modes must hybridize with the topologically protected delocalized state at $E = 0$ while at high energies it hybridizes with the bulk modes or with high lying surface states. Either, they presence of a domain wall modes prevents the full localization of states at high energies.

With these observations in mind we can consider a random surface fragmenting potential varying in space, in the case where $\langle u_{f,x} \rangle = 0$ we have puddles of positive and negative surface Chern number occurring with the same probability. At the boundary of these puddles we have propagating and counterpropagating chiral modes. Since the puddles occur with equal probability we expect the chiral modes to create a network across the whole surface. This network is remniscent of a Chalker-Coddington network of the integer quantum Hall effect at criticality [103]. Is at this point where the model predicts a percolation of states evading Anderson localization. This is the mechanism behind spectrum wide criticality since all states inside the bulk at all energies appear to be delocalized. In the case where the average of positive and negative puddles is not the same, i.e, $\langle u_{f,x} \rangle \neq 0$ we do not have a network connecting all the chiral modes and therefore we expect localization. From this argument it is clear that spectrum-wide criticality corresponds to a very specific type of disorder and that for general disorder all states at $E \neq 0$ localize. According to our diagnostic tool in equation (5.38) the localized case must show an average positive or negative surface integrated Berry curvature .

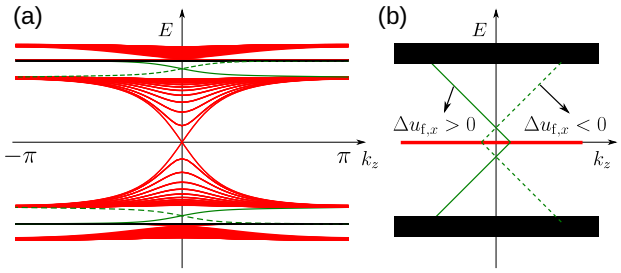

FIGURE 5.6: a) Band structure for a slab geometry of the flattened version with open boundary conditions in the x direction and two domain walls and periodic boundary conditions in y (see figure 5.5). The fragmenting potential is placed only in the outermost layer $n = 1$ and switches from 0.2 to -0.2 and back at the domain walls. The bulk, surface and domain wall part of the spectrum are show in black, red and green respectively. The solid green lines correspond to the case of a domain walls going from positive to negative and back to positive whereas the dashed green line correspond to the case of domain walls going from negative to positive and back to negative. b) In the presence of disorder only the state at $E = 0$ is delocalized. The chiral modes at the domain walls are expected to extend from the bulk all the way down to the zero energy state. Taken from [86].

5.5 CONCLUSION

In topological insulator in the Wigner-Dyson classes (class A, AI, AII) the boundary states are continously connnected to the states in the bulk which are delocalized. This connection of bulk and boundary allows for states to be transported from different boundaries through the bulk given rise to observables (e.g, the quantized Hall conductance in 2-d class A topological insulators). In this chapter we showed that topological insulators in the non-Wigner-Dyson classes do not generally have states connecting bulk and boundaries.

In the literature, non-trivial topology is associated with the obstruction to the construction of a localized basis of conduction and valence bands, reffered to as *Wannierizability*. Nevertheless, we show that topological insulators in the non-Wigner-Dyson classes enjoy this property, i.e, they are Wannier localizable and topologically non-trivial. We showed this from the bulk perspective, arguing that Wannier localizability implies the fragility of the connection between surface and bulk bands. From the boundary perspective we showed that the theory admits gap opening perturbations that respect the symmetries. At the surface we saw that the addition of disorder makes all the states Anderson

localize except the one at $E = 0$, a state that it is protected against Anderson localization by topology.

The existence of gapless surface states has been a key signature of topological insulators. However we see that this characteristic is only shared by systems in the Wigner-Dyson classes while for genuine[1] non-Wigner-Dyson surface states away from $E = 0$ can be, but not need to be, delocalized.

We showed that for a minimal model of a class AIII topological insulator with $\nu = 1$ we were able to detach surface and bulk bands, Anderson localize all the states with energies $E \neq 0$ and define a surface Chern number. Additionally at the transition point between phases with different surface Chern numbers we observe spectrum wide criticality. In the presence of disorder we use a powerful tool to probe Anderson localization, namely, the integrated Berry curvature (5.38) in which we integrate over all surface states below the energy E that we want to analyze. For energies E in which the integrated Berry curvature takes odd-integer values we see delocalization, for the other values we see localization.

Similar to the conclusions from previous chapters we see once more that for certain systems the Dirac approximation to surface states is incomplete. In the present context, they do not account for the surface Berry curvature, a phenomenon that we show to happen at high energies. From the perspective of the Dirac theory at the surface to truly describe the phenomena described in this chapter we need to add trivial bands to the minimal Dirac model. The addition of the these bands and the way the change the surface physics of the minimal model is important to determine the possibility of Wannier localizing the bulk.

For winding numbers $|\nu| = 1$ the meaning of minimal model and the tools to measure delocalization are not yet clear. It is well-established that a Wannier localizable bulk implies a gappable surface for genuine non-Wigner-Dyson classes. However, the ways in which the minimal Dirac description is fragile, and the relation between localizability and Berry curvature, need not straightforwardly generalize beyond the $\nu = 1$ AIII context.

1 Genuine non-Wigner-Dyson topological insulators are those in which the presence of chiral symmetry and/or particle-hole symmetry is essential for their topological protection.

A

APPENDIX A

A.1 REPLICA TRICK

In this appendix we give a brief account of the replica trick and its uses in field theory. In the treatment of quenched disorder systems we have to average the observables we are interested in over different disorder configurations. Formally the average of an observable $\mathcal{O}$ over a ensemble of disordered systems looks like,

$$\langle \mathcal{O} \rangle_{dis} = -\langle \frac{1}{\mathcal{Z}} \frac{\delta}{\delta J} \Big|_{J=0} \mathcal{Z} \rangle_{dis}. \tag{A.1}$$

The fact that the partition function is in the denominator makes the disorder average extremely complicated. To remedy this complication we take R copies [18] of the system described by the R-th power of the partition function. The importance of taking R copies rests on the following formal relations regarding an observable $\mathcal{O}$,

$$\begin{aligned} \mathcal{O} &= -\frac{\delta}{\delta J}\Big|_{J=0} \ln \mathcal{Z} \\ &= -\frac{\delta}{\delta J}\Big|_{J=0} \lim_{R\to 0} \frac{1}{R} \left(\exp\{(R \ln \mathcal{Z})\} - 1\right) \\ &= -\frac{\delta}{\delta J}\Big|_{J=0} \lim_{R\to 0} \frac{\mathcal{Z}^R}{R}. \end{aligned} \tag{A.2}$$

Instead of calculating the logarithm of the partition function, we calculate its R-power, making the problem of calculating the disorder average more tractable. We have, nevertheless, to analytically continue $R \to 0$, and there is, in principle, no guarantee that this procedure yields a legitimate outcome. Due to the arising issues, the method is dubbed as a mere trick. Despite the uncertainty, the trick has proven useful and it should not cause any complications in the systems considered in this thesis.

We represent the replicated partition function as a coherent state field integral

$$\mathcal{Z}^R = \int D(\bar{\psi}, \psi) \exp\left\{ \left[-\sum_{a=1}^{R} S[\bar{\psi}^a, \psi^a, J] \right] \right\}, \tag{A.3}$$

where $\psi^a, \bar{\psi}^a$, $a = 1, \ldots, R$, denote the Grassmann field of the a-th copy of the system, $D(\bar{\psi}, \psi) = \prod_{a=1}^{R} D(\bar{\psi}^a, \psi^a)$, and $S[\bar{\psi}^a, \psi^a, J] = S_0[\bar{\psi}^a, \psi^a] + S_{int}[\bar{\psi}^a, \psi^a] +$

$S_s[\bar{\psi}^a, \psi^a, J]$. Taking as an example the free electron gas, we disregard the interacting part of the action S_{int}. The non-interacting part is given by,

$$S_0[\bar{\psi}^a, \psi^a] = \int \mathrm{d}^d x\, \bar{\psi}^a(\mathbf{x}) \left(E - \frac{\nabla^2}{2m} + V(\mathbf{x}) \right) \psi^a(\mathbf{x}), \tag{A.4}$$

and S_s is the source-dependent part of the action. It is worth noting that up to this point, the action is diagonal in the replica space.

We compute the disorder average of the replicated partition function as,

$$\left\langle \mathcal{Z}^R \right\rangle_{dis} = \int D(\bar{\psi}, \psi) \exp\left\{ \left[-\sum_{a=1}^{R} S_{cl}[\bar{\psi}^a, \psi^a, J] - \sum_{a,b=1}^{R} S_{dis}[\bar{\psi}^a, \bar{\psi^b}, \psi^a, \psi^b] \right] \right\}, \tag{A.5}$$

where $S_{cl} = S|_{V=0}$, and

$$S_{dis}[\bar{\psi}^a, \bar{\psi^b}, \psi^a, \psi^b] = -\frac{\gamma^2}{2} \int \mathrm{d}^d x\, \bar{\psi}^a(\mathbf{x}) \psi^a(\mathbf{x}) \bar{\psi}^b(\mathbf{x}) \psi^b(\mathbf{x}), \tag{A.6}$$

is obtained by a direct Gaussian integration. The consequence of the disorder average is to add a quartic potential where the particles with different replica index interact. The expectation value of an observable $\mathcal{O}$ over the disorder is computed, using (A.2), as,

$$\langle \mathcal{O} \rangle_{dis} = \left\langle -\frac{\delta}{\delta J}\bigg|_{J=0} \lim_{R\to 0} \frac{\mathcal{Z}^R}{R} \right\rangle_{dis} = \lim_{R\to 0} \frac{\delta}{\delta J}\bigg|_{J=0} \frac{\left\langle \mathcal{Z}^R \right\rangle_{dis}}{R} = \lim_{R\to 0} \frac{1}{R} \sum_{a=1}^{R} \langle \mathcal{O}(\bar{\psi}^a, \psi^a) \rangle_{\psi}, \tag{A.7}$$

where we have used (a) the independence of the source J with respect to the replica index a (each replica has the same source), (b) The disorder potential does not "touch" the source term S_s in the action, and (c) $\langle \mathcal{O}(\bar{\psi}^a, \psi^a) \rangle_{\psi}$ is the expectation value with respect to the action with the new quartic potential in the coherent state representation of $\mathcal{O}$.

In this way we circumvent the problem of averaging over

A.2 SELF CONSISTENT BORN APPROXIMATION

In this appendix we discuss the self consistent Born approximation and in general the role of the parameters κ and ΔE. The starting point is the self consistent Born equation for the matrix $A(x)$,

$$A(\mathbf{x}) = W^2 \,\mathrm{tr}\, (E + i\delta\tau_3 - H - A)^{-1} (\mathbf{x}, \mathbf{x}).$$

We propose a spatially homogeneous and matrix diagonal Ansatz of the form $\bar{A} = \Delta E + i\kappa\tau_3$. Plugging in the Ansatz into the previous expression, we obtain a self-consistent equation for both ΔE and κ.

$$\Delta E + i\kappa\tau_3 = \frac{W^2}{2}\int_{BZ}\frac{\mathrm{d}^2k}{(2\pi)^2}\ \mathrm{tr}\left(\frac{1}{E - H(\mathbf{k}) - \Delta E - i\kappa\tau_3}\right).$$

The real part of the previous equation, ΔE, represents nothing more than an overall shift in the energy E of the system. The imaginary part is the self energy due to impurity scattering which is to be identified with (2 times) the scattering rate off impurities and consequently defines another quantities of interest such as the elastic scattering time τ and the mean free path ℓ.

B

APPENDIX B

B.1 DERIVATION OF THE TOPOLOGICAL ACTION

We here derive Eq.(3.34) for the topological action by explicit computation of the two contributing terms $S^{(1,2)}_{\rm top}$, i.e. the skew-derivative contributions to the first and second order gradient term in Eq. (3.32).
$S^{(2)}_{\rm top}$: The expanded representation of the second order term reads

$$\begin{aligned}
S^{(2)}[Q] &= \frac{1}{2}\int \mathrm{d}^2x(\mathrm{d}^2k)\,\mathrm{tr}(D(i\kappa\tau_3+v_\mu\sigma^\mu)F_i\Phi_i D(i\kappa\tau_3+v_\nu\sigma^\nu)F_{\bar{i}}\Phi_{\bar{i}}) \\
&\to -\frac{1}{2}\int \mathrm{d}^2x(\mathrm{d}^2k)\,\mathrm{tr}(D(i\kappa\tau_3+v_\mu\sigma^\mu)(\sigma_a\partial_i h_a\Phi_i)D(i\kappa\tau_3+v_\nu\sigma^\nu)(\sigma_b\partial_{\bar{i}}h_b\Phi_{\bar{i}})) \\
&= -i\kappa\int \mathrm{d}^2x(\mathrm{d}^2k)\,\mathrm{tr}(D\tau_3(\sigma_a\partial_i h_a\Phi_i)D(h_c\sigma_c)(\sigma_b\partial_{\bar{i}}h_b\Phi_{\bar{i}})) \\
&= -2\kappa\epsilon_{abc}\int \mathrm{d}^2x(\mathrm{d}^2k)\,\mathrm{tr}(D\tau_3\Phi_i D\Phi_{\bar{i}})\partial_i h_a\partial_{\bar{i}}h_b h_c \\
&= -2\kappa\epsilon_{ij}\int \mathrm{d}^2x(\mathrm{d}^2k)\,\mathrm{tr}(D\tau_3\Phi_i D\Phi_j)F_k, \qquad \text{(B.1)}
\end{aligned}$$

where $(\mathrm{d}^2k)=\mathrm{d}k_1\mathrm{d}k_2/(2\pi)^2$, the arrow indicates that we retain only derivative combinations $\partial_i\partial_{\bar{i}}$, $\bar{i}=(i+1)\mathrm{mod}\,2$, and we used the definition Eq. (3.36). To process the integral over k, we decompose the matrices $D=D^+P^+ + D^-P^-$, $P^s=\frac{1}{2}(1+s\tau_3)$ into advanced and retarded contributions and note that only momentum integrals over denominators D^+D^- of opposite causality are non-vanishing. In this way we arrive at

$$S^{(2)}_{\rm top}[Q] = -\frac{\theta_1}{4\pi}\int \mathrm{d}^2x\sum_s s\epsilon_{ij}\,\mathrm{tr}\big(P^s\,\Phi_i\,P^{\bar{s}}\Phi_j\big), \qquad \text{(B.2)}$$

with the momentum integral θ_2 defined in Eq. (3.35). We finally use the first of the auxiliary relations

$$\begin{aligned}
-4\epsilon_{ij}\sum_s \mathrm{tr}(sP^s\Phi_i P^{\bar{s}}\Phi_j) &= \mathcal{L}_{\rm top}(Q), \\
4\epsilon_{ij}\mathrm{tr}(\tau_3\partial_i\Phi_j) &= \mathcal{L}_{\rm top}(Q), \qquad \text{(B.3)}
\end{aligned}$$

to obtain $S^{(2)}_{\rm top}$ as given in Eq. (3.34).

$S^{(2)}_{\text{top}}$: Being first order in derivatives, the contribution from the term $S^{(1)}$ naively seems to vanish. To see that it does not, we play a trick first applied by Pruisken in his analysis of the quantum Hall effect. Noting that the energy-dependent Green function $G \equiv G_E$ can be written as $G_E = \int_E^\infty \mathrm{d}\omega\, G_\omega^2$, we represent the action as (in the same notation, $D_\omega \equiv D_{E=\omega}$)

$$\begin{aligned}
S^{(1)}_{\text{top}}[Q] &= -\int_E^\infty \mathrm{d}\omega\, \mathrm{Tr}(G_\omega F_i \Phi_i G_\omega) \\
&\to -\frac{i}{2}\int_E^\infty \mathrm{d}\omega \int \mathrm{d}^2x(\mathrm{d}^2k)\, \mathrm{tr}\big((\partial_j G_\omega)F_i(\partial_j\Phi_i)G_\omega - G_\omega F_i(\partial_j\Phi_i)\partial_j G_\omega\big) \\
&= -\frac{i}{2}\int_E^\infty \mathrm{d}\omega \int \mathrm{d}^2x(\mathrm{d}^2k)\, \mathrm{tr}\big([(\partial_j G_\omega), G_\omega]F_i\partial_j\Phi_i\big) \\
&= -\frac{1}{2}\int_E^\infty \mathrm{d}\omega \int \mathrm{d}^2x(\mathrm{d}^2k)\, \mathrm{tr}\Big(D_\omega^2[\partial_j(h_a\sigma_a), h_b\sigma_b](\partial_i h_c\sigma_c)\partial_j\Phi_i\Big) \\
&= -2i\int_E^\infty \mathrm{d}\omega \int \mathrm{d}^2x(\mathrm{d}^2k)\epsilon_{ij}\, \mathrm{tr}\Big(D_\omega^2\partial_j\Phi_i\Big)F_k. \qquad \text{(B.4)}
\end{aligned}$$

We now decompose the matrix D again, and note that only the contribution proportional to τ_3 yields a non-vanishing trace, $D^2 \to \frac{1}{2}(D^{+2} - D^{-2})\tau_3$. As a result, we obtain

$$S^{(1)}_{\text{top}}[Q] = \frac{\theta_2}{4\pi}\int \mathrm{d}^2x\, \epsilon_{ij}\, \mathrm{tr}(\tau_3\partial_i\Phi_j), \qquad \text{(B.5)}$$

with θ_2 given in (3.35). In a final step, we use the second of the auxiliary relations (B.3) to arrive at the contribution $S^{(1)}$ to (3.34).

B.2 DERIVATION OF THE GRADIENT ACTION

We here derive Eq. (3.40) by inspection of the two terms $S^{(1,2)}$ in the formal gradient expansion Eq. (3.32).

$S^{(1)}_{\text{grad}}$: Filtering symmetric derivative combinations from the explicit representation of the second order expansion we obtain

$$\begin{aligned}
S^{(2)}_{\text{grad}}[Q] &= \frac{1}{2}\int \mathrm{d}^2x(\mathrm{d}^2k)\,\mathrm{tr}\big(D(i\kappa\tau_3 + v_\mu\sigma^\mu)F_i\Phi_i D(i\kappa\tau_3 + v_\nu\sigma^\nu)F_j\Phi_j\big)\\
&\to -\frac{1}{2}\int \mathrm{d}^2x\,(\mathrm{d}^2k)\,\mathrm{tr}\Big(-\kappa^2 D\tau_3\sigma_\nu\Phi_i D\tau_3\sigma_\lambda\Phi_i + Dv_\mu\sigma^\mu\sigma_\nu\Phi_i Dv_\rho\sigma^\rho\sigma_\lambda\Phi_i\\
&\qquad\qquad + 2iE\kappa\, D\tau_3\sigma_\nu\Phi_i D\sigma_\lambda\Phi_i\Big)\partial_i v_\nu\partial_i v_\lambda\\
&= -\int \mathrm{d}^2x(\mathrm{d}^2k)\sum_a \mathrm{tr}\Big(-\kappa^2\,\tau_3 D\Phi_i\tau_3 D\Phi_i + (E^2-\epsilon^2+2h_a^2)D\Phi_i D\Phi_i\\
&\qquad\qquad + 2iE\kappa\, D\tau_3\Phi_i D\Phi_i\Big)\partial_i h_a\partial_i h_a,
\end{aligned}$$

where "$\to$" indicates that we retain only derivatives with identical i-index, and in the second equality traced over Pauli matrices. To compute the k-integrals, we again decompose $D = D^+P^+ + D^-P^-$. The product of two D's then leads to terms $D^sD^{s'}$ of equal and opposite causal index s, s', which need to be considered separately.

Using the auxiliary relations

$$\begin{aligned}
\sum_s \mathrm{tr}\left(\Phi_i\tau_3^n P^s\Phi_i\tau_3^m P^{-s}\right) &= \frac{1}{4}\,\mathrm{tr}\left(\partial_i Q\partial_i Q\right)\times\\
&\times\begin{cases} -1 & (n,m)=(0,0),\\ 1 & (n,m)=(1,1),\\ 0 & (n,m)=(0,1),(1,0)\end{cases},
\end{aligned}$$

and

$$\begin{aligned}
&\sum_s \mathrm{tr}\left(\Phi_i\tau_3^n P^s\Phi_i\tau_3^m P^s\right) f_s =\\
&\quad = -\sum_s s^{n+m}\,\mathrm{tr}\left(\frac{1}{4}\partial_i Q\partial_i Q - P^s\Phi_i^2\right) f_s,
\end{aligned}$$

where f_s is arbitrary, it is straightforward to obtain

$$S^{(2)}_{\text{grad}}[Q] = (I_+ + I_- + I_{+-})\int \mathrm{d}^2x\,\mathrm{tr}\left(\partial_i Q\partial_i Q\right) + S_{\text{A}}, \tag{B.6}$$

with $S_{\text{A}} = 4\sum_s I_s\int \mathrm{d}^2x\,\mathrm{tr}\big(P^s\Phi_i^2\big)$, and the coefficients defined in Eq. (3.41)

$S^{(1)}_{\text{grad}}$: The terms with equal indices, J_{ii} in Eq. (3.32) yield a term

$$\begin{aligned} S^{(1)}_{\text{grad}} &= \frac{1}{2}\,\text{Tr}\Big(GJ_{ii}\Phi_i^2\Big), \\ &= \frac{1}{2}\int \mathrm{d}^2x(\mathrm{d}^2k)\sum_s \text{tr}\left(G^sP^s\partial_i^2 v_\mu\sigma_\mu\Phi_i^2\right), \\ &= \frac{1}{2}\int \mathrm{d}^2x(\mathrm{d}^2k)\sum_s \text{tr}\left(G^s\partial_i v_\nu\sigma_\nu G^s\partial_i v_\mu\sigma_\mu P^s\Phi_i^2\right), \\ &= -S_{\text{A}} \end{aligned}$$

where we integrated by parts and used that $\partial_i G^s = -G^s\partial_i h_\nu\sigma_\nu G^s$. We conclude that the anomalous terms, S_{A} cancel out and arrive at the full gradient action Eq. (3.40).

B.3 DERIVATION OF EQ. (3.42)

In this appendix we take a closer look at the derivation of equation (3.42). The first thing to notice is that I can be written as the following,

$$\begin{aligned} I =& \frac{1}{4}\sum_a\int(\mathrm{d}^2k)((E+i\kappa)D^+ + (E-i\kappa)D^-)^2 + (2h_a^2-\epsilon^2)(D^+ + D^-)^2(\partial_i h_a\partial_i h_a), \\ =& \sum_a\int(\mathrm{d}^2k)\frac{E^2(E^2+\kappa^2-\epsilon^2)^2 + (2h_a^2-\epsilon^2)(E^2-\kappa^2-\epsilon^2)^2}{((E^2-\kappa^2-\epsilon^2)^2+4E^2\kappa^2)^2}(\partial_i h_a\partial_i h_a), \\ =& \sum_a\int(\mathrm{d}^2k)\frac{E^2(E^2+\kappa^2-\epsilon^2)^2 + (2h_a^2-\epsilon^2)(E^2-\kappa^2-\epsilon^2)^2}{((E^2-\kappa^2-\epsilon^2)^2+4E^2\kappa^2)(2|E|\kappa)} \\ & \times\left(\frac{2|E|\kappa}{(E^2-\kappa^2-\epsilon^2)^2+4E^2\kappa^2}\right)(\partial_i h_a\partial_i h_a). \end{aligned}$$

To make further progress we take the limit when $E\kappa \to 0$ resulting in,

$$\begin{aligned} I &= \pi\sum_a\int(\mathrm{d}^2k)\,\frac{E^2-\epsilon^2+2h_a^2}{2|E|\kappa}(\partial_i h_a\partial_i h_a)\delta(E^2-\epsilon^2), \\ &= \pi\int(dk)\frac{\sum_a h_a^2(\partial_i h_a\partial_i h_a)}{|E|\kappa}\delta(E^2-\epsilon^2). \end{aligned}$$

At this point we focus in the low energy regime, where we can take the Dirac approximation, resulting in,

$$I = \frac{E^2-m^2}{2|E|\kappa}\Theta(E^2-m^2),$$

with $m = r-c$ and $c = 2, 0, -2$ depending on the Dirac cone around which we approximate.

B.4 DERIVATION OF THE SMRCKA-STREDA COEFFICIENTS

In this appendix we show the relation between the equations 3.35 and the equations (3.43). More precisely, we want to show that $\theta_1 = 2\pi\sigma^I_{xy}$ and $\theta_2 = 2\pi\sigma^{II}_{xy}$.

$$
\begin{aligned}
\sigma^I_{xy} &= -\frac{i}{16\pi^2}\int \mathrm{d}^2k\,\epsilon_{ij}\,\mathrm{tr}\left(\tau_2 G_E \partial_i G_E^{-1}\tau_1 G_E \partial_j G_E^{-1}\right),\\
&= \frac{1}{8\pi^2}\sum_s \int \mathrm{d}^2k\, s\,\mathrm{tr}\Big((G_E\partial_1 G_E^{-1})_s (G_E\partial_1 G_E^{-1})_{-s}\Big),\\
&= \frac{1}{8\pi^2}\sum_s \int \mathrm{d}^2k\, s\,\mathrm{tr}\left((E+is\kappa+h_a\sigma_a)(\partial_1 h_b\sigma_b)(E-is\kappa+h_c\sigma_c)(\partial_2 h_d\sigma_d)\right) D^s D^{-s},\\
&= -\frac{i\kappa}{2\pi^2}\int \mathrm{d}^2k\,\mathrm{tr}(\sigma_a\sigma_b\sigma_c)h_a\partial_1 h_b\partial_2 h_c D^+ D_-,\\
&= \frac{\kappa}{\pi^2}\int \mathrm{d}^2k\, D^+D^- F_k,\\
&= \theta_1/(2\pi),\\
\sigma^{II}_{xy} &= \frac{1}{24\pi^2}\int_{-\infty}^{E}\int \mathrm{d}\omega\mathrm{d}^2k\,\epsilon_{\alpha\beta\gamma}\,\mathrm{tr}\left(\tau_3 G_\omega\partial_\alpha G_\omega^{-1} G_\omega\partial_\beta G_\omega^{-1} G_\omega\partial_\gamma G_\omega^{-1}\right),\\
&= \frac{1}{8\pi^2}\sum_s\int_{-\infty}^{E}\mathrm{d}\omega\int \mathrm{d}^2k\, s\,\mathrm{tr}\left(((G_\omega\partial_1 G_\omega^{-1})_s(G_\omega\partial_2 G_\omega^{-1}) - (G_\omega\partial_1 G_\omega^{-1})_s(G_\omega\partial_2 G_\omega^{-1})G_\omega)\right),\\
&= \frac{1}{8\pi^2}\sum_s\int_{-\infty}^{E}\mathrm{d}\omega\int \mathrm{d}^2k\, s\,\mathrm{tr}\left([(\partial_1 G_\omega)_s,(G_\omega)_s]\partial_2(G_\omega^{-1})_s\right),\\
&= \frac{1}{8\pi^2}\sum_s\int_{-\infty}^{E}\mathrm{d}\omega\int \mathrm{d}^2k\, s\,\mathrm{tr}\left([(\omega+is\kappa+h_a\sigma_a),\partial_1 h_b\sigma_b]\partial_2 h_c\sigma_c\right) D_s^2,\\
&= \frac{1}{4\pi^2}\int_{-\infty}^{E}\mathrm{d}\omega\int \mathrm{d}^2k\;\mathrm{tr}(\sigma_a\sigma_b\sigma_c)h_a\partial_1 h_b\partial_2 h_c(D_+^2 - D_-^2),\\
&= \frac{i}{2\pi^2}\int_{-\infty}^{E}\mathrm{d}\omega\int \mathrm{d}^2k\, F_k((D_+^2 - D_-^2)),\\
&= \theta_2/(2\pi).
\end{aligned}
\tag{B.7}
$$

C

APPENDIX C

C.1 TOPOLOGICAL INVARIANCE OF THE MAGNETOELECTRIC POLARIZABILITY

Here we derive equation (4.15) using the definition of the transformation for the gauge fields a with contain the sewing matrix (4.13). The sewing matrix B is a $\mathrm{U}(N)$ matrix, where N is the number of occupied bands. We start from the definition of P_3 and then we use the properties (4.14),

$$
\begin{aligned}
P_3 &= \frac{1}{16\pi^2}\int \mathrm{d}^3k\,\epsilon_{ijk}\,\mathrm{tr}\left[(f_{ij}(\mathbf{k}) - \frac{2i}{3}a_i(\mathbf{k})a_j(\mathbf{k}))a_k(\mathbf{k})\right] \\
&= \frac{1}{16\pi^2}\int \mathrm{d}^3k\,\epsilon_{ijk}\,\mathrm{tr}\left[(f_{ij}(-\mathbf{k}) - \frac{2i}{3}a_i(-\mathbf{k})a_j(-\mathbf{k}))a_k(-\mathbf{k})\right] \\
&= \frac{1}{16\pi^2}\int \mathrm{d}^3k\,\epsilon_{ijk}\,\mathrm{tr}\Big[B(\mathbf{k})f_{ij}(\mathbf{k})B^\dagger(\mathbf{k}) - \frac{2i}{3}(B(\mathbf{k})a_i(\mathbf{k})a_j(\mathbf{k})B^\dagger(\mathbf{k}) \\
&\qquad - iB(\mathbf{k})a_i(\mathbf{k})\partial_j B^\dagger(\mathbf{k}) + i\partial_i B(\mathbf{k})a_j(\mathbf{k})B^\dagger(\mathbf{k}) + \partial_i B(\mathbf{k})\partial_j B^\dagger(\mathbf{k})) \\
&\qquad \times(-B(\mathbf{k})a_k(\mathbf{k})B^\dagger(\mathbf{k}) + iB(\mathbf{k})\partial_k B^\dagger(\mathbf{k}))\Big] \\
&= \frac{1}{16\pi^2}\int \mathrm{d}^3k\,\epsilon_{ijk}\,\mathrm{tr}\Big[(-f_{ij}(\mathbf{k})a_k(\mathbf{k}) + \frac{2i}{3}a_i(\mathbf{k})a_j(\mathbf{k}))a_k(\mathbf{k}) + if_{ij}\partial_k B^\dagger(\mathbf{k})B(\mathbf{k}) \\
&\qquad + [a_i(\mathbf{k}), a_j(\mathbf{k})]\partial_k B^\dagger(\mathbf{k})B(\mathbf{k}) - 2ia_j(\mathbf{k})\partial_k B^\dagger(\mathbf{k})\partial_i B(\mathbf{k}) \\
&\qquad - \frac{2}{3}(B(\mathbf{k})\partial_i B^\dagger(\mathbf{k}))(B(\mathbf{k})\partial_j B^\dagger(\mathbf{k}))(B(\mathbf{k})\partial_k B^\dagger(\mathbf{k}))\Big] \\
&= -P_3 - \frac{1}{24\pi^2}\int \mathrm{d}^3k\,\epsilon_{ijk}\,\mathrm{tr}\left[(B(\mathbf{k})\partial_i B^\dagger(\mathbf{k}))(B(\mathbf{k})\partial_j B^\dagger(\mathbf{k}))(B(\mathbf{k})\partial_k B^\dagger(\mathbf{k}))\right] \\
&\qquad + \frac{1}{16\pi^2}\int \mathrm{d}^3k\,\epsilon_{ijk}\partial_i\,\mathrm{tr}\left[a_j(\mathbf{k})\partial_k B^\dagger(\mathbf{k})B(\mathbf{k})\right], \qquad \text{(C.1)}
\end{aligned}
$$

which implies that,

$$
2P_3 = -\frac{1}{24\pi^2}\int \mathrm{d}^3k\,\epsilon_{ijk}\,\mathrm{tr}\left[(B(\mathbf{k})\partial_i B^\dagger(\mathbf{k}))(B(\mathbf{k})\partial_j B^\dagger(\mathbf{k}))(B(\mathbf{k})\partial_k B^\dagger(\mathbf{k}))\right] \qquad \text{(C.2)}
$$

where the last term in (C.1) is a boundary terms that amounts to zero. From here we see that P_3 can only take the values 0 or $1/2$, this given that P_3 is only

defined mod 1. We have therefore two different topological phases the trivial one, with $P_3 = 0$ and a topological one with $P_3 = 1/2$.

C.2 DERIVATION OF THE NON-LINEAR σ MODEL ACTION FOR THE HOTI

In this section we derive the non-linear σ model for the surface of the inversion symmetric HOTI staring from the action 4.22. We define the SCBA Green's function,

$$G_p = (\epsilon - \mathbf{p}\cdot\boldsymbol{\sigma} - m\sigma_3 + i\kappa\tau_3)^{-1}, \tag{C.3}$$

where we have set $v = 1$ for convenience. The SCBA Green's function describes the propagation of excitations with momentum $\mathbf{p}$ in a disordered background with a damping given by κ. We rewrite the SCBA Green's function in terms of the advanced and retarded Green's functions

$$G_p = \frac{\epsilon + i\kappa\tau_3 + \mathbf{p}\cdot\boldsymbol{\sigma} + m\sigma_3}{(\epsilon + i\kappa\tau_3)^2 - (\mathbf{p}^2 + m^2)} = \sum_{s=\pm} G_p^s P^s, \tag{C.4}$$

$$G_p^s = \frac{\epsilon + is\kappa + \mathbf{p}\cdot\boldsymbol{\sigma} + m\sigma_3}{(\epsilon + is\kappa)^2 - (\mathbf{p}^2 + m^2)} = \frac{\epsilon_s + \mathbf{p}\cdot\boldsymbol{\sigma} + m\sigma_3}{\epsilon_s^2 - (\mathbf{p}^2 + m^2)}, \tag{C.5}$$

where P_s are the projectors into the advanced (+) and retarded (-) subspaces, $p = (\epsilon, \mathbf{p})$ and $\epsilon_s = \epsilon + is\kappa$. We proceed to expand the action $S_0[A]$ up to second order in $\mathbf{A} = T^{-1}(\boldsymbol{\partial} - i\mathbf{a})T$. The terms up to second order read,

$$S_0[A] = S^{(1)}[A] + S^{(2)}[A] + \dots, \tag{C.6}$$

$$S^{(1)}[A] = -i\,\mathrm{tr}(G(\mathbf{A}\cdot\boldsymbol{\sigma})), \tag{C.7}$$

$$S^{(2)}[A] = -\frac{1}{2}\int \frac{\mathrm{d}^2p\mathrm{d}^2q}{(2\pi)^4}\,\mathrm{tr}\big(G_{p+q}(\mathbf{A}\cdot\boldsymbol{\sigma})_q G_p(\mathbf{A}\cdot\boldsymbol{\sigma})_{-q}\big). \tag{C.8}$$

We begin to analyze the second order term (C.8) by neglecting the slow q momenta with respect to the fast momenta p, i.e, $G_{p+q} \simeq G_p$. Within this approximation we find,

$$S^{(2)}[A] = -\frac{1}{2}\int \frac{\mathrm{d}^2p\mathrm{d}^2q}{(2\pi)^4}\,\mathrm{tr}\big(G_p(\mathbf{A}\cdot\boldsymbol{\sigma})_q G_p(\mathbf{A}\cdot\boldsymbol{\sigma})_{-q}\big), \tag{C.9}$$

$$= -\frac{1}{2}\sum_{ij,ss'} f_{ss'}^{ij}\int \mathrm{d}^2x\,\mathrm{tr}\Big(P^s\mathbf{A}_i P^{s'}\mathbf{A}_j\Big), \tag{C.10}$$

where we have defined $f_{ss'}^{ij}$ to be the integral over the fast momenta p,

$$f_{ss'}^{ij} = \int \frac{\mathrm{d}^2p}{(2\pi)^2}\,\mathrm{tr}\big[(\epsilon_s + \mathbf{p}\cdot\boldsymbol{\sigma} + m\sigma_3)\sigma_i(\epsilon_s + \mathbf{p}\cdot\boldsymbol{\sigma} + m\sigma_3)\sigma_j\big]N_p^s N_p^{s'}, \tag{C.11}$$

where $N_p^s = (\epsilon_s^2 - (p^2 + m^2))^{-1}$.

Let us consider in the first place the case where $i = j$, $f_{ss'}^{ii} \equiv f_{ss'}$. Firstly, let us examine the case where $s = s'$. The integral reads

$$\begin{aligned} f_{ss} &= \int \frac{\mathrm{d}^2 p}{(2\pi)^2} \operatorname{tr}[(\epsilon_s + \mathbf{p}\cdot\boldsymbol{\sigma} + m\sigma_3)\sigma_i(\epsilon_s + \mathbf{p}\cdot\boldsymbol{\sigma} + m\sigma_3)\sigma_i](N_p^s)^2 \\ &= \int \frac{\mathrm{d}^2 p}{(2\pi)^2} \frac{2(\epsilon_s^2 - m^2)}{(\epsilon_s^2 - (\mathbf{p}^2 + m^2))^2} = \frac{1}{2\pi}\int_0^\infty \mathrm{d}p \frac{2p(\epsilon_s^2 - m^2)}{(\epsilon_s^2 - (p^2 + m^2))^2} \\ &= -\frac{1}{2\pi}, \end{aligned} \tag{C.12}$$

where we have used $\operatorname{tr}[(\mathbf{p}\cdot\boldsymbol{\sigma})\sigma_i(\mathbf{p}\cdot\boldsymbol{\sigma})\sigma_i)] = \sum_{j,k=1,2} p_j p_k \operatorname{tr}\left[\sigma_j\sigma_i\sigma_k\sigma_i\right] = 0$ and i takes the values $1, 2$. Now, let us consider the case where $s' = -s$.

$$\begin{aligned} f_{s-s} &= \int \frac{\mathrm{d}^2 p}{(2\pi)^2} \operatorname{tr}[(\epsilon_s + \mathbf{p}\cdot\boldsymbol{\sigma} + m\sigma_3)\sigma_i(\epsilon_{-s} + \mathbf{p}\cdot\boldsymbol{\sigma} + m\sigma_3)\sigma_i](N_p^s)(N_p^{-s}), \\ &= \int \frac{\mathrm{d}^2 p}{(2\pi)^2} \frac{2(\epsilon_s\epsilon_{-s} - m^2)}{(\mathbf{p}^2 + m^2 - \epsilon_s^2)(\mathbf{p}^2 + m^2 - \epsilon_{-s}^2)}, \\ &= \frac{1}{2\pi}\int_0^\infty \mathrm{d}p \frac{2p(\epsilon^2 + \kappa^2 - m^2)}{((p^2 + m^2 + \kappa^2 - \epsilon^2)^2 + 4\epsilon^2\kappa^2)}, \\ &= \frac{1}{2\pi}\frac{\epsilon^2 + \kappa^2 - m^2}{2\kappa} f(\epsilon, m), \end{aligned} \tag{C.13}$$

where we have defined $f(x, y) = \frac{1}{x}\left(\arctan\left(\frac{x+y}{\kappa}\right) + \arctan\left(\frac{x-y}{\kappa}\right)\right)$ [77]. With $Q = T\tau_3 T^{-1}$ and $A_i = T^{-1}(\partial_i - ia_i)T$, it is straightforward to compute the traces involving the projectors and the A_i's.

$$\sum_{s=\pm} \operatorname{tr}\left(P^s A_i P^{-s} A_i\right) = -\frac{1}{4}\operatorname{tr}[\tau_3, A_i]^2 = -\frac{1}{4}\operatorname{tr}(\nabla_i Q)^2, \tag{C.14}$$

$$\sum_{s=\pm} \operatorname{tr}(P^s A_i P^s A_i) = \frac{1}{4}\operatorname{tr}[\tau_3, A_i]^2 + \operatorname{tr}\left(A_i^2\right) = \frac{1}{4}\operatorname{tr}(\nabla_i Q)^2 + \operatorname{tr}\left(A_i^2\right), \tag{C.15}$$

where $\nabla_k Q = \partial_k Q - i[a_k, Q]$ is the covariant derivative with respect to Q.

The full contribution to the action $S_{ii}^{(2)}[A]$ from the case where $i = j$ reads,

$$S_{ii}^{(2)}[A] = \frac{1}{8}\left(\frac{1}{2\pi}\left(1 + \frac{\epsilon^2 + \kappa^2 - m^2}{2\kappa} f(\epsilon, m)\right)\right)\int \mathrm{d}^2 x \operatorname{tr}(\nabla Q)^2 + \frac{1}{4\pi}\int d^2 r \operatorname{tr}\left(\mathbf{A}^2\right), \tag{C.16}$$

$$= S_d[Q] + \frac{1}{4\pi}\int d^2 r \operatorname{tr}\left(\mathbf{A}^2\right), \tag{C.17}$$

We recognize the first term to be the diffusion term $S_d[Q]$ with longitudinal conductance $\sigma_{xx} = \frac{1}{2\pi}\left(1 + \frac{\epsilon^2+\kappa^2-m^2}{2\kappa} f(\epsilon, m)\right)$.

Let us turn our attention to the case where $i \neq j$. As before, we consider $s' = s$, and then the case $s' = -s$. The fast momenta integrals read,

$$\begin{aligned} f_{ss}^{i\neq j} &= \int \frac{\mathrm{d}^2 p}{(2\pi)^2} \operatorname{tr}\left[(\epsilon_s + \mathbf{p}\cdot\boldsymbol{\sigma} + m\sigma_3)\sigma_i(\epsilon_s + \mathbf{p}\cdot\boldsymbol{\sigma} + m\sigma_3)\sigma_j\right](N_p^s)^2, \\ &= \int \frac{\mathrm{d}^2 p}{(2\pi)^2} 4p_i p_j (N_p^s)^2, \\ &= \int_0^\infty \mathrm{d}p \int_0^{2\pi} \frac{d\theta}{(2\pi)^2} \frac{4p^2 \sin\theta\cos\theta}{(\epsilon_s^2 - (p^2+m^2))^2}, \\ &= 0 \end{aligned} \tag{C.18}$$

$$\begin{aligned} f_{s,-s}^{i\neq j} &= \int \frac{\mathrm{d}^2 p}{(2\pi)^2} \operatorname{tr}\left[(\epsilon_s + \mathbf{p}\cdot\boldsymbol{\sigma} + m\sigma_3)\sigma_i(\epsilon_{-s} + \mathbf{p}\cdot\boldsymbol{\sigma} + m\sigma_3)\sigma_j\right] N_p^s N_p^{-s}, \\ &= \frac{4s\varepsilon^{ij3} m\kappa}{2\pi} \int_0^\infty \mathrm{d}p \frac{p}{(p^2+m^2+\kappa^2-\epsilon^2)^2 + 4\epsilon^2\kappa^2}, \\ &= s\varepsilon^{ij3}\left(\frac{m}{2\pi}\right) f(\epsilon, m). \end{aligned} \tag{C.19}$$

With the previous results, we compute the trace involving $\mathbf{A}$,

$$\begin{aligned} \sum_{s=\pm} s\varepsilon^{ij3} \operatorname{tr}\left(P^s A_i P^{-s} A_j\right) = \varepsilon^{ij3} \operatorname{tr}\left(\tau_3 A_i A_j\right) &= -\frac{1}{4}\varepsilon^{ij3} \operatorname{tr}\left(Q\nabla_i Q \nabla_j Q\right), \\ \varepsilon^{ij3} \operatorname{tr}\left(\tau_3 \partial_i A_j\right) &= \frac{1}{4}\varepsilon^{ij3} \operatorname{tr}\left(Q\nabla_i Q\nabla_j Q\right) - \frac{i}{2}\varepsilon^{ij3} \operatorname{tr}\left(Q f_{ij}\right), \end{aligned} \tag{C.20}$$

where $f_{kl} = \partial_k a_l - \partial_l a_k - i[a_l, a_k]$ is the field strength tensor. We assume f_{kl} proportional to the identity in the advanced/retarded space and the replica space, $f_{jk} \propto \mathbb{I}_{ra} \otimes \mathbb{I}_R$. Under this assumption the last term in equation (C.20) vanishes. Collecting the terms, we obtain for $i \neq j$,

$$\begin{aligned} S_{ij}^{(2)}[A] &= \frac{1}{8}\left(\frac{m}{2\pi} f(\epsilon, m)\right) \sum_{ij} \int \mathrm{d}^x r \varepsilon^{ij3} \operatorname{tr}\left(Q\nabla_i Q \nabla_j Q\right), \\ &= S_{top}^I[Q]. \end{aligned} \tag{C.21}$$

We recognize this term to be the first contribution to the Pruisken term with $\sigma_{xy}^I = \frac{m}{2\pi} f(\epsilon, m)$, the Fermi surface Hall response.

Let us consider the first order correction $S^{(1)}[A]$ (C.7). We will use the trick of doubling the power of the Green's function $G(\epsilon) = \int^\epsilon d\epsilon' G(\epsilon')^2$ to obtain,

$$S^{(1)}[A] = i \int_{-\infty}^{\epsilon} \mathrm{d}\epsilon' \operatorname{tr}\Big(G(\epsilon')^2 (\mathbf{A}\cdot\boldsymbol{\sigma})\Big). \tag{C.22}$$

This term is better computed using the Moyal expansion,

$$\begin{aligned}(G(\mathbf{A}\cdot\boldsymbol{\sigma})G)(\mathbf{x},\mathbf{p}) = G(\mathbf{p})(\mathbf{A}\cdot\boldsymbol{\sigma})(\mathbf{x})G(\mathbf{p}) \\ - \frac{i}{2}\partial_{p_i}G(\mathbf{p})\partial_{x_i}(\mathbf{A}\cdot\boldsymbol{\sigma})(\mathbf{x})G(\mathbf{p}) \\ + \frac{i}{2}G(\mathbf{p})\partial_{x_i}(\mathbf{A}\cdot\boldsymbol{\sigma})(\mathbf{x})\partial_{p_i}G(\mathbf{p}),\end{aligned} \tag{C.23}$$

to bring the action (C.7) into the form,

$$\begin{aligned}S^{(1)}[A] &\simeq \frac{1}{2}\int_{-\infty}^{\epsilon}\mathrm{d}\epsilon'\int\frac{\mathrm{d}^2p}{(2\pi)^2}\int\mathrm{d}^2x\,\mathrm{tr}\big([G_p,\partial_{p_i}G_p]\partial_{x_i}(\mathbf{A}\cdot\boldsymbol{\sigma})\big), \\ &= \frac{1}{2}\sum_{s,ij}\lambda_s^{ij}\int\mathrm{d}^2x\,\mathrm{tr}\big(\partial_iA_jP_s\big),\end{aligned} \tag{C.24}$$

where the coefficients λ_s^{ij} contain the integration over energy and momentum

$$\begin{aligned}\lambda_s^{ij} &= \int_{-\infty}^{\epsilon}d\epsilon'\int\frac{\mathrm{d}^2p}{(2\pi)^2}\,\mathrm{tr}\big([\mathbf{p}\cdot\boldsymbol{\sigma}+m\sigma_3,\sigma_i]\sigma_j\big)(N_s^p)^2, \\ &= \varepsilon^{ij3}\int_{-\infty}^{\epsilon}\mathrm{d}\epsilon'\int\frac{\mathrm{d}^2p}{(2\pi)^2}4im(N_p^s)^2, \\ &= \varepsilon^{ij3}I_s(\epsilon,m).\end{aligned} \tag{C.25}$$

With this result, we find $\varepsilon^{ij3}\,\mathrm{tr}\big(\partial_iA_jP_s\big) = s\frac{1}{2}\varepsilon^{ij3}\,\mathrm{tr}\big(\tau_3\partial_iA_j\big) = s\frac{1}{8}\varepsilon^{ij3}\,\mathrm{tr}\big(Q\nabla_iQ\nabla_jQ\big)$, and the action reads

$$\begin{aligned}S^{(1)}[A] &= \frac{1}{8}\left(\sum_{s=\pm}s\frac{I_s(\epsilon,m)}{2}\right)\sum_{ij}\int\mathrm{d}^2x\varepsilon^{ij3}\,\mathrm{tr}\big(Q\nabla_iQ\nabla_jQ\big), \\ &= S_{top}^{II}[Q].\end{aligned} \tag{C.26}$$

The previous result is found to be the second contribution to the Pruisken term, $\sigma_{xy}^{II} = \sum_{s=\pm}s\frac{I_s(\epsilon,m)}{2} = \frac{m}{2\pi}f(m,e)$, the thermodynamic Hall response. The full Hall conductivity is then $\sigma_{xy} = \sigma_{xy}^{I} + \sigma_{xy}^{II} = \frac{m}{2\pi}(f(\epsilon,m)+f(m,\epsilon))$.

This is not the end of the story. We have to take into account contributions stemming from the regulator (see equation 4.22) where the terms will be of the same structure except that we take the limits $\epsilon\to 0$ and $M\to\infty$.

$$S_{\eta(ii)}^{(2)M}[A] = -\frac{1}{4\pi}\int d^2r\,\mathrm{tr}\Big(\mathbf{A}^2\Big) \tag{C.27}$$

$$S_{\eta(ij)}^{(2)M}[A] = 0 \tag{C.28}$$

$$S_{\eta}^{(1)M}[A] = \frac{1}{8}\left(-\frac{1}{2}\right)\sum_{ij}\int d^2r\varepsilon^{ij3}\,\mathrm{tr}\big(Q\nabla_iQ\nabla_jQ\big) \tag{C.29}$$

To finish the discussion, there is a little catch in the Pruisken term. The Pruisken term in the regulator can be written as,

$$\begin{aligned} -\frac{1}{16}\sum_{ij}\int d^2r\varepsilon^{ij3}\,\mathrm{tr}\big(Q\nabla_i Q\nabla_j Q\big) = -\frac{1}{16}\Big(\sum_{ij}\varepsilon^{ij3}\int d^2r\,\mathrm{tr}\big(Q\partial_i Q\partial_j Q\big) \\ -4i\int d^2r\,\mathrm{tr}\big((\partial_i Q)a_j\big) \\ +2\int d^2r\,\mathrm{tr}\big(Q[a_i,a_j]\big)\Big). \end{aligned} \tag{C.30}$$

Let us take a closer look at the second term in equation (C.30),

$$\begin{aligned} \frac{i}{4}\sum_{ij}\varepsilon^{ij3}\int \mathrm{d}^2x\,\mathrm{tr}\big((\partial_i Q)a_j\big) = &\frac{i}{4}\sum_{ij}\varepsilon^{ij3}\int \mathrm{d}^2x\,\mathrm{tr}\big(\partial_i(Qa_j)\big) \\ &-\frac{i}{8}\sum_{ij}\varepsilon^{ij3}\int \mathrm{d}^2x\,\mathrm{tr}\big(Q(\partial_i a_j-\partial_j a_i)\big) \end{aligned} \tag{C.31}$$

The first term in equation (C.31) we recognize it to be a boundary term. Since our space is closed, this integral vanishes. We can combine the second term in equation (C.31) with the third term in equation (C.30) to form a term proportional to the field strength tensor, namely, $\frac{i}{8}\sum_{ij}\varepsilon^{ij3}\int d^2r\,\mathrm{tr}\big(Qf_{ij}\big)$. This term is zero as mentioned before. We are left with the first term only. We have shown then, that the Pruisken term in the regulator can be written with derivatives instead of covariant derivatives.

D

APPENDIX D

D.1 SADDLE POINT FOR THE AIII MODEL

We derive a saddle point equation for the disordered AIII model. Taking the variation with respect to fields A_+ and A_- results in the following coupled equations,

$$\begin{aligned}\bar{A}_+ &= \gamma^2 \operatorname{tr}\left(\begin{pmatrix}\bar{A}_+ & -h\\ -h^\dagger & \bar{A}_-\end{pmatrix}^{-1}\begin{pmatrix}1 & 0\\ 0 & 0\end{pmatrix}\right),\\ \bar{A}_- &= \gamma^2 \operatorname{tr}\left(\begin{pmatrix}\bar{A}_+ & -h\\ -h^\dagger & \bar{A}_-\end{pmatrix}^{-1}\begin{pmatrix}0 & 0\\ 0 & 1\end{pmatrix}\right).\end{aligned} \tag{D.1}$$

We make the following ansatz, $\bar{A}_+ = \bar{A}_- = i\kappa\tau_3$, which solves the coupled equations and gives a self-consistent equation for the parameter κ,

$$\kappa = 2\gamma^2 \int \frac{\mathrm{d}^3k}{(2\pi)^2} \operatorname{tr}\left(\frac{\kappa}{\kappa^2 + h(\mathbf{k})h^\dagger(\mathbf{k})}\right), \tag{D.2}$$

At this point to obtain a low energy action we introduce a spatially dependent saddle point solution, such that $\bar{A}_+ = i\kappa\tau_3 M(x)$ and $\bar{A}_- = i\kappa M^{-1}(x)\tau_3$, which are precisely the Goldstone modes of theory.

D.2 DERIVATION OF THE AIII NON-LINEAR σ MODEL

In this section we show how we can derive an effective non-linear σ model for $E = 0$ in the case where we take the Hamiltonian of the system to be the low energy version of (5.11),

$$H_D = \sum_{i=1}^{3} k_i \tau_1 \sigma_i + m\tau_2\sigma_0 \tag{D.3}$$

where m is a parameter that depends around which point we take the low energy approximation. In this approximation the off-diagonal component of the Hamiltonian takes the form,

$$h = \sum_{i=1}^{3} k_i\sigma_i - im. \tag{D.4}$$

The first order contributions vanish, and therefore the interesting contributions come from the second order and third order.

To obtain the gradient term we look at the second order contribution when $i = j$,

$$\frac{1}{2}\,\mathrm{Tr}(G_0 F G_0 F) = \frac{1}{2}\int \frac{\mathrm{d}^3k}{(2\pi)^3}\,\frac{\mathrm{Tr}\big(h^\dagger \partial_i h\, h^\dagger \partial_i h\big)}{(\kappa^2+|h|^2)^2}\int \mathrm{d}^3x\ \mathrm{Tr}(\phi_i\phi_i) \tag{D.5}$$

We develop the trace in the momentum integrals,

$$\begin{aligned}\mathrm{Tr}\Big(h^\dagger \partial_i h\, h^\dagger \partial_i h\Big) &= \mathrm{Tr}\left((\sum_{i=l}^{3} k_l\sigma_l + im)\sigma_i(\sum_{i=m}^{3} k_m\sigma_m + im)\sigma_i\right)\\ &= \sum_{l,m} k_l k_m\,\mathrm{Tr}(\sigma_l\sigma_i\sigma_m\sigma_i) - m^2\,\mathrm{Tr}(\sigma_i\sigma_i)\\ &= -\frac{2}{3}|k|^2 - 2m^2,\end{aligned} \tag{D.6}$$

where from the first to second line we have ignored the terms that are zero under the trace. From the second to the third line we have used the fact that only for $l = m$ the integral would be non-zero, we aslo used that $k_l^2 = |k|^2/3$ under the integral. And finally we used that $\sum_{l=1}^{3} Tr(\sigma_l\sigma_i\sigma_l\sigma_i) = -2$.

The momentum integral takes the following form,

$$-\int_0^\infty \frac{\mathrm{d}|k|}{2\pi^2}\,\frac{|k|^4/3 + m^2|k|^2}{(\kappa^2+|k|^2+m^2)^2}, \tag{D.7}$$

This integral is UV divergent. To fix this issue we do a Pauli-Villars regularization, where we substract the same integral but we do the following changes $\kappa \to \eta$, $m \to \mu$, where $\eta \to 0$ and $\mu \to \infty$. In this limit the integral yields the following value,

$$-\int_0^\infty \frac{\mathrm{d}|k|}{2\pi^2}\,\frac{|k|^4/3 + m^2|k|^2}{(\kappa^2+|k|^2+m^2)^2} \overset{\text{Reg.}}{=} \frac{1}{8\pi}\,\frac{\kappa^2}{\sqrt{m^2+\kappa^2}} \tag{D.8}$$

Therefore the second order contribution yields the gradient term,

$$S_{\mathrm{grad}}[M] = \frac{1}{8\pi}\frac{\kappa^2}{\sqrt{m^2+\kappa^2}}\int \mathrm{d}^3x\,\mathrm{Tr}\Big(\partial_i M^{-1}\partial_i M\Big) \tag{D.9}$$

We consider now the third order term and we consider the case where $i \neq j \neq k$ which would yield the topological term,

$$-\frac{1}{3}\,\mathrm{Tr}(G_0 F G_0 F G_0 F) = -\frac{1}{3}\int \frac{\mathrm{d}^3k}{(2\pi)^3}\,\frac{\mathrm{Tr}\big(h^\dagger \partial_i h\, h^\dagger \partial_j h\, h^\dagger \partial_k h\big)}{(\kappa^2+|h|^2)^3}\int \mathrm{d}^3x\ \mathrm{Tr}\big(\phi_i\phi_j\phi_k\big) \tag{D.10}$$

From the previous expression we notice that the trace in the momentum integral yields a lot of terms, nevertheless it is easily simplified once we notice that odd powers of the components of k will yield 0. We consider therefore the following terms,

$$\begin{aligned} 3im\sum_{l,m} k_l k_m \operatorname{Tr}\left(\sigma_l\sigma_i\sigma_m\sigma_j\sigma_k\right) &= im|k|^2\sum_l \operatorname{Tr}\left(\sigma_l\sigma_i\sigma_l\sigma_j\sigma_k\right) \\ &= -2im|k|^2\epsilon_{ijk}, \end{aligned} \tag{D.11}$$

and

$$-im^3\operatorname{Tr}\left(\sigma_i\sigma_j\sigma_k\right) = -2im^3\epsilon_{ijk}. \tag{D.12}$$

The momentum integral that we need to solve is,

$$\frac{i}{3\pi^2}\int_0^\infty \frac{m|k|^4+m^3|k|^2}{(\kappa^2+|k|^2+m^2)^3} \overset{\text{Reg.}}{=} \frac{i}{64\pi}\left(\frac{4m^3+3m\kappa^2}{(m^2+\kappa^2)^{3/2}}-4\right) \tag{D.13}$$

With this consideration the third order term is therefore the topological action,

$$S_{\text{top}} = \frac{i}{48\pi}\left(\frac{4m^3+3m\kappa^2}{(m^2+\kappa^2)^{3/2}}-4\right)\int \mathrm{d}^3x\,\epsilon_{ijk}\operatorname{Tr}\left(M^{-1}\partial_i M\,M^{-1}\partial_j M\,M^{-1}\partial_k M\right) \tag{D.14}$$

Within this derivation we have the following identification for the coupling constants of the theory,

$$\begin{aligned} g &= \frac{1}{8\pi}\frac{\kappa^2}{\sqrt{m^2+\kappa^2}}, \\ \vartheta &= \frac{\pi}{2}\left(\frac{4m^3+3m\kappa^2}{(m^2+\kappa^2)^{3/2}}-4\right). \end{aligned} \tag{D.15}$$

BIBLIOGRAPHY

1. Klitzing, K. v., Dorda, G. & Pepper, M. New method for high-accuracy determination of the fine-structure constant based on quantized Hall resistance. *Physical review letters* **45**, 494 (1980).
2. Laughlin, R. B. Quantized Hall conductivity in two dimensions. *Physical Review B* **23**, 5632 (1981).
3. Thouless, D. J., Kohmoto, M., Nightingale, M. P. & den Nijs, M. Quantized Hall conductance in a two-dimensional periodic potential. *Physical review letters* **49**, 405 (1982).
4. Haldane, F. D. M. Model for a quantum Hall effect without Landau levels: Condensed-matter realization of the" parity anomaly". *Physical review letters* **61**, 2015 (1988).
5. Altland, A. & Zirnbauer, M. R. Nonstandard symmetry classes in mesoscopic normal-superconducting hybrid structures. *Physical Review B* **55**, 1142 (1997).
6. Anderson, P. W. Absence of Diffusion in Certain Random Lattices. *Phys. Rev.* **109**, 1492 (5 1958).
7. Wegner, F. J. Electrons in disordered systems. Scaling near the mobility edge. *Zeitschrift für Physik B Condensed Matter* **25**, 327 (1976).
8. Pruisken, A. M. On localization in the theory of the quantized hall effect: A two-dimensional realization of the θ-vacuum. *Nuclear Physics B* **235**, 277 (1984).
9. Pruisken, A. M. in *The quantum Hall effect* 117 (Springer, 1987).
10. Ryu, S., Schnyder, A. P., Furusaki, A. & Ludwig, A. W. Topological insulators and superconductors: tenfold way and dimensional hierarchy. *New Journal of Physics* **12**, 065010 (2010).
11. Altland, A., Bagrets, D. & Kamenev, A. Topology versus Anderson localization: Nonperturbative solutions in one dimension. *Physical Review B* **91**, 085429 (2015).
12. Altshuler, B. L. & Simons, B. Universalities: From Anderson localization to quantum chaos. *Mesoscopic Quantum Physics, Les Houches*, 1 (1994).
13. Lifshitz, I. M. Energy spectrum structure and quantum states of disordered condensed systems. *Soviet Physics Uspekhi* **7**, 549 (1965).

14. Edwards, J. & Thouless, D. Numerical studies of localization in disordered systems. *Journal of Physics C: Solid State Physics* **5**, 807 (1972).

15. Thouless, D. Resistance and localization in thin films and wires. *Journal of Non-Crystalline Solids* **35**, 3 (1980).

16. Abrahams, E., Anderson, P. W., Licciardello, D. C. & Ramakrishnan, T. V. Scaling theory of localization: Absence of quantum diffusion in two dimensions. *Physical Review Letters* **42**, 673 (1979).

17. König, E., Ostrovsky, P., Protopopov, I. & Mirlin, A. Metal-insulator transition in two-dimensional random fermion systems of chiral symmetry classes. *Physical Review B—Condensed Matter and Materials Physics* **85**, 195130 (2012).

18. Edwards, S. F. & Anderson, P. W. Theory of spin glasses. *Journal of Physics F: Metal Physics* **5**, 965 (1975).

19. Efetov, K. *Supersymmetry in disorder and chaos* (Cambridge university press, 1999).

20. Kamenev, A. & Levchenko, A. Keldysh technique and non-linear σ-model: basic principles and applications. *Advances in Physics* **58**, 197 (2009).

21. Wegner, F. Four-loop-order β-function of nonlinear σ-models in symmetric spaces. *Nuclear Physics B* **316**, 663 (1989).

22. Efetov, K., Larkin, A. & Kheml'Nitskiĭ, D. Interaction of diffusion modes in the theory of localization. *Soviet Journal of Experimental and Theoretical Physics* **52**, 568 (1980).

23. Schäfer, L. & Wegner, F. Disordered system with n orbitals per site: Lagrange formulation, hyperbolic symmetry, and Goldstone modes. *Zeitschrift für Physik B Condensed Matter* **38**, 113 (1980).

24. Jüngling, K. & Oppermann, R. Effects of spin interactions in disordered electronic systems: loop expansions and exact relations among local gauge invariant models. *Zeitschrift für Physik B Condensed Matter* **38**, 93 (1980).

25. Von Klitzing, K. The quantized Hall effect. *Reviews of Modern Physics* **58**, 519 (1986).

26. Byers, N. & Yang, C. Theoretical considerations concerning quantized magnetic flux in superconducting cylinders. *Physical review letters* **7**, 46 (1961).

27. Bloch, F. Josephson effect in a superconducting ring. *Physical Review B* **2**, 109 (1970).

28. Halperin, B. I. Quantized Hall conductance, current-carrying edge states, and the existence of extended states in a two-dimensional disordered potential. *Physical review B* **25**, 2185 (1982).

29. Nakahara, M. *Geometry, topology and physics* (CRC press, 2018).

30. Smrcka, L. & Streda, P. Transport coefficients in strong magnetic fields. *Journal of Physics C: Solid State Physics* **10**, 2153 (1977).

31. Khmelnitskii, D. Quantization of Hall conductivity. *ZhETF Pisma Redaktsiiu* **38**, 454 (1983).

32. Zirnbauer, M. R. The integer quantum Hall plateau transition is a current algebra after all. *Nuclear Physics B* **941**, 458 (2019).

33. Zirnbauer, M. R. Reprint of: Marginal CFT perturbations at the integer quantum Hall transition. *Annals of Physics* **435**, 168691 (2021).

34. Evers, F. & Mirlin, A. D. Anderson transitions. *Reviews of Modern Physics* **80**, 1355 (2008).

35. Janssen, M. Multifractal analysis of broadly-distributed observables at criticality. *International Journal of Modern Physics B* **8**, 943 (1994).

36. Huckestein, B. Scaling theory of the integer quantum Hall effect. *Reviews of Modern Physics* **67**, 357 (1995).

37. Evers, F., Mildenberger, A. & Mirlin, A. Multifractality at the quantum Hall transition: Beyond the parabolic paradigm. *Physical review letters* **101**, 116803 (2008).

38. Li, J., Chu, R.-L., Jain, J. K. & Shen, S.-Q. Topological anderson insulator. *Physical review letters* **102**, 136806 (2009).

39. Groth, C., Wimmer, M., Akhmerov, A., Tworzydło, J. & Beenakker, C. Theory of the topological Anderson insulator. *Physical review letters* **103**, 196805 (2009).

40. Berry, M. V. Quantal phase factors accompanying adiabatic changes. *Proceedings of the Royal Society of London. A. Mathematical and Physical Sciences* **392**, 45 (1984).

41. Tong, D. The quantum Hall effect: TIFR infosys lectures. *arXiv preprint arXiv:1606.06687* (2016).

42. Qi, X.-L., Wu, Y.-S. & Zhang, S.-C. Topological quantization of the spin Hall effect in two-dimensional paramagnetic semiconductors. *Physical Review B—Condensed Matter and Materials Physics* **74**, 085308 (2006).

43. Jackiw, R. & Rebbi, C. Solitons with fermion number 1/2. *Physical Review D* **13**, 3398 (1976).

44. Moreno-Gonzalez, M., Dieplinger, J. & Altland, A. Topological quantum criticality of the disordered Chern insulator. *Annals of Physics* **456**, 169258 (2023).

45. Altland, A., Offer, C. & Simons, B. in *Supersymmetry and Trace Formulae: Chaos and Disorder* 17 (Springer, 1999).

46. Altland, A. & Simons, B. D. *Condensed matter field theory* (Cambridge university press, 2010).

47. Mirlin, A. & Evers, F. Multifractality and critical fluctuations at the Anderson transition. *Physical Review B* **62**, 7920 (2000).

48. Rodriguez, A., Vasquez, L. J., Slevin, K. & Römer, R. A. Multifractal finite-size scaling and universality at the Anderson transition. *Physical Review B—Condensed Matter and Materials Physics* **84**, 134209 (2011).

49. Puschmann, M., Cain, P., Schreiber, M. & Vojta, T. Integer quantum Hall transition on a tight-binding lattice. *Physical Review B* **99**, 121301 (2019).

50. Puschmann, M. & Vojta, T. Green's functions on a renormalized lattice: An improved method for the integer quantum Hall transition. *Annals of Physics* **435**, 168485 (2021).

51. Dresselhaus, E. J., Sbierski, B. & Gruzberg, I. A. Scaling collapse of longitudinal conductance near the integer quantum Hall transition. *Physical Review Letters* **129**, 026801 (2022).

52. Kane, C. L. & Mele, E. J. Z 2 topological order and the quantum spin Hall effect. *Physical review letters* **95**, 146802 (2005).

53. Kane, C. L. & Mele, E. J. Quantum spin Hall effect in graphene. *Physical review letters* **95**, 226801 (2005).

54. Fu, L., Kane, C. L. & Mele, E. J. Topological insulators in three dimensions. *Physical review letters* **98**, 106803 (2007).

55. Su, W.-P., Schrieffer, J. & Heeger, A. Soliton excitations in polyacetylene. *Physical Review B* **22**, 2099 (1980).

56. Kitaev, A. Y. Unpaired Majorana fermions in quantum wires. *Physics-uspekhi* **44**, 131 (2001).

57. Volovik, G. Fermion zero modes on vortices in chiral superconductors. *Journal of Experimental and Theoretical Physics Letters* **70**, 609 (1999).

58. Cartan, É. Sur une classe remarquable d'espaces de Riemann. *Bulletin de la Société mathématique de France* **54**, 214 (1926).

59. Cartan, É. Sur une classe remarquable d'espaces de Riemann. II. *Bulletin de la Société Mathématique de France* **55**, 114 (1927).

60. Schnyder, A. P., Ryu, S., Furusaki, A. & Ludwig, A. W. Classification of topological insulators and superconductors in three spatial dimensions. *Physical Review B—Condensed Matter and Materials Physics* **78**, 195125 (2008).

61. Kitaev, A. *Periodic table for topological insulators and superconductors* in *AIP conference proceedings* **1134** (2009), 22.

62. Ando, Y. & Fu, L. Topological crystalline insulators and topological superconductors: From concepts to materials. *Annu. Rev. Condens. Matter Phys.* **6**, 361 (2015).

63. Fu, L. Topological crystalline insulators. *Physical review letters* **106**, 106802 (2011).

64. Benalcazar, W. A., Bernevig, B. A. & Hughes, T. L. Electric multipole moments, topological multipole moment pumping, and chiral hinge states in crystalline insulators. *Physical Review B* **96**, 245115 (2017).

65. Benalcazar, W. A., Bernevig, B. A. & Hughes, T. L. Quantized electric multipole insulators. *Science* **357**, 61 (2017).

66. Schindler, F., Cook, A. M., Vergniory, M. G., Wang, Z., Parkin, S. S., Bernevig, B. A. & Neupert, T. Higher-order topological insulators. *Science advances* **4**, eaat0346 (2018).

67. Langbehn, J., Peng, Y., Trifunovic, L., von Oppen, F. & Brouwer, P. W. Reflection-symmetric second-order topological insulators and superconductors. *Physical review letters* **119**, 246401 (2017).

68. Benalcazar, W. A., Li, T. & Hughes, T. L. Quantization of fractional corner charge in C n-symmetric higher-order topological crystalline insulators. *Physical Review B* **99**, 245151 (2019).

69. Bradlyn, B., Elcoro, L., Cano, J., Vergniory, M. G., Wang, Z., Felser, C., Aroyo, M. I. & Bernevig, B. A. Topological quantum chemistry. *Nature* **547**, 298 (2017).

70. Geier, M., Trifunovic, L., Hoskam, M. & Brouwer, P. W. Second-order topological insulators and superconductors with an order-two crystalline symmetry. *Physical Review B* **97**, 205135 (2018).

71. Trifunovic, L. & Brouwer, P. W. Higher-order bulk-boundary correspondence for topological crystalline phases. *Physical Review X* **9**, 011012 (2019).

72. Qi, X.-L., Hughes, T. L. & Zhang, S.-C. Topological field theory of time-reversal invariant insulators. *Physical Review B—Condensed Matter and Materials Physics* **78**, 195424 (2008).

73. Essin, A. M., Moore, J. E. & Vanderbilt, D. Magnetoelectric polarizability and axion electrodynamics in crystalline insulators. *Physical review letters* **102**, 146805 (2009).

74. Bernevig, B. A. *Topological insulators and topological superconductors* (Princeton university press, 2013).

75. Qi, X.-L. & Zhang, S.-C. Topological insulators and superconductors. *Reviews of modern physics* **83**, 1057 (2011).

76. Pauli, W. & Villars, F. On the invariant regularization in relativistic quantum theory. *Reviews of Modern Physics* **21**, 434 (1949).

77. Ostrovsky, P., Gornyi, I. & Mirlin, A. Quantum criticality and minimal conductivity in graphene with long-range disorder. *Physical review letters* **98**, 256801 (2007).

78. König, E., Ostrovsky, P., Protopopov, I., Gornyi, I., Burmistrov, I. & Mirlin, A. Half-integer quantum Hall effect of disordered Dirac fermions at a topological insulator surface. *Physical Review B* **90**, 165435 (2014).

79. Essin, A. M. & Gurarie, V. Bulk-boundary correspondence of topological insulators from their respective Green's functions. *Physical Review B—Condensed Matter and Materials Physics* **84**, 125132 (2011).

80. Schulz-Baldes, H. & Stoiber, T. *Harmonic analysis in operator algebras and its applications to index theory and topological solid state systems* (Springer Nature, 2022).

81. Prodan, E. Disordered topological insulators: a non-commutative geometry perspective. *Journal of Physics A: Mathematical and Theoretical* **44**, 113001 (2011).

82. Sbierski, B., Karcher, J. F. & Foster, M. S. Spectrum-wide quantum criticality at the surface of class AIII topological phases: An "energy stack" of integer quantum Hall plateau transitions. *Physical Review X* **10**, 021025 (2020).

83. Foster, M. S., Xie, H.-Y. & Chou, Y.-Z. Topological protection, disorder, and interactions: Survival at the surface of three-dimensional topological superconductors. *Physical Review B* **89**, 155140 (2014).

84. Karcher, J. F. & Foster, M. S. How spectrum-wide quantum criticality protects surface states of topological superconductors from Anderson localization: Quantum Hall plateau transitions (almost) all the way down. *Annals of Physics* **435**, 168439 (2021).

85. Ghorashi, S. A. A., Liao, Y. & Foster, M. S. Critical percolation without fine-tuning on the surface of a topological superconductor. *Physical Review Letters* **121**, 016802 (2018).

86. Altland, A., Brouwer, P. W., Dieplinger, J., Foster, M. S., Moreno-Gonzalez, M. & Trifunovic, L. Fragility of surface states in non-Wigner-Dyson topological insulators. *Physical Review X* **14**, 011057 (2024).

87. Thouless, D. Wannier functions for magnetic sub-bands. *Journal of Physics C: Solid State Physics* **17**, L325 (1984).

88. Kuchment, P. Tight frames of exponentially decaying Wannier functions. *Journal of Physics A: Mathematical and Theoretical* **42**, 025203 (2008).

89. Ludewig, M. & Thiang, G. C. Large-scale geometry obstructs localization. *arXiv preprint arXiv:2204.12895* (2022).

90. Soluyanov, A. A. & Vanderbilt, D. Wannier representation of Z 2 topological insulators. *Physical Review B—Condensed Matter and Materials Physics* **83**, 035108 (2011).

91. Thonhauser, T. & Vanderbilt, D. Insulator/Chern-insulator transition in the Haldane model. *Physical Review B—Condensed Matter and Materials Physics* **74**, 235111 (2006).

92. Winkler, G. W., Soluyanov, A. A. & Troyer, M. Smooth gauge and Wannier functions for topological band structures in arbitrary dimensions. *Physical Review B* **93**, 035453 (2016).

93. Cornean, H. D., Monaco, D. & Teufel, S. Wannier functions and Z 2 invariants in time-reversal symmetric topological insulators. *Reviews in Mathematical Physics* **29**, 1730001 (2017).

94. Cornean, H. D. & Monaco, D. *On the construction of Wannier functions in topological insulators: the 3D case* in *Annales Henri Poincaré* **18** (2017), 3863.

95. Read, N. Compactly supported Wannier functions and algebraic K-theory. *Physical Review B* **95**, 115309 (2017).

96. Trifunovic, L. Bulk-and-edge to corner correspondence. *Physical Review Research* **2**, 043012 (2020).

97. Lapierre, B., Neupert, T. & Trifunovic, L. N-band Hopf insulator. *Physical Review Research* **3**, 033045 (2021).

98. Alexandradinata, A., Nelson, A. & Soluyanov, A. A. Teleportation of Berry curvature on the surface of a Hopf insulator. *Physical Review B* **103**, 045107 (2021).

99. Gade, R. & Wegner, F. The n= 0 replica limit of U (n) and U (n) SO (n) models. *Nuclear Physics B* **360**, 213 (1991).

100. Altland, A. & Simons, B. Field theory of the random flux model. *Nuclear Physics B* **562**, 445 (1999).

101. Altland, A., Simons, B. & Zirnbauer, M. Theories of low-energy quasiparticle states in disordered d-wave superconductors. *Physics Reports* **359**, 283 (2002).

102. Nersesyan, A., Tsvelik, A. & Wenger, F. Disorder effects in two-dimensional d-wave superconductors. *Physical review letters* **72**, 2628 (1994).

103. Chalker, J. & Coddington, P. Percolation, quantum tunnelling and the integer Hall effect. *Journal of Physics C: Solid State Physics* **21**, 2665 (1988).

ACKNOWLEDGEMENTS

The completion of this PhD thesis would not have been possible without the support and guidance of many people to whom I am deeply indebted. First and foremost, I would like to express my gratitude to my advisor, Prof. Dr. Alexander Altland, for his mentorship, support, and great insights from which I was able to learn a lot. I also thank the second examiner Prof. Dr. Achim Rosch and the chair of the evaluation committee Prof. Dr. Joachim Krug for their time, for reading my thesis and for taking part in the examination committee. I also would like to thank Dr. Romain Daviet for taking on the role of the minute-taker.

I would like to thank of all the collaborators I had the chance to work with in the last years and whose contributions have been integral to the success of this research. They are Johannes Dieplinger, Matthew Foster, Piet Brouwer, Luka Trifunovic, Adam Chaou, Omri Lesser and Carolin Wille. It has been an enriching experience and I have learned so much from all the countless hours of discussions we had. Your insights, feedback, and expertise have greatly broadened my own understanding of disorder in topological matter.

I would like to extend my thanks to Dr. Dmitry Bagrets for his generous time and invaluable guidance throughout my time in the group. I am truly grateful for your support and for the many insightful discussions. I deeply appreciate the dedication and patience you have shown.

A big thank you to Petra Neubauer-Guenter, Andreas Sindermann, Dinna Schäfer, Sophie Hinzmann for their help and support in various technical and administrative matters.

After seven years in Cologne I have had the pleasure of meeting truly wonderful people, people that I now call my friends. Your support, encouragement, and companionship have been invaluable to me during this journey. Whether it was celebrating successes, providing a listening ear during challenging times, or simply sharing everyday moments, each of you has made my time in Cologne more meaningful and fulfilling. Roberto, Mario, Jana, Camila, Aggelos, Elena, Marc, Lorenz, Felipe, Efe, Spencer, Saurabh, Vaishnavi and Changjun made the first couple years away from home easier. I have wonderful memories and I always cherish the nice moments we spent together. To Aurelio, Laura, Julian, Arnau, Elisa, Stephan, Maedeh, Sanam, Matthijs, Sreya, Denny, Yaren, Dennis, Muna, Luis, Berta, Rodolfo, Rene, Jonas, Andressa, Maksi, Matteo and many more thank you all for the wonderful moments during these 4 years of PhD, from silly conversations to serious discussions about life at mensa, from discussions about physics to dancing all night at parties, from cake fridays to

beer at the wall, and many more fun activities you have certainly made this journey through my PhD (which was not easy) much more fun. Special thanks to Rohan, thanks for proofreading parts of this thesis, for all the nice enlightning discussions around physics and about life that we had. Thanks to Konni also for proofreading parts of the thesis and for many interesting conversations about basically every topic in the world and all the nice moments we spent with the rest of the group. A wholeheartdly thanks to Blanca, thank you very much for proofreading parts of this thesis and thank you for all the wonderful moments: the classic "descansito a las y media", the protein bar reviews, the crosswords, the political conversations, the parties, bouldering, and many more special moments... Thank you for always being such a supportive and amazing friend and for being there in the difficult moments.

Gracias enormes a mis amigos de Colombia, Miguel, JuanDa, S. Vergara, D. Sepúlveda, Javi, Dani, JuanSa, JuanGui, Pipe, Santi Gómez gracias por hacerme sentir un poco más cerca de Colombia en la distancia. Por su apoyo, por las conversaciones acerca de migrar y estar lejos de casa y por los buenos momentos tanto en Colombia como en Europa.

Finalmente, gracias desde el fondo de mi corazón a mi familia. A mis padres Armando y Omaira, a mis hermanas, Laura y Karol y a mis hermanos Andrés y Santi. Gracias por la paciencia, por todo el apoyo y amor incondicional en los momentos más difíciles. Su amor y apoyo han sido mi base, y no podría haber alcanzado este hito sin ustedes.

ERKLÄRUNG ZUR DISSERTATION

Hiermit versichere ich an Eides statt, dass ich die vorliegende Dissertation selbstständig und ohne die Benutzung anderer als der angegebenen Hilfsmittel und Literatur angefertigt habe. Alle Stellen, die wörtlich oder sinngemäß aus veröffentlichten und nicht veröffentlichten Werken dem Wortlaut oder dem Sinn nach entnommen wurden, sind als solche kenntlich gemacht. Ich versichere an Eides statt, dass diese Dissertation noch keiner anderen Fakultät oder Universität zur Prüfung vorgelegen hat; dass sie - abgesehen von unten angegebenen Teilpublikationen und eingebundenen Artikeln und Manuskripten -noch nicht veröffentlicht worden ist sowie, dass ich eine Veröffentlichung der Dissertation vor Abschluss der Promotion nicht ohne Genehmigung des Promotionsausschusses vornehmen werde. Die Bestimmungen dieser Ordnung sind mir bekannt. Darüber hinaus erkläre ich hiermit, dass ich die Ordnung zur Sicherung guter wissenschaftlicher Praxis und zum Umgang mit wissenschaftlichem Fehlverhalten der Universität zu Köln gelesen und sie bei der Durchführung der Dissertation zugrundeliegenden Arbeiten und der schriftlich verfassten Dissertation beachtet habe und verpflichte mich hiermit, die dort genannten Vorgaben bei allen wissenschaftlichen Tätigkeiten zu beachten und umzusetzen. Ich versichere, dass die eingereichte elektronische Fassung der eingereichten Druckfassung vollständig entspricht.

Teilpublikationen:

1. Topological quantum criticality of the disordered Chern insulator. **M. Moreno–Gonzalez**, J. Dieplinger, A. Altland. Annals of Physics (2023): 169258.

2. Fragility of spectral flow for topological phases in non-Wigner-Dyson classes. A. Altland, P. Brouwer, J. Dieplinger, M. Foster, **M. Moreno–Gonzalez**, L. Trifunovic. Physical Review X 14, 011057 (2024) .

Pre-prints:

1. Disordered topological crystalline phases. A. Chaou, **M. Moreno Gonzalez**, A. Altland, P. Brouwer. arXiv:2412.01883.

Mateo Moreno Gonzalez

01.09.2024, Köln